FINITE ELEMENT MODELING OF THE ANTHROPOID MANDIBLE: MANDIBLE MODEL, EXPERIMENTAL VALIDATION, AND ANTHROPOLOGIC APPLICATION

By

RUXANDRA CRISTIANA MARINESCU TANASOCA

A DISSERTATION PRESENTED TO THE GRADUATE SCHOOL
OF THE UNIVERSITY OF FLORIDA IN PARTIAL FULFILLMENT
OF THE REQUIREMENTS FOR THE DEGREE OF
DOCTOR OF PHILOSOPHY

UNIVERSITY OF FLORIDA

2006

To my husband, Razvan.

ACKNOWLEDGMENTS

I give special thanks to Dr. Andrew Rapoff and Dr. David Daegling for their assistance and guidance throughout my graduate studies. I wish to thank Dr. William Ditto, Dr. Raphael T. Haftka, Dr. Frank Bova and Dr. Malisa Sarntinoranont for their assistance and for serving on my supervisory committee. Special thanks go to Dr. Nam-Ho Kim, Dr. William Ditto and Dr. Johannes van Oostrom for their constant support and guidance.

I wish to thank and express sincere appreciation to my friend, Dr. Nicoleta Apetre, for her help on my research and moral support during the years.

Special thanks to my mentor, Dr. Jean Wright, for her unending support, encouragement and invaluable advice.

I would like to thank all my professors and colleagues from whom I learned so much. Special thanks go to my husband, my son, my parents, my sister and my friends, for their continual love, support, and encouragement throughout my time in graduate school.

TABLE OF CONTENTS

page

ACKNOWLEDGMENTS iv

LIST OF TABLES vii

LIST OF FIGURES ix

ABSTRACT xi

CHAPTER

1 INTRODUCTION 1

Bone Structure 9
Cortical Bone 10
Trabecular Bone 10
Mechanical Properties of Bones 11
Measuring the Mechanical Properties of Bone 13
Mechanical Tests 13
In Vitro or in Vivo Strain Gage Measurements 14
Ultrasonic Pulse Transmission Technique 14
Microindentation and Nanoindentation Tests 15
Computed Tomography Method 15
Measurements of the Elastic Modulus of Bones 16
Mandible 17
Masticatory Muscles 18
Measurements of the Elastic Modulus of the Mandible 19
State of the Art — Mandible Models 21
Methods of Model Building 21
FE Mandible Models 23
SED and Functional Adaptation 25
Adaptation to Environment 25
Mechanobiology of Bone 26
Strain Energy Density (SED) 29

2 FINITE ELEMENT MODELING OF THE ANTHROPOID MANDIBLE: MANDIBLE MODEL AND EXPERIMENTAL VALIDATION 40

Introduction 40

Finite Element Modeling 41
Mathematical Method 41
Photoelastic method 42
Strain Gauge Analysis 42
Materials and Methods 44
Experimental Strain Analysis 44
Finite Element Analysis 45
Mandible model 45
Finite element simulations 47
Factors that Influenced the FEA 48
FEA—nodal constraints 49
FEA—degrees of freedom 49
FEA—force direction 49
FEA—material properties assignment 50
Validation of the FE Model 54
Method to Record Principal Strain Values 60
Results 60
FEA—Nodal Constraints 61
FEA—Force Direction 61
FEA—Degrees of Freedom 62
FEA—Material Properties Assignment 62
Discussion 63

3 RELATIONSHIP OF STRAIN ENERGY DENSITY TO MORPHOLOGICAL VARIATION IN MACACA MANDIBLE 85

Introduction 85
Regional Variation in Cortical Bone 86
Loading Patterns, Strain Gradients and Mandible Morphology 88
Edentulous vs. Dentate Mandible Models 91
Strain Energy Density 93
Materials and Methods 99
Strain Energy Density Criterion 99
Finite Element Analysis 100
Results 107
Strain Energy Density 108
Strain 110
FE Model Accuracy in Terms of Cortical Asymmetry 112
Discussion 116

4 CONCLUSIONS AND PERSPECTIVES 149

LIST OF REFERENCES 155

BIOGRAPHICAL SKETCH 168

LIST OF TABLES

Table page

1-1 Elastic modulus values for trabecular bone and cortical bone 31

1-2 The 9 independent constants for human and canine mandibles 31

1-3 Elastic moduli of symphysis, canine and molar region.....31

1-4 Comparison between elastic modulus values for human and macaque mandibles..32

2-1 Experimental and theoretical principal strain data. Principal strains and the principal strain ratios are calculated from the lateral aspect of the corpus. 69

2-2 Experimental and theoretical principal strain data. Principal strains and the principal strain ratios are calculated from the medial aspect of the corpus 69

2-3 FE Material properties assignment.....70

2-4 Effect of nodal constraint on principal strain values. Principal strains and the principal strain ratios are calculated from the lateral aspect of the corpus.. 71

2-5 Effect of nodal constraint on principal strain values. Principal strains and the principal strain ratios are calculated from the medial aspect of the corpus 71

2-6 Influence of force orientation on principal strain values. Principal strains and the principal strain ratios are calculated from the lateral aspect of the corpus 72

2-7 Influence of force orientation on principal strain values. Principal strains and the principal strain ratios are calculated from the medial aspect of the corpus. 73

2-8 Influence of the degrees of freedom on principal strain values. Principal strains and the principal strain ratios are calculated from the lateral aspect of the corpus..73

2-9 Influence of the degrees of freedom on principal strain values. Principal strains and the principal strain ratios are calculated from the medial aspect of the corpus. 74

2-10 Influence of material properties assignment on principal strain values. Principal strains and the principal strain ratios are calculated from the lateral aspect of the corpus.. 75

2-11 Influence of material properties assignment on principal strain values. Principal strains and the principal strain ratios are calculated from the medial aspect of the corpus.. 76

3-1 Regional cortical thickness for macaque jaws 129

3-2 Mastication model. SED, maximum and minimum principal strain and cortical thickness data for lateral midcorpus region....129

3-3 Mastication model. SED, maximum and minimum principal strain and cortical thickness data for basal region. 130

3-4 Mastication model. Sed, maximum and minimum princpal strain and cortical thickness data for medial midcorpus. 130

3-5 Clench model. SED, maximum and minimum principal strain and cortical thickness data for lateral midcorpus region....131

3-6 Clench model. SED, maximum and minimum principal strain and cortical thickness data for basal region. 131

3-7 Clench model. SED, maximum and minimum principal strain and cortical thickness data for medial midcorpus region. 132

3-8 SED and principal strain values for mastication and clench models when one or more vectors are used to simulate the masseter-pterygoid sling load. The values are reported for the lateral midcorpus.. 132

3-9 SED and principal strain values for mastication and clench models when one or more vectors are used to simulate the masseter-pterygoid sling load. The values are reported for the medial midcorpus.. 133

3-10 Cortical thickness comparison for the lateral midcorpus region. 133

3-11 Cortical thickness comparison for the medial midcorpus region. 134

LIST OF FIGURES

Figure page

1-1 Hierarchical structural organization of bone 32

1-2 Bone section of proximal end of femur 33

1-3 Macro and micro structure of cortical bone 33

1-4 Trabecular bone structure. 34

1-5 A typical stress-strain curve: elastic region, yield point, plastic region, fracture.. ..34

1-6 Lateral view of a mandible 35

1-7 Distribution of the cortical and trabecular bone in a mandible 35

1-8 The four muscles involved in mastication. 36

1-9 Gupta and Knoell model: mathematical model of mandible. 36

1-10 Hart model: mandible model developed by reconstruction from CT scans. 37

1-11 Korioth mandible model. 38

1-12 Vollmer mandible model. 38

1-13 Physiologic and pathologic strain levels. 39

2-1 Photoelastic method.. 77

2-2 Rectangular rosette strain gauge. 77

2-3 *Macaca fascicularis* specimen. 78

2-4 Experimental strain analysis—lateral strain gauge.. 78

2-5 Experimental data variation. 79

2-6 Digitized CT cross sections. 80

2-7 Geometric mandible model 80

2-8 FE mandible models: dentate and edentulous FE models. 80
2-9 Prediction of surface strains from the FE dentate model. 81
2-10 Variation in the number of constrained nodes in finite element models. 81
2-11 Relaxing boundary conditions by reducing the degrees of freedom. 82
2-12 Alteration of direction of the applied force. 82
2-13 Heterogeneous transverse isotropic model showing specification of local material axes for three regions 83
2-14 Convergence test. 83
2-15 Method to record principal strain values. 84
2-16 Effect of nodal constraint on predicted maximum principal strain values 84
3-1 Mandibular cross-sections. 135
3-2 Calculated lazy zone interval. 136
3-3 The masseter-pterygoid sling and the temporalis muscles simulation. 136
3-4 Mandible model subjected to combined loading 137
3-5 Mandibular sections. 137
3-6 SED and thickness data for various mandibular regions 138
3-7 SED profile along midcorpus 139
3-8 Regional SED values for the mastication model. 140
3-9 Regional SED values for the clench model. 141
3-10 Regional SED values and the calculated lazy zone interval 142
3-11 Principal strain ratio and thickness data for various mandibular regions 143
3-12 Regional principal strain values for the mastication model. 144
3-13 Regional strain values for the clench model. 145
3-14 Regional strain values and the lazy zone interval. 146
3-15 Principal strain profiles in mandibular cross-sections 147
3-16 Cortical thickness comparison. 148

Abstract of Dissertation Presented to the Graduate School
of the University of Florida in Partial Fulfillment of the
Requirements for the Degree of Doctor of Philosophy

FINITE ELEMENT MODELING OF THE ANTHROPOID MANDIBLE:
MANDIBLE MODEL,
EXPERIMENTAL VALIDATION,
AND ANTHROPOLOGIC APPLICATION

By

Ruxandra Cristiana Marinescu Tanasoca

December 6, 2006

Chair: W. Ditto
Major Department: Biomedical Engineering

Finite element modeling (FEM) provides a full-field method for describing the stress and strain environment of the bone. The main objectives of the current study were to create and validate a FE mandible model. The overall goal of the project was to explore the connection between the mandible's morphology and strain history. Experiments established that usually bones respond to mechanical loads imposed on them, but the functional relationship of the mandible is controversial.

Initially, an in vitro strain gauge experiment on a *Macaca fascicularis* mandible was conducted and strain data were recorded. Subsequently, the mandible was scanned and dentate and edentulous models were obtained through volumetric reconstruction from CT scans. Several FE simulations were performed under various conditions of material and structural complexity. The validation of the FE models was achieved by comparing experimental and FE data and using convergence study. In addition, the study offers a

prospective assessment of the difficulties encountered when attempting to validate complex FE models from *in vivo* strain data.

Many functional and nonfunctional theories attempted to explain the fascinating mandibular morphology. However, the justification for the asymmetrical distribution of bone is still ambiguous. The previous modeling efforts are improved by simulating the masticatory muscles. Strain interval and strain energy density (SED) criterion are used to evaluate the functional adaptation process and to predict variations in the mandibular bone mass (thickness) when the mandible is subjected to combined loading.

The results suggest that strain and SED do not consistently correlate with bone mass (thickness) variation. According with the mechanostat model, the goal of bone is to maintain strain within a physiologic strain range or equilibrium interval. The "equilibrium" proposed by the mechanostat model seems to fit the mandibular strains. However, only 50% of the SED values are within the equilibrium interval. In addition, the results reject a null hypothesis of uniform SEDs everywhere, which is the implicit assumption underlying Wolff's Law.

CHAPTER 1
INTRODUCTION

The mandible is characterized by a very odd and fascinating geometry, and it has attracted much attention due to its complexity. The bone is distributed asymmetrically in the mandible. The mandibular thickness varies significantly throughout the entire mandible and significant differences exist between lower (basal) or upper (alveolar) regions, anterior (symphysis) or posterior (molar) region, and medial (lingual) or lateral (buccal) aspects of the mandibular corpus. The mandibular cross-section is asymmetrical, and presents considerable geometric dissimilarity between the lingual and lateral aspects of the corpus. In macaques, the mandibular thickness is greatest along the lingual aspect at the symphysis (Daegling 1993). However, in the molar region, the lingual aspect of the corpus is thinner than the lateral aspect. Especially at midcorpus, the mandibular bone is thicker on the lateral aspect than on the lingual aspect. Under the premolars, the thin lingual bone is much less apparent. Experimental studies showed that not only the geometrical properties but also the mechanical properties differ considerably throughout the mandible. The mandible is very stiff in the longitudinal direction and usually stiffer on the medial aspect than on the lateral aspect.

The mandible is the largest mobile bone of the skull and thus it plays a major role in mastication. The alveolar bone present in the mandible provides support and protection for the teeth. Because of the insertion of the lower teeth in the mandibular bone, the mandible plays an important role in feeding and mastication. The primary activities of the

mandible include elevation (jaw closing), depression (jaw opening) and protrusion (jaw protruding forward).

Despite extensive research on the morphology of the mandible, mastication system and profiles of stress and strain, the justification for this unique, asymmetrical distribution of cortical bone is still ambiguous. A direct relationship among mandible form and function, although crucial from a biomechanical point of view, has been often assumed but has never been established. Understanding the functional morphology of the mandible is critical for uncovering the evolutionary transformations in facial bones form and expanding our knowledge of primate origin.

Why is the mandibular bone distributed asymmetrically? Numerous functional and nonfunctional explanations have been presented over the years, but currently there is no consensus regarding the mandibular asymmetry and the unusual bone tissue distribution in the mandible.

The underlying assumption in the functional explanations is that a functional link between the morphology of the mandible and the masticatory forces to which the mandible is subjected during mastication exists, and thus, the unusual bone distribution can be explained in biomechanical terms. Hylander (1979a) proposed that the morphology of the mandible is an adaptation to countering mastication forces and consequently, there is a functional correlation between the morphology and function of the mandible. The mandible is vertically deep in the molar region to counter bending stress during unilateral mastication and transversely thick in the molar region to counter torsion about the long axis. In 1984, Demes et al. (1984) proposed a theory according to which the mandible unusual form could be explained by the mandibular function. Demes

et al. used shear and bending moment diagrams to prove their theory. The mandible is vertically deep to counter the bending stress and transversely thick to counter the added effects of torsion and direct shear. Moreover, shearing and torsional stresses add up on the lateral side and are subtracted on the lingual aspect of the mandible which correlates with the mandibular corpus being thicker on the lateral aspect and thinner on the lingual aspect. Daegling and Hotzman (2003) performed several in vitro experimental strain analyses on human mandibles by superposing torsional and occlusal loads to test Demes et al. theory. The study partially supported the theory and showed that the lingual strains are indeed diminished and the lateral basal corpus strains are increased when the mandible is subjected to combined loading. However, the authors obtained different results for the midcorpus and alveolar aspects of the mandible. Various other researchers supported the hypothesis according to which the facial bones are especially optimized for countering and dissipating mastication forces. In 1985, Russell proposed a novel theory for that time regarding the morphology of the facial bones. The author postulated that the stress obtained from chewing hard food leads to developing more pronounced supraorbital region.

Research shows that the mandible morphology can be related to dietary specialization. Consistency of food could significantly affect the strain gradients in the mandible during mastication and ultimately alter the anatomy of the mandible. In a study performed by Bouvier and Hylander (1981), hard-diet monkeys exhibited higher mandibular bone remodeling in their mandibles than soft-diet monkeys. Moreover, the hard—diet monkeys had deeper mandibles, probably due to the higher stress levels that occur during mastication of hard foods. However, other studies brought contradictory

evidence and showed that the mandibular morphology does not reflect differences in diet for all primate species (Daegling and McGraw 2001). Other studies examined the influence of diet on the material properties of the mandible. Soft diet (decreased mechanical loading on the mandible) affected the density of the bone and the bone mass (Kiliaridis et al. 1996). Other studies are concerned with the change in material properties of the mandibular bone after loss of teeth (Giesen et al. 2003). The conclusion of the study was that reduced mechanical load decreases the density, stiffness, and strength of the mandibular bone.

Another factor related to mastication and believed to significantly impact the mandible morphology is the fatigue strength of bone. Various primates spend a great amount of time chewing food. The number of chewing cycles could be as high as 51,000 bites per day (Hylander 1979a). The structure of the mandible needs to be adapted to withstand such prolonged, repetitive cyclical loads. Hylander assumed that the increased depth of the jaw, characteristic for primates whose diet consists of leaves, could be explained as an adaptation to counter repetitive cyclical loads.

Not only the frequency and the magnitude of the masticatory forces, but also the location of the masticatory forces could affect the mandible's anatomy and trigger the asymmetrical distribution of bone. During incisal biting or unilateral mastication in macaques, the load is positioned asymmetrically, lateral to the long axis of the mandibular corpus (Hylander 1979a). The lower border of the mandible, the mandibular base, is everted while the upper border, the alveolar process, is inverted. The asymmetrically applied load will produce locally a certain deformation in the bone. The

amount of stress and strain produced will therefore be distributed asymmetrically in the mandibular bone.

The direction of the applied load could play an important role in development of bone asymmetry. Experimental work showed that mastication force is not applied vertically, perpendicular on the mandible. Usually the mastication force is inclined laterally, up to 15° from the vertical plane (Daegling and Hotzman 2003). Depending on how the load is applied, different stress gradients will affect the mandible's structure and trigger bone modeling and remodeling activities. In agreement with other studies, the resulting difference in stress distribution between the lateral or medial aspects of the same mandibular corpus or between the left mandibular corpus and right mandibular corpus, due to asymmetrical distribution of mastication loads, is the main cause for the development of mandibular asymmetry (Ueki et al. 2005).

Nonfunctional theories presume that the mastication forces are not functionally linked to the mandible's morphology and in fact, the mandibular structure could be the result of genetic determinants or numerous non-mechanical factors that occurred during evolution (Knoell 1977, Ward 1991). Their conclusions are based on the fact that large stress values were collected from mandibular regions characterized by thin and porous bone tissue. The studies questioned the biomechanical significance of mandibular structure and advanced the hypothesis that the mandible could be in fact "overdesigned." One of the non-functional theories which tried to explain the asymmetry is that the mandibular corpus is deep and thick to accommodate large teeth, more specifically their long roots (Hylander 1988). However, this theory was not accepted as the roots do not extend all the way down to the mandibular base. Many studies show that there is actually

no relationship among the mandibular corpus dimensions and teeth size (Daegling and Grine 1991).

Many researchers challenge the functional correlation theory based on experimental bone strain data. A large body of experimental work proves that the facial bones and mandibular bone, in particular, exhibit a totally different behavior than expected. Facial bones do not exhibit maximum strength with minimum material. Hylander et al. (1991) explored the functional significance of well-developed browridges in of Macaca fascicularis using strain gauges. The strains recorded were very low. Many other studies showed that bone strain values collected for various "robust" facial bones during mastication, including the mandible, were very low and they suggested that facial bones could be overdesigned for feeding (Hylander 1979b, 1984, Daegling 1993, Daegling and Hotzman 2003, Hylander and Johnson 1997, Fütterling et al. 1998, Dechow and Hylander 2000). This body of research does not support the theory according to which the facial bones are properly adapted to counter mastication forces. The facial bones could be "robust" to withstand forces experienced during traumatic blows to the head. Perhaps the size of some bones, such as the enlarged browridge, is primarily the result of genetic factors.

As can be seen, there are many theories proposed that could offer non-mechanical or functional explanations, but there is no consensus concerning the unusual morphology of the mandible and the mandible's structural asymmetry. Thus, one of the most essential questions concerning the mandible's morphology still remains unanswered. The objectives of the present study were to use FEA to create and validate a mandible FE model and then to use the model to explore the cortical asymmetry concept. Two primary

sub-problems will be addressed. First, does the transverse thickness of bone at various locations have a predictable relationship to strain energy density (SED) and strain values, and second, if the equilibrium that ought to exist under the mechanostat model fit the mandibular strains and SED.

The main contribution of this dissertation is the development of a validated mandible model using Finite Element Analysis (FEA). Experimental methods are considered limited field methods. Due to spatial limitations, the mandible is usually analyzed only in certain regions "of interest." The loading environment cannot be controlled in an in vivo experiment. The physiologic loading environment is very difficult to recreate in an in vitro experiment. Furthermore, strain gradients could be obtained only from a few sites "of interests." Finite element analysis is successfully used in biomechanical studies because it offers many advantages over the limited field methods: the load magnitude and the loading environment can be controlled during the analysis; the stress and strain results can be obtained inside and throughout the model, not just in some regions of interest. Finite element analysis predicts regions with maximum stress and/or maximum strain values, provides quick and accurate results for any large and complex structures, and allows optimization and numerous simulations.

An in vitro strain gage experiment was performed on a fresh *Macaca fascicularis* mandible. During the experiment, the mandible was constrained bilaterally at the condyles and angle, and an occlusal load was applied on the left incisor. Experimental strain data were recorded from the specimen. The mandible was then scanned in sagittal planes and 90 computed tomography (CT) sections were obtained. A FE model of the mandible was obtained through volumetric reconstruction from the CT scans. Because

the model is reconstructed from CT scans, a very accurate mandible model was obtained which reflected in great detail the size and shape of the real mandible. Two mandible models were developed, a dentate and an edentulous model. FE analyses were performed using different boundary conditions and assignment of spatial variation (homogeneity vs. heterogeneity) and directional dependence (isotropy vs. orthotropy) of elastic properties in both dentate and edentulous models. Thus, the model developed exhibited not only very accurate geometrical properties but also complex, realistic mechanical properties. Validation of the models was achieved by comparing data obtained from the experimental and FE analyses and convergence studies. In this dissertation, the validated FE mandible models provide an excellent testing tool for performing full-field analysis that cannot be performed using conventional testing methods.

The second significant contribution of this dissertation is successfully using the validated mandible model to address issues that have been the source of scientific controversy in physical anthropology and bioengineering, and to bring light on a fundamental biological problem. A novel approach to investigate the mandible's morphology is presented in this study: SED and principal strain values are correlated with bone mass (thickness) variation.

This dissertation will be organized into four chapters. Chapter 1 is the introduction and presents the background of the study, the research problem and information about mandible's form and function. Chapter 2 presents the development and validation of the FE mandible models. Chapter 3 describes how the model was used to explore an anthropological problem. The conclusions of the study will be presented in Chapter 4.

Bone Structure

The skeletal system consists of bones, cartilage, ligaments and tendons. The skeleton has multiple functions: to offer support for the body and protection of soft parts, to produce body movement, to store and release minerals when needed, to produce blood cells (in the red marrow), etc. The bone consists of 65% mineral and 35% organic matrix, cells and water (Cowin 2001). The cells are embedded within the organic matrix, which consists mostly of collagen fibers. Collagen fibers are responsible for flexibility in bones. The mineral part of the bone consists of hydroxyapatite crystals in forms of rods or plates.

The bone structure is usually described using hierarchical levels. Each hierarchical level has a particular structure and mechanical properties imposed by that structure. One of the most comprehensive studies regarding bone structure was proposed by Rho et al. (1998) (Figure 1-1). The levels of hierarchical structural organization proposed by Rho et al. are:

- The macrostructure (trabecular and cortical bone)
- The microstructure (osteons, trabeculae)
- The sub—microstructure (lamellae)
- The nanostructure (fibrillar collagen and embedded mineral)
- The sub—nanostructure (mineral, collagen, non—collagenous organic proteins)

Bones can be classified according to their size and shape, position and structure. Based on their shape, bones can be flat, tubular or irregular. According to their size bones can be classified as long and short bones (Yang and Damron 2002). Based on matrix arrangement, bone tissue can be classified as lamellar bone (secondary bone tissue) characterized by lamellae arranged parallel to each other and woven bone (primary bone tissue) characterized by collagen fibers arranged in irregular arrays. Depending on the

relative density of the tissue present in the bones, there are two types of bone: cortical (also called Haversian or compact bone) and trabecular (also called spongy or cancellous bone) (Hayes and Bouxsein 1997) (Figure 1-2).

Cortical Bone

The cortical bone is the stronger, less porous outer layer of a bone and it is found predominantly in long bones. It accounts for approximately 80% of the skeletal mass (Cowin 2001). The cortical bone provides mechanical and skeletal strength and protects the internal structures of the bone. The cortical bone consists of osteons, the basic units, which are cylindrical concentric structures, 200μm in diameter that surround neuro-vascular canals called Haversian canals (Martin et al. 1998). The Haversian canal is surrounded by lamellae—concentric rings comprising a matrix of mineral crystals and collagen fibers. Between the rings of matrix, osteocytes (bone cells) are present, located in spaces called lacunae. Haversian canals, through which nutrients are brought in, contain capillaries and nerves and are approximately 50 μm in diameter. Osteons with the Haversian canals run generally parallel with the longitudinal axis of the bone. Volkmann's canals are another type of neuro-vascular canals. They are transverse canals that connect Haversian canals and they also contain capillaries and nerves (Figure 1-3).

Trabecular Bone

The trabecular bone tissue is a more porous bone tissue that is found usually inside the bones, in cubical and flat bones. The porosity in the trabecular bone is 75%-95% (Martin et al. 1998). Besides providing mechanical and skeletal strength, the trabecular bone has also an important metabolic function. The trabecular bone consists of small plates and rods called trabeculae, usually randomly arranged (Figure 1-4). The individual

trabecula constitutes the actual load-bearing component of the entire structure (Cowin 2001). The trabeculae are very small, approximately 200 μm thick, which makes measuring mechanical properties of trabecular bone very difficult. It is extremely important to determine, for example, trabecular bone strength because trabecular bone tissue can be responsible for bone failure and increased fracture risks.

Mechanical Properties of Bones

Determining the mechanical properties of bones throughout the skeleton is of tremendous practical importance. Known mechanical properties of bones are essential in a variety of fields, from medicine (studying the strength of a bone in the skeleton for selecting a suitable bone grafts or the influence of forces exerted on bone by an implant device) to the automobile or aerospace industry (determining the bone's limit of tolerance to various types of impacts to design protective outfits and equipment) (Evans 1973). The mechanical properties of bone were determined gradually over the years as the research on mechanics of solids developed progressively. One of the first and most important sources of information are the Galileo notes on mechanics (1564-1642). He was among the first to discuss the shape of the bones and the mechanical implication of the geometrical shapes. In 1676, Robert Hooke discovered that force is a linear function of elongation based on experiments with wires and springs and postulated his law of elasticity. In 1729, Pieter Van Musschenbroek, a scientist from the Netherlands, published a book in which he described testing machines for tension, compression, and flexure. In 1807, Thomas Young published *Lectures on Natural Philosophy*. He defined the term "modulus of elasticity" and, through his studies, he greatly contributed to the study of mechanics. The development of these testing tools and laws of mechanics helped

the research on mechanics of bones to expand progressively. In 1892 the Wolff law of bone remodeling was published. Wolff established that bones react to the loads to which they are subjected and adapt accordingly (Martin et al. 1998). In 1917, Koch published *The Laws of Bone Architecture* in which he defined the laws of mechanics and applied them in studying the bone (human femur).

The use of animals in orthopedic research had a great role during the years in helping to explore the biomechanics of the human bone. Some scientists argue that the bone structure varies greatly from species to species and it is strongly influenced by multiple factors such as age, level of activity and disease. However, many animal studies are done today because of multiple similarities between the human and the animal mechanical properties of the bone (Dechow and Hylander 2000). The animal studies have the advantages that the specimens are smaller, easy to control and less expensive. Moreover, the process involves fewer ethical concerns.

Depending on the purpose of the orthopedic research, an appropriate animal model should be carefully selected. For example, the dog model is usually used in studying the spinal fusion, the bovine model for studying long bones, rat model for studying effects of aging, etc. (Liebschner 2004). For studying the mandible, canine or monkey models are regularly used (Ashman et al. 1985, Hylander 1986, Nail et al. 1989, Dechow and Hylander 2000). Monkey models are most often used because of similarities in anatomy and physiology between monkeys and humans. The macaque model is an excellent model for studying mastication because of abundant available data. There are other reasons for which monkeys were chosen for research: handling is easily done in the lab, the models are smaller and simpler, less expensive, etc.

Measuring the Mechanical Properties of Bone

The orthopedic research on determining the bone mechanical properties is an ongoing process. Many scientists, especially in the last half of the twentieth century, are more and more concerned with how bones should be tested and examined from a mechanical and material point of view (Yamada and Evans 1970, Evans 1973, Martin et al. 1998, Cowin 2001, Currey 2002). Determining mechanical properties is vital for numerous clinical interventions, including dental implants, hip replacement, bone grafting, for preventing and treating bone fractures frequently encountered in various diseases and aging and bone research.

Mechanical Tests

Mechanical tests are usually used to study the mechanical properties of the bone, tests that are based on the fundamental principles of mechanics. Depending on the type of applied load, the mechanical tests usually performed on a bone are: tension (Kotha and Guzelsu 2003), compression (Carter and Hayes 1977, Hvid et al. 1989, Ciarelli et al. 1991, Giesen et al. 2003), bending (Remmler et al. 1998, Lettry et al. 2003) and torsion (Taylor et al. 2003). A mechanical testing machine is used to apply different loads to bone specimens. By determining the relationship among applied load and displacement, mechanical tests provide information about the integrity of the bone, the stiffness of the structure, maximum force at failure and maximum energy required to break the bone. When load is transformed into stress and displacement converted into strain, the stress-strain curve can be obtained (Figure 1-5). Other important biomechanical parameters can be determined using the stress-strain curve. The slope of the stress-strain curve, the elastic modulus, gives information about the bone stiffness. Other measurable biomechanical parameters are: the maximum stress or the ultimate strength, the

maximum or the ultimate strain, the energy required to fracture the bone and the yield point (Cowin 2001).

In Vitro or in Vivo Strain Gage Measurements

The material properties of the cortical mandibular bone can be determined from in vitro or in vivo strain gage measurements (Carter et al. 1981). In vivo strain gage measurements are performed on animal subjects (dogs, monkeys) who were previously sedated while strain gauges were inserted through small surgical incisions and bonded on the bone (Hylander 1986, Dechow and Hylander 2000, Coleman et al. 2002). Rosette strain gage are glued to the bone and bone surface strains are recorded while a certain activity of interest is performed (chewing, biting, walking, etc.). In the study performed by Dechow and Hylander (2000), a monkey is sedated and a surgical incision is performed along the lower border of the mandible. The strain gages are applied on the cortical surface of the mandible. The subject is fed and strain data is recorded. For in vitro strain gage measurements, strain data is obtained by mechanically testing the bone on which strain gages were glued previously (Dally and Riley 1991). In vitro strain gage measurements are used generally for studying the biomechanics of the bone and can be successfully performed on almost any type of bone: mandible (Knoell 1977, Vollmer et al. 2000), skull (Evans 1957), femur (Lengsfeld et al. 1998), ulna (Lee et al. 2002), pelvic bone (Dalstra et al. 1995), vertebra (Guo et al. 2002).

Ultrasonic Pulse Transmission Technique

Elastic moduli, shear moduli and Poisson's ratio of bones can be determined successfully using an ultrasonic pulse transmission technique, by measuring the ultrasonic velocities (Ashman and Van Buskirk 1987, Rho et al. 1995, Schwartz-Dabney and Dechow 2003). The ultrasonic pulse transmission technique consists in passing an

ultrasonic wave through a bone specimen. A pulse generator is used and ultrasonic waves are recorded. The time delay between the transmitted and the received waves is determined. Studies performed on mandibles using ultrasonic pulse transmission techniques, showed that the mandibular bone is anisotropic. However, an orthotropic mandibular structure is considered a "reasonable simplification", with the stiffest axis being along the longitudinal direction of the bone (Dechow and Hylander 2000). Significant differences were found between elastic modulus values function of the direction and the lingual or buccal portion of the mandible. The cortical bone was stiffer in the longitudinal axis of the mandible and on the lingual area. There is not enough available data about the mandibular trabecular bone mainly due to the difficulty of analyzing it. The specimens are usually small and the trabecular portion in their mandible is very friable and has a reduced thickness.

Microindentation and Nanoindentation Tests

Microindentation and nanoindentation tests are used to measure the hardness of bone tissue. The hardness is obtained by measuring the size of the indentation made by a diamond indenter. The indenter is pressed with a small known load into the bone tissue. Microindentation gives spatial resolution from 30 to 100μm. Nanoindentation provides spatial resolution from 1 to 5μm (Cowin 2001). Important mechanical properties as microhardness or elastic modulus can be successfully determined using indentation tests (Hengsberger et al. 2003).

Computed Tomography Method

Noninvasive methods could also be used in analyzing the bones-for example determining mechanical properties through computed tomography (Snyder and Schneider

1991, Rho et al. 1995, Vollmer et al. 2000, Lettry et al. 2003). The method is based on predicting mechanical properties (elastic modulus) from density and CT numbers. The results of the studies performed on mandibles indicate that CT numbers may be successfully used in predicting mechanical properties of the mandibular bone (Vollmer et al. 2000, Lettry et al. 2003). Some studies investigated the anisotropy of the trabecular bone in the proximal humerus and the proximal femur of *Macaca* using the micro-CT analysis but data on the mandibular trabecular bone of *Macaca* it has yet to be collected (Fajardo and Muller 2001) (Table 1-1).

Measurements of the Elastic Modulus of Bones

One of the major limitations in creating a bone model is choosing the appropriate material properties. Despite extensive research, the actual mechanical properties of bone are largely unknown. Assigning elastic properties of bone (Young's modulus, shear modulus and Poisson's ratio) to a bone model presents a significant challenge due to the bone structural complexity. Usually the mechanical properties of the cortical bone are extracted from tibial or femoral diaphyses and from vertebral bodies for the trabecular bone (Carter and Spengler 1978, Van Buskirk and Ashman 1981). Using compression and tension tests, Reilly et al. (1974) reported the elastic moduli for human femur in the range of 17.1 ± 3.15 GPa, for bovine femur in the range of 23.9 ± 5.57 GPa and for bovine tibia in the range of 21.2 ± 4.15 GPa. Bonfield and Datta (1974) used two different microstrain measuring techniques for determining the elastic modulus of bovine tibia. They reported the elastic modulus of bovine tibia in the range of 22.5 - 30.0 GPa.

The microscopic properties of human cortical and trabecular bone have been well documented by Rho and his colleagues. Rho et al. (1997) observed that significant

variations in elastic modulus may exist between microstructural components of the bone (single osteons, thin cortical shell, etc.) and dense cortical bone. Rho et al. used nanoindentation to determine the material properties of bone's microstructural components. The elastic modulus for human tibia for the osteons was found to be 22.5 ± 1.3 GPa and 25.8± 0.7 GPa for the interstitial lamellae. The average elastic modulus for human vertebral trabeculae was found to be 13.5 ± 2.0 GPa. Later, Rho and his colleagues investigated the possible variations in the individual lamellar properties within osteons of the human femur using nanoindentation (Rho et al. 1999). They showed significant differences between elastic modulus values obtained from the inner osteonal lamellae (20.8 ± 1.3 GPa) and from outermost osteonal lamellae (18.8 ± 1.0 GPa).

Mandible

The mandible is the inferior maxillary bone, the largest mobile part of the skull. It is the largest and the strongest bone of the face (Gray 2000). The mandible provides support and protection for the mouth, and because of the insertion of the lower teeth in the mandibular bone, it plays an important role in feeding and mastication (Figure 1-6). The mandible has three principal parts: a horizontal curved part called the body (corpus) of the mandible and two vertical parts called the rami. The body of the mandible has a horseshoe shape and can be divided in an upper portion, near the teeth, called the alveolar process (supports the teeth), and a lower portion, near the base of the mandible, called the inferior or basal corpus. The alveolar border has many cavities for the insertion of the teeth. The basal border consists of cortical bone and it is very strong and much thicker than the alveolar border (Figure 1-7).

The vertical part of the mandible, the ramus, has a rectangular shape and is inserted in the temporo-mandibular joint (TMJ). The upper part of the ramus has two processes, the coronoid process in front and the condylar process in the back, separated by a concavity called the mandibular notch. The posterioinferior margin of the angle of the mandible is called the gonion (Gray 2000). The mandibular canal, the canal traversing the mandible, initiates at the mandibular foramen and continues in the ramus. The mandibular canal passes horizontally in the body of the mandible, below molars (Berkovitz et al. 1988).

The asymmetrical pattern of cortical bone distribution in the mandible is unique. Even more intriguing is that this cortical asymmetry is stereotypical among anthropoid primates regardless of variations in mandible dimensions or dietary preferences (Daegling 2002, Daegling and Hotzman 2003). Considerable differences in cortical bone can be observed between the basal or alveolar regions, symphysis or molar region, and medial or lateral aspects of the mandible. The mandibular thickness varies significantly throughout the mandible (Daegling 1993, Futterling et al. 1998). In *Macaca*, the lingual aspect of the mandibular corpus is thinner than the lateral aspect in the molar region. The distribution of cortical bone changes from the molars toward the symphysis, such that under the premolars the thin lingual bone is much less apparent. The base of the mandibular corpus in the molar region is the thickest part. At midcorpus, the mandibular corpus is thicker on the lateral aspect than on the medial aspect (Daegling 1993).

Masticatory Muscles

There are four muscles involved in mastication: masseter, temporalis, pterygoideus externus and pterygoideus internus (Figure 1-8). The masseter is a large, quadrilateral muscle that originates from the inferior border and medial surface of the zygomatic arch

and has insertion points into the lateral and upper half surface of the ramus and into the lateral surface of the coronoid process of the mandible. The principal role of the masseter muscle is to raise the mandible against the maxilla with a very large force. It also helps with the protrusion and the retrusion of the chin and its side-to-side movements.

The temporalis or the temporal muscle is a broad shaped muscle situated on the lateral side of the skull. The origin of the temporal muscle is on the surface of temporal fascia. The insertion points are on the surface of coronoid process and anterior border of the ramus of the mandible. The temporalis acts along with the medial pterygoid and masseter muscles in closing the mouth, retruding the chin and in side-to-side movements, as grinding and chewing.

The pterygoideus externus, the external pterygoid muscle or the lateral pterygoid muscle is a short muscle with two origin heads. One origin head of the muscle is on the sphenoid bone while the second one is on the lateral pterygoid plate. The insertion point is located on the neck of the mandible and the articular disc. The pterygoideus externus helps to open the mouth, to protrude the chin and also helps in producing side-to-side movements of the mandible.

The pterygoideus internus, the internal pterygoid muscle or the medial pterygoid muscle is a quadrilateral shaped muscle. The two origin points are located on the pterygoid plate and on the tuberosity of the maxilla. The pterygoideus internus is inserted on the medial surface of ramus of mandible. It helps in elevating the mandible, protruding the chin and producing a grinding motion.

Measurements of the Elastic Modulus of the Mandible

Studies addressing the elastic properties of a human mandible indicate that the human mandibular bone is elastically homogeneous but anisotropic. Elastically, it the

mandible seems comparable with a long bone bent into the shape of a horseshoe (Ashman and Buskirk 1987). The mandibular bone is usually considered having orthotropic material properties, i.e. different material properties in 3 different perpendicular directions, having 9 independent constants (Ashman and Buskirk 1987, Dechow et al. 1992) or transversely isotropic material properties, i.e. the same properties in one plane and different properties in the direction normal to this plane, having 5 independent constants (Nail et al. 1989) (Table 1-2).

Dechow and his colleagues investigated the elastic properties of the human mandibular corpus, especially the regional variation in elastic properties between different directions and sites in the mandible (Dechow et al. 1992). By propagating longitudinal and transverse ultrasonic waves through the bone specimens, they studied the regional variations in material properties within the corpus of the mandible and found that the mandibular bone is stiffer and denser in the anterior region of the mandible than in the molar region. The results of their study indicate also that the mandibular bone is orthotropic (Table 1-3).

Another study concerned with the regional distribution of the mechanical properties of human mandible was performed by Lettry et al. (2003). The authors used a three-point bending test to obtained elastic modulus values from different bone specimens. They obtained lower values of elastic modulus than those previously published.

One of the most comprehensive studies investigating the elastic properties of the macaque mandible was the study of Dechow and Hylander (2000). Using an ultrasonic technique, Dechow and Hylander measured the elastic, shear moduli and Poisson's ratios in 12 macaque mandibles (buccal and lingual sites). The conclusion of the study is that

the elastic properties of the macaque mandible are very similar with those of human mandible. The macaque mandible is stiffer in the longitudinal direction, less stiff in the inferosuperior direction and least stiff in the direction normal to the bone's surface. As in the human mandible, the lingual aspect of the macaque mandible is stiffer than the buccal aspect (Table 1-4).

State of the Art — Mandible Models

Methods of Model Building

There are mainly two methods available for creating a virtual model: designing the model by using the dimensions of the bone (the indirect methods) or performing reconstruction from images or points (the direct methods). The geometry of the model can be reconstructed from CT scans (geometry or voxel-based reconstruction) or from a three dimensional cloud of points. Reconstruction from CT scans usually generates an improved virtual model because simplifying assumptions of geometry are avoided (Futterling et al. 1998, Hart and Thongpreda 1988, Hart et al. 1992, Hollister et al. 1994, Keyak et al. 1990, Korioth et al. 1992, Lengsfeld et al. 1998, van Rietbergen et al. 1995, Vollmer et al. 2000). Obtaining geometry by CT is the preferred method since it offers more accuracy than reconstructions based on planar radiographs. The advantage of CT scanning is that it gathers multiple images of the object from different angles and then combines them together to obtain a series of cross-sections.

A virtual model can be obtained using a computer-aided design system (CAD). The measurements of a real bone are used to build a virtual, mathematical bone model. Usually the bone (a mandible) is cut into many slices and data from each slice is recorded and used in building the virtual bone model. The model obtained in this way is in fact an idealized model, an approximation of the real object. This was mainly a method used

when finite element was at the beginning, when, because of the software limitations, virtual models were very difficult to obtain (Gupta et al. 1973, Knoell 1977, Meijer et al. 1993).

Reconstruction from CT scans usually gives a better virtual model because the geometry and shape of the real model are preserved. Reconstruction from CT scans can be performed using a geometry-based approach or a voxel-based one. Geometry-based reconstruction is performed in several stages: first, the CT scans of the bone (mandible) are obtained, then each cross section is digitized (contours or outlines are obtained) using a reconstruction software or an edge detection algorithm (Hart and Thongpreda 1988, Hart et al. 1992, Lengsfeld et al. 1998, Korioth et al. 1992). The volume is built as a stack from all the contours previously obtained and used as input in a FE software. The voxel-based reconstruction is performed by subdividing each cross-section in rectangles or squares (Keyak et al. 1990, Hollister et al. 1994, van Rietbergen et al. 1995, Lengsfeld et al. 1998, Futterling et al. 1998, Vollmer et al. 2000). By aligning all the slices, the rectangles or squares will form voxels which in turn will be converted usually in bricks or other 3D finite elements. In this way a voxel-oriented finite element mesh is obtained that preserves the dimensions of the real model and more importantly, the material properties of the original bone. Voxel-based reconstruction takes into account the Hounsfield Units (HU) within each CT slice. The HU from each rectangle or square is averaged and the resulted value assigned to the corresponding voxel. A complex distribution of material properties can be assigned to the virtual bone model. This method is usually performed through a succession of in-house developed applications.

Reconstruction from a cloud of points can be achieved by using a three dimensional digitizer. The real model is scanned with a hand-held digitizer and three-dimensional coordinates from the surface of the model are recorded. The geometry of the original model is reconstructed from the cloud of points obtained. The model is obtained by using a modeling software that does the conversion from the cloud of points to a geometric model. The geometric model is then imported in a finite element package, meshed and analyzed (Lee et al. 2002).

FE Mandible Models

There are a few mandible FE models developed during the years that greatly influenced the work in this field. One of the first mandible models developed 30 years ago, was a half mandible model, symmetric about the symphysis (Gupta et al. 1973) (Figure1-9). The authors attempted to study the stress distribution and the deformation that occur in the mandible during biting. The model was designed from measurements, had limited anatomical description, low number of elements, three materials properties assigned (dentin, alveolar bone, bone mixture).

The Gupta et al. model is still a reference model today because they pioneered how a FE mandible model can be obtained and the idea that such a model can be used for studying the mandibular bone. An improved model was designed four years later (Knoell 1977). The main improvement was the full mandibular dentition. The material properties assigned were accounting for dentin, cortical and trabecular bone. The model was more complex and had 4 times more finite elements.

Another noteworthy model is the 3D FEM developed by Hart and Thongpreda (Hart and Thongpreda 1998). They developed the geometric model through reconstruction from CT scans and converted it into a FEM. The meshing was done using

bricks finite elements. The main purpose of the study was to investigate the relationship among the mandible's form and its function. The model was subjected to a biting force while condyles were held fixed. Two material properties were assigned, for the trabecular and the cortical region. In 1992, Hart et al. presented an improved, more complex mandible model, and this is probably one of the most comprehensive mandible studies in this field (Figure 1-10). The study shows the patterns of strain in the mandible when subjected to occlusal forces. Five models with increasing number of nodes and elements were analyzed. In this study the method of investigating the mandible biomechanics through FE method is more refined. The author discussed the difficulties in making a mandible model, the weaknesses in the finite element model, the numerous simplifying assumptions that needs to be made, the necessity of convergence tests, etc.

Studies by Korioth et al. (1992) present the complexity of modeling and analyzing a mandible using FEM. Korioth developed one of the most complex finite element mandible models. Various anatomical structures were simulated in great detail such as periodontal ligament and masticatory muscles. Isotropic and orthotropic material properties were assigned to the FE model (Figure1-11).

A more recent study shows that FE model could be a valid, noninvasive approach in investigating the biomechanical behavior of a mandible (Vollmer et al. 2000). The model was obtained through reconstruction from CT images, using the voxel-based approach (Figure 1-12). A good correlation was found between the experimental strain gage data and the strain values resulted from the FEA. In the article, the authors discussed about the multiple difficulties in making a FE mandible model, about the lack

of information about material properties, the uncertainty of load distribution or assigning the proper boundary conditions.

SED and Functional Adaptation

The capability of the living systems to adapt to their surroundings is a process that does not stop to amaze scientists. Functional adaptation is the process which helps a living system to adjust to its changing environment. Usually, the living systems respond to various stimuli (mechanical, chemical, hormonal etc) from their surroundings and adapt accordingly.

Adaptation to Environment

A well-known example of adaptation to environment is the adaptation of respiratory functions of lungs to altitude (Wilson et al. 2002). Another remarkable example of adaptation is the adaptation of living systems to a low temperature environment by reducing the metabolic demand (Johnston 2003). Biological tissues adapt to surroundings very differently, from visible and obvious adaptation — as in adaptation of muscles to intense physical exercises (Blazevich et al. 2003) — to less noticeable transformations as in vascular adaptation (Driessen et al. 2004).

The functional adaptation of bone has been studied a long time but it is still a very controversial issue. It was shown through numerous studies that usually bone adapts itself to exercise, disuse, diet and disease. However there is not always an obvious relationship among the bone's function and its morphology.

One of the most well-known cases of functional adaptation of bone is modification in the bone mass due to high physical training, i.e. increasing the mechanical stimulus will accelerate the bone formation and therefore increasing the bone mass (Pettersson et al. 1999). A very active research area in bone adaptation is the influence of decreased

mechanical loading on the mechanical properties of the bone in limb immobilization after trauma (Ulivieri et al. 1990), extensive bed rest (Bischoff et al. 1999) and long term stay in low gravity (Vico et al. 1998). All these studies show that decreasing the mechanical loading will directly affect the density and the strength of the bone. There are also many conditions that can affect bones and can trigger their functional adaptation. One of the most important is obesity in small kids. Orthopedic prosthesis can also cause bone adaptation, usually with an undesired effect, because they alter the normal stress distribution in bones.

Mechanobiology of Bone

Mechanobiology of bone refer to the regulation of bone adaptation by mechanical forces. Understanding the mechanobiology of bone is important for several reasons. Understanding the bone adaptation is paramount in clinical applications, for treatment and prevention of various bone disease and injuries, bone grafts, implants and reconstructive surgeries. In the mandible's case, understanding the adaptation process is important not only for clinical situations (extractions, edentulation, dental and orthodontic treatment, dental implants) but also for uncovering the factors that determined the current mandibular morphology.

One of the first studies on bone adaptation, published in 1892, is the Wolff's law. Wolff's law states that bones react to the loading environment to which they are subjected and adapt accordingly (Martin et al. 1998). Wolff was among the first scientist to recognize that bones react to the loading environment to which they are subjected. However, the mechanisms responsible for bone adaptation were unknown. Wolff suggested that bone is an optimal structure that exhibit maximum efficiency with minimum mass. In 1917, Koch published an article about the "inner architecture" of the

human bone in which he investigated how the inner structure is adapted to resist to different loads.

In recent years, the Wolff's law was improved and redefined by other scientists. Frost redefined the Wolff's law by studying the adaptation of bone to mechanical usage (Frost 1964, 1986, 1990a,b, 1994). Frost developed mathematical theories, which explain some of the phenomena in bones that could not be explained before. Frost proposed first the mechanostat theory according to which bones adapt to mechanical loads in order to sustain those loads without hurting or breaking (Frost 1998, Schoenau and Frost 2002). Four mechanical usage windows or strain ranges are usually defined: below 50με (disuse characterized by bone loss), between 50-1500με (the adapted window, normal load), 1500-3000με (mild overload characterized by bone gain) and above 4000με (irreversible bone damage) (Figure 1-13) (Frost 1994, Mellal et al. 2004). According to this theory, most of the values are expected to be generally situated in the adapted window range and therefore bone homeostasis is predicted. Homeostasis means that no adaptation will take place, the bone is in an equilibrium state and therefore the strain values should be near uniform throughout the bone. In 1980, Pauwels examined the functional adaptation of bones by emphasizing the "essential characteristics" of the adaptation process, namely "the economy of the material" in the skeleton. He investigated and described limping as a "pure functional" adaptation.

Bouvier and Hylander (1981) performed a study on in macaques to determine the effects of a diet of hard food compared to a diet of soft food. Low levels of remodeling were determined in the mandibles of soft-diet monkeys and as well as large regions of unremodeled bone. Higher mandibular bone remodeling levels were encountered in the

hard-diet monkeys. Moreover, hard-diet monkeys had deeper mandibles. The conclusion of the study was that the mandible adapts itself to higher stress levels associated with the mastication of hard foods.

Later, Bouvier and Hylander (1996) performed another study concerning the distribution of secondary osteonal bone in high- and low-strain regions of the macaque face. Four mature macaques and three immature macaques received fluorescent labels over a period of time to investigate the face remodeling activity. Bone samples were analyzed from the zygomatic arch (high strain region), mandibular corpus (high strain region) and mid-supraorbital bar (low strain region). The study proved that, contrary to expectations, there are not consistent differences in remodeling between low and high levels of strain for the adult Macaca and consequently, there is no direct relationship among remodeling and strain levels. A low rate of remodeling was found in the adult Macaca face. However, the results for the immature macaques were different. The pattern of remodeling was consistent. Moreover, increased remodeling activity was found in the mandibular corpus (high strain region) and lower remodeling activity was found in the mid-supraorbital bar (low strain region). The conclusion of the study was that in the mature macaques mechanical and metabolic factors contribute equally to trigger remodeling, whereas in the immature macaques, mechanical factors are predominantly responsible for remodeling initiation.

Theoretical and experimental studies on the mechanobiology of bone performed by numerous researchers explored the relationship among mechanical stress histories and bone tissues biology (Carter et al. 1981, Lanyon et al. 1982, Rubin and Lanyon 1982, 1985, Rubin 1984, Carter 1987, Frost 1990a,b, Rubin et al. 1994). Lanyon stated in one

of his studies based on his extensive work in the mechanobiology of bone field, that the existence of a relationship among mechanical stress histories and bone tissues biology is undisputed. The nature of this relationship is, however, totally unknown (Lanyon et al. 1982).

For the mandibular bone, this functional relationship is not obvious or undeniable. Even more, the nature of this relationship remains unrevealed. As described previously, studies performed on the facial bones including the mandible show that the morphology of bones of the skull is deeply affected by the mastication forces whereas other studies bring overwhelming evidence that actually there is not a functional correlation between morphology of bones and their mechanical demands.

Strain Energy Density (SED)

The functional adaptation of the mandible is triggered by mechanical or non mechanical stimuli. Today it is accepted that mechanical stimuli govern bone adaptation (Cowin 2001). The most common mechanical stimuli are: strain, stress, strain energy, SED, strain rate and fatigue microdamage. SED has been considered by many researchers a valid stimulus for bone adaptation (Huiskes et al. 1987, Katona et al. 1995, Cowin 2001, Mellal et al. 2004).

Strain energy is the energy stored in the material as a function of deformation of the material. Strain energy can be expressed by the stress (σ) and strain (ε) using the following formula:

$$U = \frac{1}{2}\{\sigma\}\{\varepsilon\}$$

Brown and his colleagues investigated twenty-four mechanical parameters that are related to functional adaptation in bone (Brown et al. 1990). The results of the study

reveal that only four parameters are directly related to adaptation: SED, shear stress and tensile principal stress and strain. Huiskes and his colleagues were among the first to consider SED the main mechanical stimulus instead of strain (Huiskes et al. 1987). They developed an adaptive model and used SED to predict the shape or bone density adaptations. Fyhrie and Carter (1990) developed later another theory using SED as the main stimulus. Their study showed that SED can successfully predict the adaptation activity in the femur.

Since then, SED was successfully used to investigate adaptation in bones (Katona et al. 1995, Turner et al. 1997, Barbier et al. 1998, Cowin 2001, Mellal et al. 2004). A strain energy density criterion was developed in which SED is the main stimulus. The rate of change of apparent density at a particular location in the mandible is described by the following formula:

$$\frac{\partial \rho}{\partial t} = B\left(\frac{u}{\rho} - k\right)$$

where ρ is the apparent density, t is the time, B and k constants that quantify bone gain or loss, and u is the strain energy density. The area, in which no net change of bone density occurs, the zone between bone densification and bone resorption, is the lazy zone.

Theoretical and experimental studies on the mandible seem to convey conflicting conclusions regarding a possible relationship among the strain field and the distribution of bone mass. The current study aims to explore questions related to functional morphology of the mandible, in an attempt to explain patterns of cortical asymmetry. The hypotheses that mandibular thickness is related to SED and strain patterns will be tested.

Table 1-1. Elastic modulus values for trabecular bone (Etrabecular) and cortical bone (Ecortical) for various bone specimens obtained using different testing techniques.*

Bone type	Testing technique	$E_{trabecular}$ (GPa)	$E_{cortical}$ (GPa)
Human iliac crest	Three-point bending	3.81	4.89
Human tibia	Four-point bending	5.72	6.75
Human tibia	Tensile test	10.4	18.6
Human tibia	Ultrasonic test	14.8	20.7
Human vertebra	Nanoindentation	13.4	22.5
Human vertebra	Four-point bending	2.11	2.50
Human femur	Nanoindentation	18.14	20.02
Human femur	Acoustic microscopy	17.50	17.73
Bovine femur	Ultrasonic test	10.9	-
Bovine femur	Tensile test	1.0	18.6
Porcine femur	Microindentation	5.9	11.6
Porcine femur	Nanoindentation	21.5	16.4

*Cowin 2001

Table 1-2. The 9 independent constants for human and canine mandibles determined by Ashman and Buskirk (1987) using an ultrasonic technique.

Elastic coefficients	Human mandible (GPa)	Canine mandible (GPa)
C11	15.9	16.2
C22	18.8	17.1
C33	27.1	15.9
C44	4.63	2.51
C55	4.12	2.73
C66	3.81	2.72
C12	8.33	10.9
C13	9.79	11.5
C23	9.79	11.5

Table 1-3. Elastic moduli of three mandibular sites (symphysis, canine and molar region) for facial and lingual aspect of the mandible. E1 is the modulus found in the direction normal to the surface of the bone, E2 in the direction tangential to the bone surface and E3 in the longitudinal direction. Values are in GPa.*

Elastic Modulus	Symphysis region		Canine region		Molar region	
	facial	lingual	facial	lingual	facial	Lingual
E1	11.3	10.0	10.1	10.3	10.0	10.5
E2	14.9	13.5	14.7	14.2	13.3	13.9
E3	20.5	4.1	24.0	27.0	19.1	19.8

*Dechow et al. 1992

Table 1-4. Comparison between elastic modulus values for human and macaque mandibles. E1 is the elastic modulus in the direction normal to the surface of the bone, E2 is the elastic modulus in the infero-superior direction and E3 is the elastic modulus in the longitudinal direction. Values are in GPa.

Elastic Modulus	Human mandible* (molar region)		Macaque mandible** (molar region)	
	facial	lingual	facial	Lingual
E1	10.0	10.5	9.0	9.3
E2	13.3	13.9	15.9	17.6
E3	19.1	19.8	21.0	23.9

*Dechow et al. 1992, **Dechow and Hylander 2000

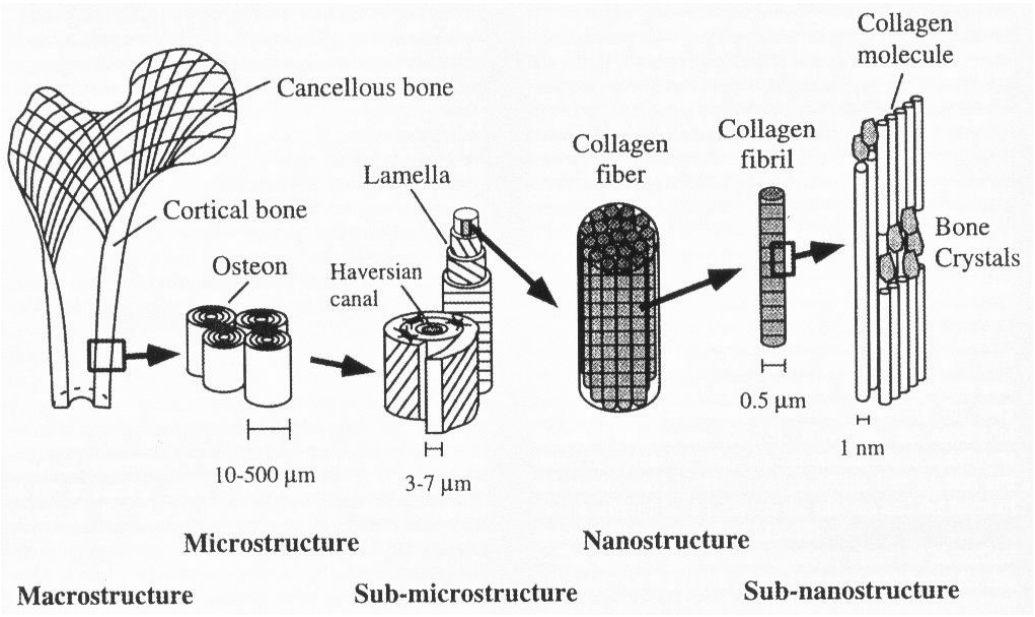

Figure 1-1. Hierarchical structural organization of bone. Taken from: Rho JY, Kuhn-Spearing L, Zioupos P. 1998. Mechanical properties and the hierarchical structure of bone. Med Eng Phys. 20(2):92-102.

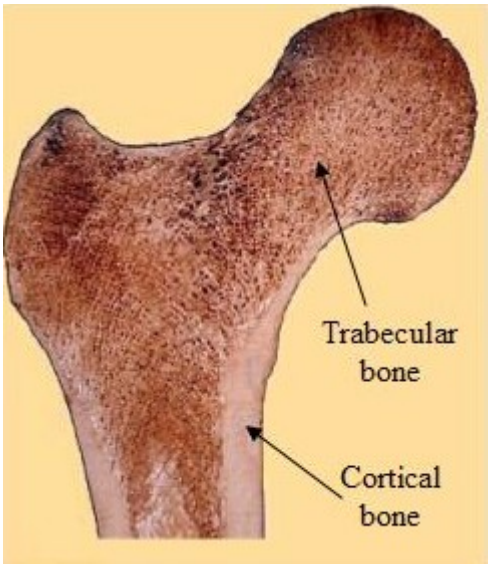

Figure 1-2. Bone section of proximal end of femur. The cortical bone is the outer layer of a bone while the trabecular bone is found usually inside the bones.

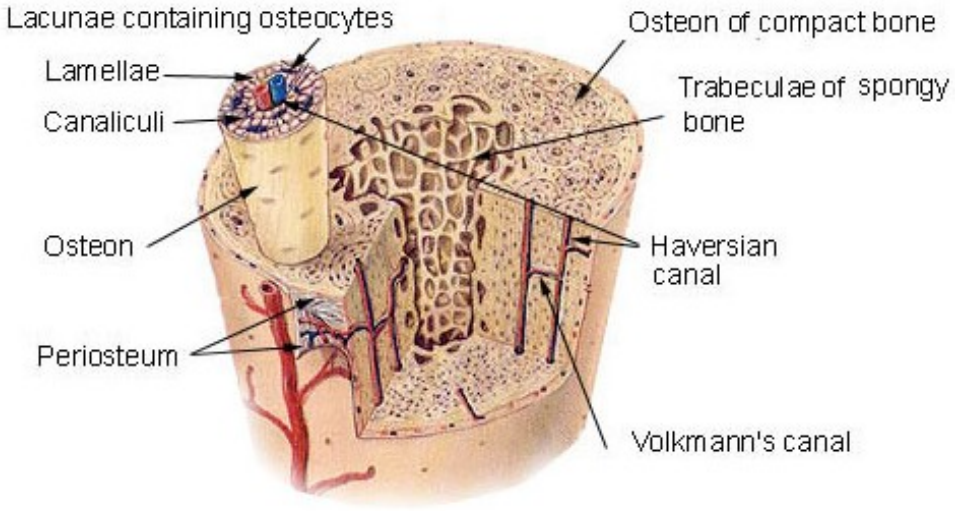

Figure 1-3. Macro and micro structure of cortical bone. Taken from Emory University, Atlanta SEER Cancer Registry, Atlanta, Georgia, U.S.A. (February 12, 2005)

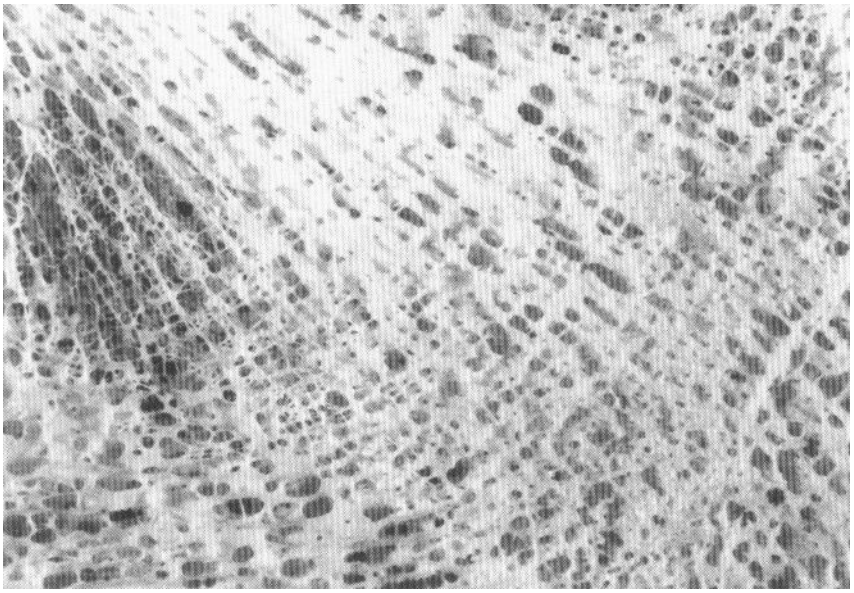

Figure 1-4. Trabecular bone structure. Taken from Martin RB, Burr DB, Sharkey NA, Skeletal Tissue Mechanics, 1998 Springer-Verlag New York, Inc.

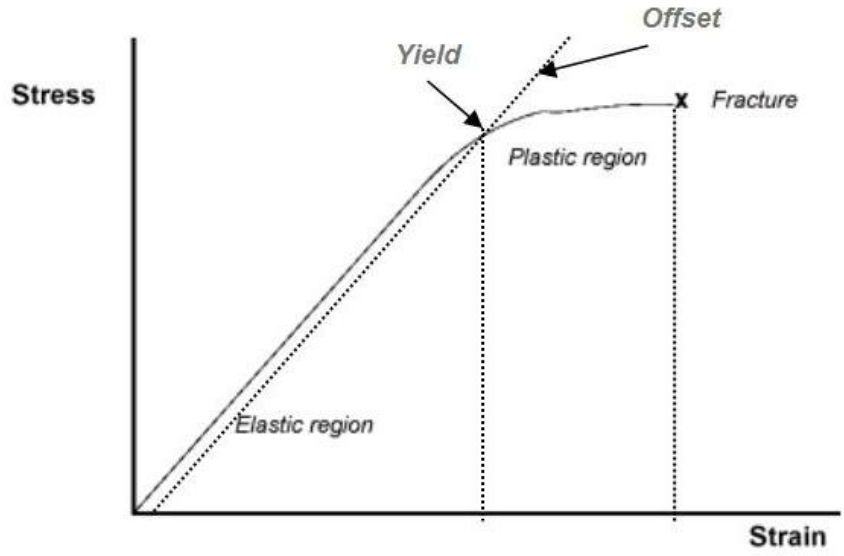

Figure 1-5. A typical stress-strain curve: elastic region, yield point, plastic region, fracture.

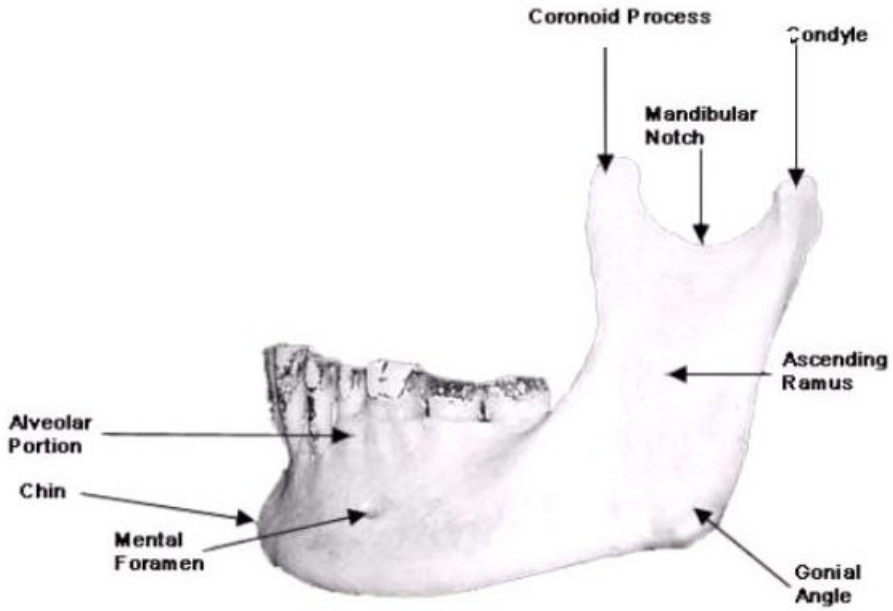

Figure 1-6. Lateral view of a mandible. Adapted image from University of Utah, Salt Lake City, Utah (February 12, 2005) http://medlib.med.utah.edu/kw/osteo/osteology/osteohtm/bonemand.html

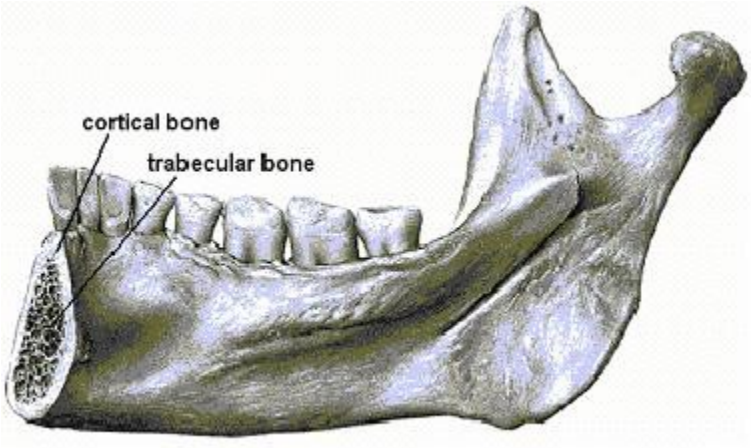

Figure 1-7. Distribution of the cortical and trabecular bone in a mandible. (Adapted image from www.zib.de/SciSoft/kardos/projects/mandible.html)

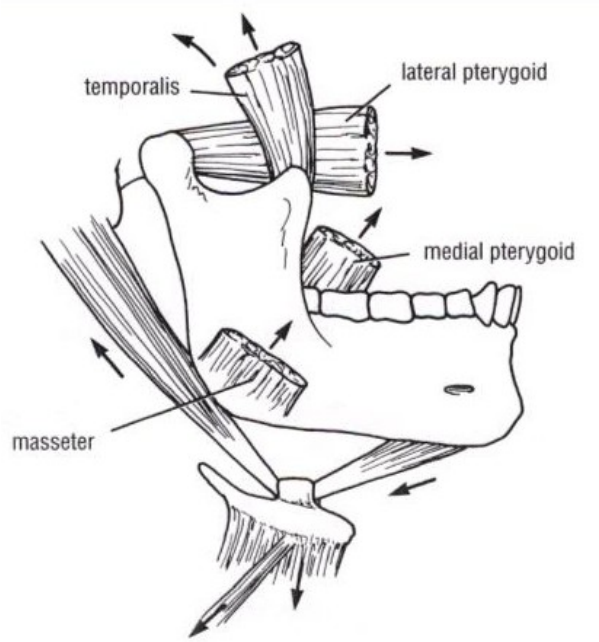

Figure 1-8. The four muscles involved in mastication: masseter, temporalis, lateral pterygoid and internal pterygoid.

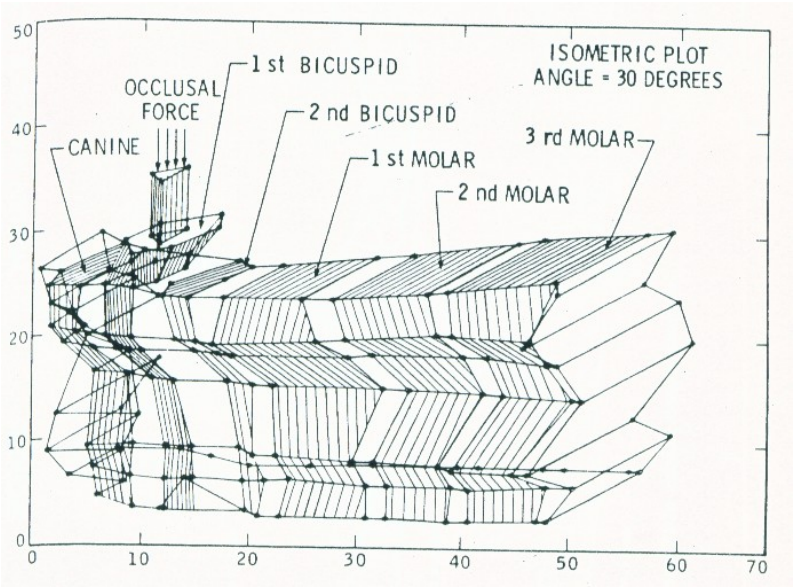

Figure 1-9. Gupta and Knoell model: mathematical model of mandible (Gupta and Knoell 1973).

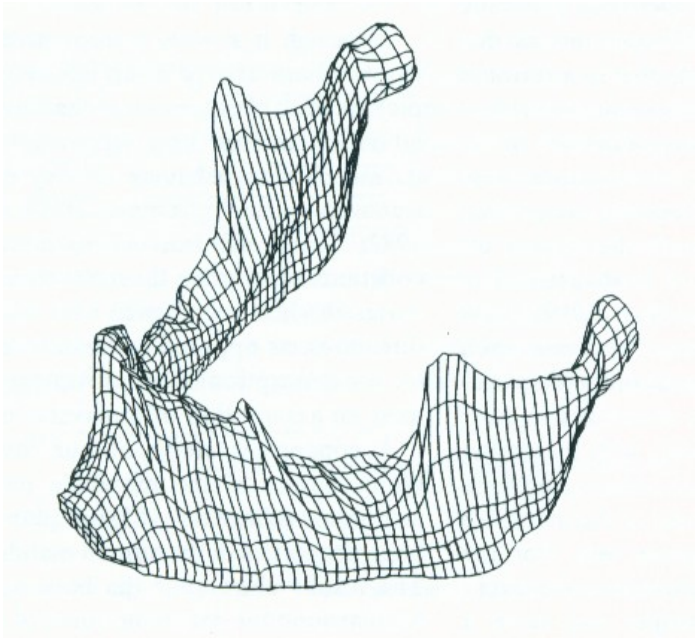

Figure 1-10. Hart model: mandible model developed by reconstruction from CT scans (Hart et al. 1992).

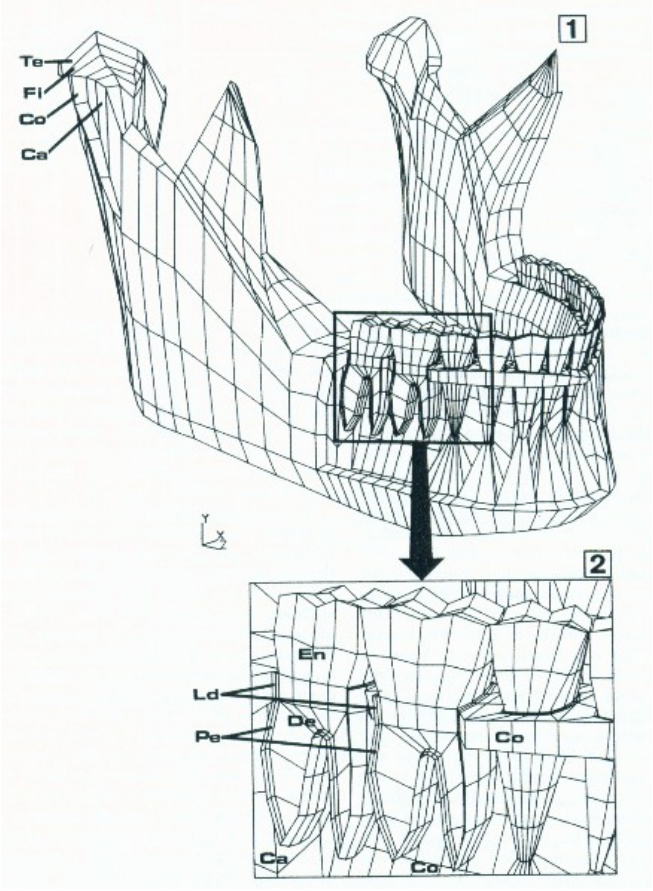

Figure 1-11. Korioth mandible model (Korioth et al. 1992) (1 - right condyle, 2 - corpus, Te - temporal cortical bone; Fi - fibrocartilage; Co - cortical bone; Ca - cancellous bone; En - enamel; De - dentin; Ld - lamina dura; Pe - periodontium).

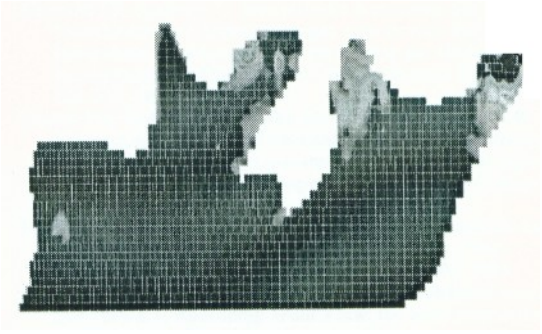

Figure 1-12. Vollmer mandible model: mandible model obtained through reconstruction from CT images, voxel-based approach (Vollmer et al. 2000).

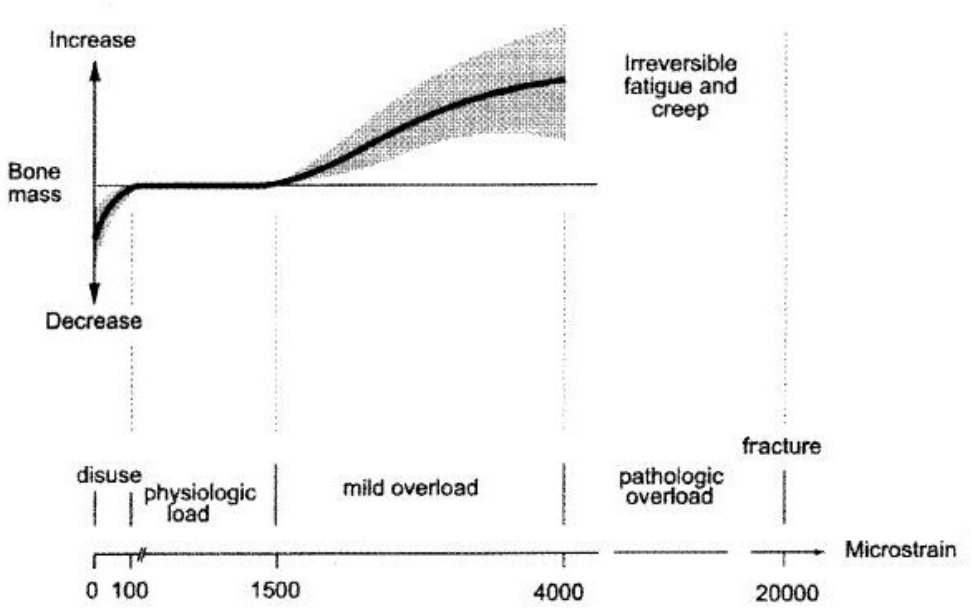

Figure 1-13. Physiologic and pathologic strain levels (Wiskott and Belser 1999).

CHAPTER 2
FINITE ELEMENT MODELING OF THE ANTHROPOID MANDIBLE: MANDIBLE MODEL AND EXPERIMENTAL VALIDATION

Introduction

Finite element analysis (FEA) is the method of choice for theoretical analysis of the mechanical behavior of complex shapes in biology. The FE method approximates real geometry using a large number of smaller simple geometric elements (e.g., triangles, bricks, tetrahedrons). Since complex shapes defy simple mathematical solution (i.e., in terms of engineering formulas), FEA simplifies a problem by analyzing multiple simple elements of known shapes with established mathematical solutions. These multiple solutions are in the end combined together to depict states of stress and strain through the entire structure.

There are many FE studies that investigate the stress-strain behavior of the mandibular bone (Hart and Thongpreda 1988, Hart et al. 1992, Korioth et al. 1992). However, the complex geometry of the mandible, lack of information about material properties, the ambiguity of correct load distribution or assigning the proper boundary conditions make the validation of the FE models very difficult. In this chapter, some of the important issues involved in FE model validation are explored.

The focus in this chapter was on the impact of the decisions that need to be made concerning assignment of material properties and specification of boundary conditions and FE validation. A FE model of a fresh *Macaca fascicularis* mandible was reconstructed from CT scans. Previously, i*n vitro* strain data from the mandible specimen

were recorded under controlled loading conditions. The validation of the FE model was achieved by comparing the strain data obtained from the in vitro experiment with data obtained from the FE analyses and convergence studies. Several simulations are performed to elucidate differences in the model mechanical responses assuming various combinations of heterogeneity-homogeneity and anisotropy-isotropy.

There are several methods to study the stress or strain behavior in a mandible. These can be in vivo or in vitro methods. Many studies present in vitro methods of recording strains because in vivo experiments are much more difficult to perform. The most important methods of recording stresses or strains are: FE method, mathematical method, photoelastic method and strain gauge analysis.

Finite Element Modeling

The basic idea of FE method is that a continuous function can be approximated using a discrete model (Hart et al. 1992, Korioth et al. 1992, Meijer et al. 1993). Therefore, FE method is a very convenient and useful method to study a complex structure such as the mandible. Experimental methods have sometimes limited opportunities to investigate bones with complex morphology. For example, experimental analyses cannot provide enough information abut the stress or strain gradients throughout the mandible. Finite Element Analysis can be successfully used to address these limitations.

Mathematical Method

This method consists of developing a mathematical model of a mandible and analyzing it. The geometry of the mandible can be approximated by a simpler shape, a bar for example, and an approximate stress or strain pattern can be obtained. This method

gives good insight into the overall stress or strain behavior of the mandible but it is not suitable for detailed biomechanical studies (Hylander 1984).

Photoelastic method

Photoelastic resin is used to coat the mandible or to make a resin mandible model (Daegling and Hylander 2000). The coated mandible or the resin mandible model is then analyzed in order to investigate the stress or strain behavior. Another similar method developed to observe the distribution of stress and strain in bones was based on using an aluminum undercoating and a brittle lacquer. The layers were applied with a spray gun and allowed to dry (Figure 2-1). The bone specimen was then tested together with some calibration strips and the cracks pattern was analyzed (Evans 1957). The main disadvantage of this method is that it gives information about the stress or strain environment of a mandible that has different material properties than it should, and consequently, the results are not ideal.

Strain Gauge Analysis

The experimental strain analysis is performed by attaching strain gages on the surface of the mandible, testing the mandible in various loading conditions and recording the surface strains (Figure 2-2). The strain gage experiments can be performed in vivo or in vitro. Both approaches have the major drawback of recording only the strains at the surface of the mandible model. The gage elements A, C are positioned on the mandible according to an x, y axis. The principal strain directions are denoted by x_p and y_p. The surface strains ε_A, ε_B and ε_C are recorded during the experiment. The principal strains (ε_1 and ε_2), the principal direction (φ) and the maximum shear strain (γ_{max}) can be calculated function of the experimental surface strains (ε_A, ε_B, ε_C) using the following relations:

$$\varepsilon_{1,2} = \frac{1}{2}(\varepsilon_A + \varepsilon_C) \pm \frac{1}{2}\sqrt{(\varepsilon_A - \varepsilon_C)^2 + (2\varepsilon_B - \varepsilon_A - \varepsilon_C)^2}$$

$$\varphi = \frac{1}{2}\tan^{-1}\left(\frac{2\varepsilon_B - \varepsilon_A - \varepsilon_C}{\varepsilon_A - \varepsilon_C}\right)$$

$$\gamma_{\max} = \left|\varepsilon_1 - \varepsilon_2\right|$$

FE method was used in this study to investigate the behavior of a mandible. The necessary steps in performing a FEA are: obtaining the FE model, meshing the model, assigning material properties, boundary conditions and analyzing the model. The major challenges in obtaining a FE model are the following:

- *Obtaining accurate geometry of the model.* It is widely appreciated that the geometry of the FE model plays a crucial role in obtaining accurate results. The construction of a FE model proceeds by first obtaining a geometric model and then converting that geometry into a FE model. The geometric model can be obtained through direct or indirect methods; i.e., by reconstruction of a 3D model from a stack of CT scan images or from a cloud of coordinate points or by using the dimensions of the bone to build an approximate model with a computer—aided design system (Gupta et al. 1973, Knoell 1977, Meijer et al. 1993). Building precise geometry is critical for FE model validation.

- *Meshing the model*. A mandible has a very complex shape and therefore the process of finding the right type of FEs (considering also the FE types available in the software used) and meshing the model is a very challenging one. For example, it is well-known that the thickness varies strongly throughout the mandible, which makes the meshing process very difficult and cumbersome, especially in very thin or arched regions.

- *Obtaining detailed information on material properties*. Usually, one or two material properties are assigned in a model. The data is obtained usually from previous mandible studies or from other bone studies (humerus, femur etc). The density and the type of the mandibular bone are changing very much throughout the mandible (Futterling et al. 1998). Generally, for simplification, the material property assigned to the model is an averaged value and consequently, the results will be greatly influenced.

- *Assigning material properties.* This is one of the most important and challenging tasks in obtaining a FE model. The process of assigning material properties to the mandible model depends on the method of obtaining the initial geometric model and on the capabilities of the FE software used. If the model is built using a CAD

system or reconstructed (from CT images, geometry-based approach or cloud of points) the material properties are averaged and assigned to a few mandibular regions. There is a great limitation in the number of materials assigned (usually up to three materials). If the model is obtained through the voxel-based approach, more material properties can be assigned to the model. The material properties are assigned automatically to each voxel according to the density grey level in each CT scan. These properties are then assigned to the FEs. An averaging of data also takes place but overall, the latter method is more successful in assigning material properties.

Materials and Methods

Experimental Strain Analysis

The experimental strain analysis was performed on a fresh mandible of a six-year old adult female macaque. Prior to excision of the mandible, the skull was wrapped in gentamicin-doped saline-soaked gauze and frozen at -20°C. The mandible was thawed and cleaned using conventional techniques (scalpel, scissors) and stored in soaked gauze when not being tested or scanned (Figure 2-3).

One rectangular rosette strain gauge was bonded to the lateral and one to the medial aspect of the mandibular corpus, below the left second molar. Surface bone strain data were obtained from mechanical testing of the mandible. From the raw strain data from the individual gauge elements, principal strain magnitude and direction were calculated. The tests were performed using MTS 858 MiniBionix Test System (Eden Prairie, MN) in displacement mode with a 407 Controller. The steel fixture that restrained the mandible during the procedure was composed from a base that supported the mandible at each angle along its base and a roller which prevented movement at the condyles (Figure 2-4.). The mandible was subjected to a vertical occlusal load (70 N) applied to the left central incisor.

The symmetrical steel fixture did not constrain the mandible completely during the experiment as it was observed later from strain and load curves. The variation of the

principal strain values versus the applied load for the lateral and medial aspects of the mandible was analyzed. In both cases, the ratio of maximum to minimum principal strains increases as the load does. This is an indication that the specimen slightly moved during the experiment, the restraints were not fixing the specimen in three planes as it was intended and that the nature of the load changed during the experiment. The strain values for the medial aspect show a larger variation. The boundary conditions were not totally controlled during the experiment which makes the FEM validation even more challenging.

To determine the variation in the experimental data, the coefficient of determination R^2, the square of the correlation coefficient, was obtained for the strain data corresponding to lateral and medial gages. The maximum principal strain values obtained from the experiment were plotted versus the applied load for the lateral and medial gages. For the lateral corpus, the coefficient of determination $R^2 = 0.97$. For the medial corpus, the coefficient of determination $R^2 = 0.90$. As it can be seen, the coefficient of determination for the strain data obtained from the medial aspect of the mandible is smaller. The smaller coefficient of determination suggests larger variation in the experimental data (Figure 2-5). The increased variation in the experimental data makes the validation process more difficult, especially for the medial gage. It also could explain the incongruence between FE strain ratios (maximum principal strain divided to minimum principal strain, absolute value) and experimental strain ratios.

Finite Element Analysis

Mandible model

In the current study, the geometric model of the mandible was obtained through volumetric reconstruction from CT scans. The mandible was scanned in a series of

parasagittal planes. The thickness of each slice was 0.63 mm giving a total of 90 cross sections through the mandible. Each cross section was converted from a DICOM (Digital Imaging and Communications in Medicine) file to a BMP (Bitmap) file. Each scan was segmented to obtain 2D digitized contours (Figure 2-6).

The volume (three-dimensional geometry) of the mandible was reconstructed from the 90 digitized contours obtained using commercial software (SURFdriver, Kailua, HI) (Figure 2-7). Because of the limits of spatial resolution in conventional CT, the soft tissue interface between the teeth and alveolar bone, the periodontal ligament, was not visualized and consequently was not modeled. The model was developed from a stack of 90 digitized outer contours and therefore lacks a high degree of internal anatomical detail.

The role of teeth as load-bearing structures in the absence of occlusal loads in the mandible is ambiguous (cf. (Daegling et al. 1992; Daegling and Hylander 1994a,b). Since most FE models ignore the periodontal ligament (e.g., Gupta et al. 1973, Knoell 1977, Hart and Thongpreda 1988, Hart et al. 1992, Strait et al. 2003), this question is not easily addressed with reference to single models. Because the periodontal ligament could not be simulated in the model and the teeth were rigidly inserted into the mandibular bone, without an interface between the teeth and alveoli, the dentate model always behaved as a very stiff, rigid structure. As expected, low strain values were obtained when the model was analyzed. The dentate model was therefore unrealistically stiff and it did not reflect the behavior of the mandible during the strain gage experiment. For this reason, it was necessary to develop a second mandible model, a mandible model without teeth.

The edentulous model was reconstructed from the same CT cross sections used for reconstructing the dentate model. Teeth were “extracted” (not digitized) and gaps were

created where the tooth roots were visualized. Both models were imported into the MSC Patran finite element analysis package (MSC Software Corporation, Santa Ana, CA) (Figure 2-8). The models were transformed into solids and then meshed with a tetrahedral mesh using quadratic elements. The dentate model had 13,616 quadratic tetrahedral elements. The edentulous model had 9,735 quadratic tetrahedral elements.

As with any model developed to simulate a biological structure, there are some limitations in this model. Characteristic to FEA, many assumptions and simplifications need to be made during the entire model development, especially when assigning material properties (for example choosing density values, Poisson's ratio, average HU, average elastic modulus etc) and simulating the physiological loading environment (mastication forces). The dentate model is unrealistically stiff. The edentulous model performs better but it was created by teeth removal and therefore, the overall amount of the material was reduced. Periodontal ligament influences stress-bearing capabilities in the mandible. Due to volumetric reconstruction from CT images, the periodontal ligament could not be simulated in the model and consequently, the results obtained do not reflect its contribution.

Finite element simulations

The FEA was planned to replicate as close as possible the conditions from the experimental setup. Thus, the models were subjected to a vertical occlusal load of 70 N which was applied to the left central incisor (this tooth was preserved in the edentulous models) and the models were constrained bilaterally at condyles and angles. The locations for the virtual lateral and medial gauges in the FEA model correspond as much as possible to the strain gauge locations on the real mandible. The virtual gauges were "placed" as much as possible at the same location for the dentate and the edentulous

models. Strain analyses were performed in order to determine the principal strains at the strain gauge sites and compare these values with the experimental data (Figure 2-9). Initially a homogeneous isotropic mandible model was analyzed, with condyles and angles completely constrained (Daegling et al. 2003). The maximum and minimum principal strains for the dentate model (lateral strain gauge: 231με and - 247με; medial strain gauge: 161με and -67με) and for edentulous model (lateral strain gauge: 528με and - 174με; medial strain gauge: 154με and -84με) showed poor agreement with experimental values (Table 2-1, Table 2-2).

The steel bar constrained the mandible at the base against horizontal movements and the steel roller prevented movement at the condyles in the vertical direction. As it was evident later, during and after the experiment, the mandible was not totally constrained in the transverse direction. Subsequently, efforts were made to replicate the unpredicted change in boundary conditions which took place during the experiment. To replicate the altered boundary conditions, the mandible was totally constrained at the left condyle and the left base (the force was applied on the left side of the mandible), and partially constrained (not constrained in the transverse direction) at the right condyle and the right base. Realistic boundary conditions were investigated further by decreasing the number of nodes constrained, altering the degrees of freedom and changing the force orientation.

Factors that Influenced the FEA

There are many factors that could influence the results. Changing the location and the orientation of the force has a huge impact on the principal strain results. Relaxing the model by decreasing the number of nodes constrained or by altering the degrees of

freedom in the constrained nodes has, as expected, a large impact on the strain results. Material properties assignment (isotropy vs. orthotropy, homogeneity vs. heterogeneity) will greatly influence the outcome.

FEA—nodal constraints

Reduction of nodal constraints bilaterally below the condyles and at gonion from 25 nodes to 1 node at each location has predictably large effects. Initially was assumed that the mandible was not moving, consequently that the "virtual" mandible was not deflecting in the angular region, which served (in retrospect) to over-constrain the model. Over-constraining the model will result in stiffening the model and consequently producing incorrectly low principal strains. Simulations were performed by reducing the nodal constraints bilaterally below the condyles and at gonion from 25 to 12, 6, 3 and 1 at each location in successive iterations (Figure 2-10).

FEA—degrees of freedom

To account for the deflection of the specimen during the experiment, simulations were performed by reducing the number of degrees of freedom at condyles and angles in the transverse direction (the only unrestricted plane). Three analyses were performed (isotropic case) for each model: altering the nodal constraints at the right condyle and right base, at the right condyle and left base and changing the nodal constraints simultaneously in the right condyle, left condyle and right base (Figure 2-11).

FEA—force direction

The influence of variation in orientation of the external force applied at the incisor on model principal strain values was investigated. Four analyses were performed using the homogeneous isotropic model in which 4 different inclination angle values ($\theta = 0°$, 5°, 10°, 20°) were considered. The force vector was tilted in the frontal plane in an

attempt to replicate the conditions of the experiment, given the likely deflection of the specimen (Figure 2-12).

FEA—material properties assignment

The effects on model behavior of spatial variation and directional dependence of elastic properties were also investigated. Based on material properties assignment, three models were developed: an isotropic homogeneous model, an isotropic heterogeneous model (with material properties assigned based on CT density) and a transverse isotropic heterogeneous model (by considering the mandible made from regions, with each region of the mandible having a different orientation of the local material axes). Material properties assignment is reported in Table 2-3.

The simplest assignment was an isotropic homogeneous model; that is, all model elements had the same material properties assigned, independent of direction (Young's modulus E = 15 GPa and Poisson's ratio $\nu = 0.3$). Elastic properties assigned to the isotropic homogeneous model were obtained from micromechanical tests performed on the specimen in another study (Rapoff et al. 2003) completed after the strain experiment and the CT scanning.

The second model, the isotropic heterogeneous model, was developed using Bonemat program (Laboratorio di Technologia Medica, Bologna, Italy, Zannoni et al. 1998 and Taddei et al. 2004). The Bonemat program was used to assign material properties based on CT density. The materials properties are automatically calculated using a linear relationship between CT numbers (expressed in HU—Hounsfild Units) and apparent bone density, and a power relationship between apparent density and Young’s

modulus. Bonemat program reads the CT dataset and the FEA mesh generated from it and assigns to each element of the mesh a Young's modulus value..

Step 1: Input. Three inputs are required to use Bonemat program: mesh input, CT dataset input and a parameter file.

- Mesh input. A mesh file was created in the finite element analysis package. The element types usually supported in Bonemat are: tetrahedron, hexahedron, wedge and quadratic tetrahedron. The finite element mesh file created contained information about each of the quadratic tetrahedron elements contained in the mandible mesh. Mesh data was transferred between software using a neutral file format.

- CT dataset input. The CT scans were initially in the DICOM format (Digital Imaging and Communications in Medicine) which is not supported by Bonemat. The images were converted in .vtk file format (Visual Toolkit) using the free DataManager application, a software used for medical data sharing and developed by Marco Viceconti and colleagues at Istituti Ortopedici Rizzoli, Bologna, Italy.

- Parameters input. The parameter file is a text file that contains information on mesh input, CT dataset input, density calibration of the CT images (two points to define the CT numbers and density from CT images), and parameters to define the equation between density and elastic modulus.

Once the input files are introduced, Bonemat calculate first an average HU value based on CT images for each finite element contained in the mesh file. The average HU value (HU) is composed by integrating over the entire volume of the finite element. Two coordinate systems are used: (x, y, z) are the coordinates provided by the CT dataset and (r, s, t) are the coordinates provided in the mesh file, the coordinates of the finite element reference system. A great feature of the program is that Bonemat allows controlling the number of material properties created. The elements with similar elastic modulus are grouped together and several groups of elements are created. In the end, one material property will be assigned within a group.

Step 2: Calibration. Ideally, a calibration phantom containing known CT numbers is measured to perform proper scanner calibration. For the current mandibular CT dataset,

unfortunately, no information on scanner calibration is available. Mimics software (Materialise Ann Arbor, MI, USA) was use to evaluate the CT numbers in the CT images available. 65,536 CT numbers were obtained and imported in an excel file. CT numbers for the trabecular bone, cortical bone and teeth were situated in the interval 1545 HU ÷ 3055 HU. The average calculated value was 2060 HU. In addition, HU values were carefully examined and manually collected from known cortical and teeth regions in mandibular CT images. The examination confirmed that the cortical HU values were situated close to 2000HU value and the teeth HU values were situated close to the 3000HU value. Cortical bone has a density between 1.7 and 2.0 g/cm^3. Other calibration points for cortical bone available in the literature are: 1840 HU, 1.73 g/cm^3 (Zannoni et al. 1998) and 1650 HU and 1.8 g/cm^3 (Taddei et al. 2004).

In the current study, the first calibration point used in the parameters file representing the radiological and apparent density of cortical bone was 2060 HU and 1.8 g/cm^3. The second calibration point chosen was 0 HU, 1 g/cm^3 representing the radiological and apparent density of water (Zannoni et al. 1998, Taddei et al. 2004). The calibration equation between the average density value and average HU value is linear and based on the calibration points provided by the user. An average density value obtained from an average HU value will be calculated and assigned to each finite element of the mesh.

Step 3: Evaluation of the Young's modulus. Bonemat program uses the information provided to calculate the elastic modulus as a function of bone density. The relationship between modulus and density is given by:

$$E_n = k\rho_n^c$$

where E_n is the Young's modulus assigned to a finite element n, ρ_n is the apparent density of the element and k, c are coefficients provided by user. The relationship between elastic modulus and density was described as a cubic relationship (Carter and Hayes 1977, Zannoni et al. 1998).

Three different materials were obtained and assigned to three groups of elements (A, B, C). The three groups of elements were determined automatically, based on the material property derived from the CT density of the tissue, as stored in the CT scan data. The model made from the 3 groups of elements was consequently isotropic but heterogeneous (E_A = 15.4 GPa, E_B = 9.08 GPa, E_C = 3.7 GPa, and $\nu_A = \nu_B = \nu_C = 0.3$). Material properties were assigned using MSC Patran according to a local coordinate system: the 3-axis was defined as following the length of the mandible, with the 1-axis mediolaterally oriented and 2-axis superoinferiorly oriented.

The third model, the heterogeneous transversely isotropic model, was developed by assigning two sets of material properties, for cortical and trabecular bone. A few studies having succeeded in assigning directionally dependent material properties considered the mandible made from regions, with each region of the mandible having a different orientation of the local material axes. In these studies three main mandibular regions were defined: the left mandible, the chin and the right mandible (Hart and Thongpreda 1988, Hart et al. 1992). Similar mandibular regions were defined in Korioth's study (Korioth et al. 1992): the symphyseal region, the gonial angle region and the rest of the mandible. The same approach was used in the present study. As such, the third model was divided into three regions: right region (posterior corpus and ramus), symphyseal region (anterior corpus) and left region (posterior corpus and ramus). One local coordinate system was

built for each region, which followed the longitudinal axis from one condyle to the other (Figure 2-13).

The groups of elements defined previously (group A, representing the cortical region and groups B and C representing the trabecular region) were each further divided in 3 subgroups: right, symphyseal, and left regions. MSC Patran was used to assign material properties for cortical and trabecular bone to each region, according to their local coordinate system. Using the same groups of elements determined in the previous case, two materials were defined: group A, representing the cortical bone and groups B and C representing the trabecular bone. The model combines material information data obtained through micromechanical testing. For cortical bone, the material properties were assigned in the frontal plane and in the longitudinal direction ($E_{1,2\text{cortical}} = 13$ GPa, $G_{12} = 5$ GPa, $E_{3\text{cortical}} = 17$ GPa, $G_{23} = 6.91$ GPa, $\nu_{12} = 0.3$ and $\nu_{23} = 0.229$). The trabecular region was modeled as isotropic ($E_{\text{trabecular}} = 1.5$ GPa and $\nu_{\text{trabecular}} = 0.3$).

Validation of the FE Model

The finite element method is an essential tool for analyzing complex biomechanical models. FEM is widely used today to analyze bone models and predict stress and strain patterns. However, the accuracy of numerical models depends upon the accuracy of the input data. When biological structures are considered, many assumptions are to be made because several input parameters are unknown. Simulating in a FE model the exact geometry, material properties of the bone and the complex biological microstructures within the bone is a major challenge. To establish the validity of the resulted numerical models is therefore a very difficult and challenging task.

Many authors consider the numerical models to be an excellent tool for predicting the behavior of a real, physical model (Demes 1984, Turner et al. 1997, Koolstra and Van Eijden 1997b, 1999, Carter et al. 1998, Spencer 1998, 1999). FE stress and strain results will be used to predict the performance of a biological structure and often, the FE predictions will be used for clinical applications. Other researchers strongly disagree with using numerical models to predict the behavior of real world because in their opinion, it is absolutely impossible to verify and validate a numerical model (Oreskes el at 1994, Dalstra et al. 1995). Only a closed system can be verifiable. Several input parameters are unknown, the output is often unclear and many assumptions and predictions need to be made. A numerical model is therefore a complex open system and consequently, cannot be actually validated. Moreover, all the assumptions and the predictions are introducing auxiliary hypotheses. If the verification of the numerical model cannot be performed, it will be impossible to determine if the principal hypothesis or the auxiliary hypotheses are at fault.

However, verifiable or not, the FE models are increasingly used in biomechanics due to their ability to represent very complex biological systems. In an effort to minimize the lack of consensus regarding the verification and the validation of numerical models, guidelines for validation and publication of FE studies were proposed (Viceconti et al. 2005). The authors agree that no numerical model can be totally validated when applicable to biological structure. However, three levels of validation were proposed. For publishing theoretical studies, a first level of validation is proposed: explaining the model selection and performing the verification of the model using a convergence study. For clinical recommendations, sensitivity analysis should be considered.

Often, the only method of validation encountered in FE studies of biological structures is the comparison of the predicted FE values with values published in the literature (Korioth et al. 1992, Korioth and Hannam 1994a,b, Barbier et al. 1998, Liebschner et al. 2003). However, this method of validation is a very subjective method and provides only a general comparison between FE values and published data. Because of different conditions, assumptions and simplifications made in each study by different authors, the comparison between analyses is very difficult. Usually terms as “good agreement”, “good fit”, “compares favorably with published data” or “correlate well” are used in these studies to establish the validity of the models.

If the FE study is proposed for publication in journals of applied biomechanics research for clinical validation, a second validation step is necessary, validation against experiments. Validation at this stage is performed usually by using linear regression between experimental and FEA results and the regression parameters are reported. However, a “safe” range for experimental variation is not available and the matter is still a source of disagreement. Unfortunately, the most important question for FE validation against in vitro experiments, how good is good enough, remains answered.

For some FE studies, the validation was performed but the results are not presented in the article (Akay and Aslan 1996, “the finite element models generally agree well with the experimental strain gauge measurements”, Barker et al. 2005 “FE results were in good agreement with those in vitro”). For many studies the experimental validation was performed and some of the results are mentioned in the article (Dalstra et al. 1995 “the FE results corresponded well to the experimental values”).

Usually, for most of the FE studies, the experimental validation was performed and the results are published: correlation coefficient, coefficient of determination, standard error, slope and intercept. Some of the successful FE studies accepted for publication in highly respectable journals in the biomechanics field reported the error between FE and experimental values to be: 10% (Gross et al. 1997), less than 30% (McNamara et al. 1997), more than 30% (Dalstra et al. 1995) or more than 50% (Keyak et al. 1993, Gupta et al. 2004, Barker et al. 2005). In all these studies, the validation of the bone models was performed against in vitro strain gage experiments. All these studies are presenting FE validated bone models. None of the articles mentioned discuss a "safe" interval for the FE-experimental variation.

Sometimes, for a very complex model, even if all the necessary validation steps were performed and the results thoroughly reported, the validation of the bone model cannot be attained (Metzger et al. 2005). The published comparison between the experimental and predicted values indicated a lack of any statistically significant correlations, at any of the locations of interest. Incongruence between experimental and FE values may be attributed to a range of factors, such as model complexity, geometric differences, inaccurate material properties, unknown loading conditions, etc. Generally, the validation process for a simple structure such as ulna or a metallic implant (Gross et al. 1997, 2002) is more attainable and easier to perform than for a model with complicated geometry with complex material properties, for example a crocodilian skull (Metzger et al. 2005).

For clinical recommendations and publication in clinical journals, a third level of validation is proposed. The validation of FE models which will be used directly in

clinical practice should include risk-benefit analysis, retrospective studies and prospective studies. However, there is always a risk when model predictions, even from "validated" models, are used. A complex open system, such as a bone model, cannot be totally verifiable when applicable to biological structures.

In the current study, a convergence test was performed to determine the accuracy of the numerical model (Figure 2.14). FE meshes, from coarse to a very refined mesh with increased degrees of freedom, were created by assigning different GEL (global edge length) values. The bigger the edge length of an element, the bigger the element and the smaller the number of total elements created. For the edentulous model, the coarsest mesh was created using the global edge length 10 (7,772 elements were created). The most refined mesh was created using the global edge length 0.5 (16,906 elements were created). The maximum principal strain results were obtained at the lateral gage location for each mesh. The relative error was calculated by considering the maximum principal strain results obtained from the finest mesh and from the coarsest mesh by the using the formula (Barbier et al. 1998):

$$Mesh\ error = \frac{\varepsilon_{fine} - \varepsilon_{coarse}}{\varepsilon_{fine}} * 100$$

The total mesh error for the edentulous model is approximately 10%. The model used for simulations was created using a global edge length of 2 (9735 elements were created). Therefore according to the convergence test, the error of the strain results obtained by using the edentulous model should be less than 10%. Generally, a model is considered to have converged if the error between a mesh and the most fine mesh is less than 2% (Liebschner et al. 2003). The error between the mesh used in the simulations and the most refined mesh in the current study is very small (0.37%).

The comparison between experimental and finite element principal strain data was performed for the current study. The maximum and minimum principal experimental strains recorded during the strain gauge experiment were: lateral strain gauge: 755με and - 221με; medial strain gauge: 273με and -108με. The maximum and minimum principal finite element strains (lateral strain gauge: 528με and - 174με; medial strain gauge: 154με and -84με) recorded for the edentulous homogeneous isotropic model, fully constrained bilaterally at condyles and angles were lower than the experimental strain values. During the strain experiment, the mandible was supposed to be restrained by the symmetrical steel fixture. However, the specimen deflected during the experiment because of the mandible asymmetrical geometry and movement occurred in the transverse direction at the constraint locations. The steel bar constrained the mandible in the horizontal direction and the steel roller in the vertical direction. Therefore, the mandible was not totally constrained in the transverse direction. A 70 N load was applied asymmetrically, to the left incisor. To replicate the altered boundary conditions, the mandible was totally constrained at the left condyle and the left base, and partially constrained (not constrained in the transverse direction) at the right condyle and the right base. Very congruent finite element results were obtained by simulating the altered boundary conditions: the maximum and minimum principal finite element strains (lateral strain gauge: ε_1=769με; ε_2=-241με, medial strain gauge: ε_1=295με; ε_2=-371με). The overall percent error is below 10% (1.85% for the lateral gauge and 8.05% for the medial gauge).

According to the FE principal strain results, both values are below 10% error which seems to be the assumed accepted error in the FE studies even if many of the published

FE models of biological structures report a higher value. The convergence study performed on the edentulous model adds extra confidence in the FE results.

Method to Record Principal Strain Values

The method used for recording and evaluating the principal strain data generated by the FE models consists of averaging principal strain values of a node common to the neighboring elements, following similar methods used by other researchers (Remmler et al. 1998, Lengsfeld et al. 1998, Coleman et al. 2002, Guo et al. 2002). The strain gauge location on the virtual mandible on each side is subject to a small, but undetermined error with respect to the location of the strain gauge in the real mandible. Rather than rely on single element values, an averaged strain value was calculated (Figure 2-15).

The necessary steps to record principal strains using the current method are:

- Find the location in the model where the strain gage would be placed.
- Pick the closest node to that location ("Common node").
- Find the neighboring elements for the common node (all the elements around that have in common that node).
- Find their "skin" faces.
- Record the strain values for all the neighboring elements.
- Average the strain values for each common node.

The elements situated at the gauge location were found and their principal strain values for these elements were averaged. This method is introducing one unique local coordinate system. The force and the boundary constraints are assigned in reference to this unique coordinate system. The principal strains from the various models were determined from these same elements in all simulations.

Results

The experimental principal strains and the principal strain ratio for lateral and medial regions of the mandible are presented in Table 2-1 and Table 2-2. The lateral

maximum principal strain found was 755 με and the lateral minimum principal strain was -221 με, yielding a ratio of maximum to minimum principal strain of 3.41. The medial maximum principal strain found was 273 με and the medial minimum principal strain was -108 με, yielding a ratio of maximum to minimum principal strain of 2.52. The principal strains and the principal strain ratios for the lateral and medial location obtained using the FEA (homogeneous isotropic model, fully constrained bilaterally at condyles and angles) are also reported in Table 2-1 and Table 2-2. The lateral and medial principal strain values obtained from the edentulous model are more compatible to the experimental values.

FEA—Nodal Constraints

The absolute number of constrained nodes has the predictable effect of influencing model stiffness. An equal number of nodes were constrained on each side, at condyles and angles (Figure 2-10). The greater number of nodes constrained results in a stiffer model and consequently produces lower principal strains (Figure 2-16, Table 2-4, Table 2-5). Reduction of nodal constraints from 25 nodes to 1 node at each location has predictably large effects, resulting in a more than 50% increase in principal strain magnitudes. The dentate model yields a principal strain ratio near 1.0 throughout these iterations while the edentulous model fits the experimental data better in all cases.

FEA—Force Direction

Changing the orientation of the applied force has a large impact on model principal strains (Figure 2-12). As the inclination of the applied force deviates from a purely sagittal orientation to having a progressively greater lateral component, the principal strain ratio values increase, due to the more rapid increase in the maximum principal

strain (Table 2-6, Table 2-7). Altering occlusal point load directions by as little as 10° alters maximum principal strains by 11-18%.

FEA—Degrees of Freedom

Further FE analyses were performed by relaxing successively the degrees of freedom at condyles and angles in an attempt to simulate the deflection of the specimen during the experiment (Figure 2-11). Relaxation of the degrees of freedom in the transverse direction causes a significant increase in principal strain values (Table 2-8, Table 2-9). In particular, allowance for translation in the transverse direction on the right side of the edentulous model (the right condyle and the right base) yields strain results very congruent with the experimental data.

FEA—Material Properties Assignment

Principal strain values are influenced by different assignment of spatial variation (homogeneity vs. heterogeneity) and directional dependence (isotropy vs. orthotropy) of elastic properties in both dentate and edentulous models (Table 2-10, Table 2-11). The decision to employ isotropic and homogeneous models results in different errors depending on the analysis of the dentate versus edentulous case. Introducing structural heterogeneity and directional dependence of material behavior by regional assignment of material properties results in an increase in principal strains in the edentulous model (Table 2-10, Table 2-11). In the case of this particular mandible, the choice of material properties assignment and structural simplicity introduce large differences in predicted strains. In the edentulous model, introduction of heterogeneity and directional dependence actually increases departure of the predicted strain ratio values from the experimentally observed value. This is also true of the dentate model, although this

model is always in marked disagreement with experimental values regardless of the nature of perturbations.

Discussion

The application of FEA to skeletal mechanics has changed since this method was first introduced. Initially, this method was used to investigate questions of structural failure (Huiskes and Hollister 1993). Currently this method is successfully used in the context of understanding the biomechanical behavior of the bone under physiological loading conditions. Despite advances in techniques and hypothesis specification, the accuracy and reliability of using FEA to address functional morphological questions are incompletely established.

It is widely appreciated that the geometry of the FE model plays a crucial role in obtaining accurate results. In the present case, the geometry of the dental alveoli rather than the teeth themselves is more informative of actual behavior. The edentulous virtual mandible model's better match with the experimental data suggests that in the absence of occlusal loads, teeth may not function as load bearing structures. The dentate model is always too stiff; that is, the strain values obtained from it are extremely low when compared with the experimental strain values. The periodontal ligament was not modeled and consequently no interface existed between the teeth and alveoli. This increases the structural stiffness of the model and explains the low strain values obtained. The strain results obtained from analyzing the edentulous model are more congruent with the experimental strain data not only because the edentulous model is less stiff, but also because the removal of teeth lowers the neutral axis in bending (which readily explains the better fit of the principal strain ratio values to those observed in the experiment). An

increase in strain values can be explained by tooth removal given reduction in the overall amount of material resisting deformation.

Correct boundary conditions are also critical for FE model validation. As expected, constraining the model excessively produces inaccurately low principal strain values. In contrast, applying minimal constraints produces strain results more compatible with the experimental strain data, even if single-node constraints are not biologically reasonable. If the purpose of the experimental tests were to provide benchmarks for simulation validation, then the loading and constraints most reproducible in the simulations should be used in the tests even if the tests do not represent physiologic conditions. Whether the model constraints are at all appropriate for in vivo caseloads is arguable and also irrelevant; the point of the above analysis is to establish a baseline for understanding the sensitivity of the whole mandible model to changes in boundary conditions. The main difficulty in correlating strain data with FE model predictions arises from the difficulty in recreating identical parameters in experimental and virtual contexts. A multitude of variables act simultaneously during a strain gauge experiment (e.g., orientation and magnitude of the applied load, nature of constraints, material property variation, and geometric subtleties of the real specimen) whereas in a FEA these variables are necessarily subject to a number of simplifying assumptions. This discrepancy might lead to different results and interpretations of the stress-strain behavior of the mandibular bone (Hylander et al. 1998, Dechow and Hylander 2000). The objective was to obtain a validated model and to portray the difficulties encountered when attempting to validate FE models from an in vitro context where some parameters are ostensibly under

investigator control. For the in vivo context, the specification of appropriate boundary conditions and material properties assignment will be more difficult.

Relaxing the FE model by decreasing the number of nodes constrained or by altering the degrees of freedom in the constrained nodes has, as expected, a large impact on the strain results. During the strain experiment, the mandible was restrained by a symmetrical steel fixture; however, mandibles are not perfectly symmetrical structures. It was assumed initially that the mandible was totally constrained in three dimensions below the condyles and at the angles during the experiment. Deflection of the specimen during the experiment, however, suggests movement occurred in the transverse direction at the constraint locations. The validation of the model was successful when simulating the altered boundary conditions. Thus, very congruent finite element results were obtained by relaxing the degrees of freedom in the transverse direction. The FE principal strain ratio for the lateral gage was similar to the experimental principal strain ratio. However, the ratio for the medial gage differs from the experimental value. The incongruence in the medial results is not surprising given the large variation in the experimental data (Figure 2-5). A smaller coefficient of determination (R^2) was obtained for the medial gage, suggesting large variation in the medial data. This proves that the boundary conditions were not controlled during the experiment and makes the exact matching of the results very difficult.

Modest errors in specifying the direction of the applied force in the FE simulation can have substantial impact on principal strain values, and the critical point here is that this is true even at locations remote to the point of load application. As the mandible deflected during the experiment, the loading environment became modified such that a

horizontal force component was introduced. Because of the oblique orientation of the mandibular angles on the supporting rod during the experiment, a horizontal reaction force was induced at those points. Because of the relationships between force and displacement, and displacement and strain, modifying the direction of the applied load produces a novel load case in the present context, in terms of the relative contributions of bending and torsion to recorded and predicted strains. Unfortunately, the precise magnitude of this horizontal force component introduced when the specimen deflected is unknown.

Spatial variation (homogeneity vs. heterogeneity) and directional dependence (isotropy vs. orthotropy) of elastic properties greatly influence principal strain values, sufficiently so that the convenience of using isotropic models entails a significant cost in model accuracy. The first analysis considered an isotropic homogenous model obtained by assigning the same material property to all elements, independent of direction. The second analysis was performed on an isotropic heterogeneous mandible model in which three different isotropic properties were assigned to three different groups of elements. The third analysis employed a transverse isotropic heterogeneous model with spatial variation and directional dependence of elastic properties. As expected, introduction of heterogeneity and transverse isotropy in the less stiff edentulous model increases principal strain values because approximately 14% of the FEs are assigned a relatively low modulus corresponding to the trabecular region. As in all the previous simulations, the edentulous model performs better than the dentate one. Incorporating heterogeneity and transverse isotropy into the FE models improves the congruence of experimental and

theoretical values. This will not be obvious in cases where the effects of load direction and boundary conditions have not been satisfactorily controlled.

In the absence of precise information about the material properties of the mandible or because of the need for simplicity, FE mandible models are idealized as isotropic, linearly elastic solids (Gupta et al. 1973, Knoell 1977, Meijer et al. 1993). The material properties assigned to the models are therefore directionally independent, consequently eliminating one of the most cumbersome steps in the process of obtaining a realistic FE model, that of assigning directionally dependent material properties.

Multiple studies performed to determine the elastic properties of the mandible showed how complex the mandibular bone is. The elastic properties vary directionally between different regions in the mandible (Dechow and Hylander 2000). Developing a model without directional dependence of elastic properties, although very convenient and significantly less time consuming, will provide only a first approximation of the strain field in a loaded mandible.

The material properties for the second type of FEA, the isotropic heterogeneous mandible model, were assigned according to a single local coordinate system (the 3-axis in the longitudinal direction and the other two axes oriented in the frontal plane) without variation throughout the mandible. The chosen coordinate system facilitates recording the principal strains from the region of interest where the strain gauge was attached – the lateral and medial aspects of the left basal corpus, below the second molar. Although the second model is heterogeneous, it is an isotropic model and therefore unrealistic.

The material properties for the third type of FEA, the heterogeneous transverse isotropic model, were assigned according to three local coordinate systems corresponding

to three regions in the mandible: right region, symphysis and left region. Introducing structural heterogeneity and directional dependence of material behavior produces an increase in principal strains in the edentulous model as it can be seen in Table 2-10 and Table 2-11.

A case of using strain data from two points (i.e., two strain gauges) was presented to validate a model. Utilizing multiple strain gauge sites would allow for mapping strain gradients, which would offer additional insight into the influences of the modeling parameters. This would not be an option in the in vivo context due to experimental limitations or size and geometry of the specimen (Hylander et al. 1998, Dechow and Hylander 2000).

Table 2-1. Experimental and theoretical principal strain data. Principal strains and the principal strain ratios are calculated from the lateral aspect of the corpus. The reported values are for homogeneous isotropic models, fully constrained bilaterally at condyles and angles (4 nodes). The models were subjected to a vertical occlusal load of 70N, applied to the left central incisor.

	$\varepsilon_1(\mu\varepsilon)$	$\varepsilon_2(\mu\varepsilon)$	$\varepsilon_1/\varepsilon_2$
Experiment	755	-221	3.41
FE dentate model*	288	- 225	1.28
FE dentate model+	231	-247	0.93
FE edentulous model+	542	-181	2.99

*Daegling et al. 2003;
+ In the current study predicted strains were determined by averaging strains from five elements while in the 2003 study the strains were taken from a single element. The coordinate systems used in the 2003 study (a global system) and the present study (a local system) also differed slightly.

Table 2-2. Experimental and theoretical principal strain data. Principal strains and the principal strain ratios are calculated from the medial aspect of the corpus. The reported values are for homogeneous isotropic models, fully constrained bilaterally at condyles and angles (4 nodes). The models were subjected to a vertical occlusal load of 70N, applied to the left central incisor.

	$\varepsilon_1(\mu\varepsilon)$	$\varepsilon_2(\mu\varepsilon)$	$\varepsilon_1/\varepsilon_2$
Experiment	273	-108	2.52
FE dentate model*	159	51	3.11
FE dentate model+	161	-67	2.40
FE edentulous model+	213	-174	1.22

Table 2-3. Material properties assignment. The isotropic heterogeneous model had three sets of material properties assigned based on CT density using BoneMat. The transverse isotropic heterogeneous model considered the mandible to have regional dependence of material properties, with three regions of the mandible having a different orientation of the local material axes.

Material	Young's modulus (GPa)	Poisson's ratio	Shear Modulus (GPa)	N of elements	
				Dentate	Edentulous
Isotropic Homogeneous	15	0.3	-	13616	9735
Isotropic Heterogeneous	E_A=15.4	ν_A=0.3	-	A: 12353	A: 8428
	E_B=9.08	ν_B=0.3	-	B: 65	B: 62
	E_C=3.7	ν_C=0.3	-	C: 1198	C: 1245
Transverse Isotropic Heterogeneous	$E_{1,2cortical}$=13	ν_{12}=0.3	G_{12}=5	12353	8428
	$E_{3cortical}$=17	ν_{23}=0.229	G_{23}=6.91		
	$E_{trabecular}$=1.5	ν=0.3	-	1263	1307

Table 2-4. Effect of nodal constraint on principal strain values. Principal strains and the principal strain ratios are calculated from the lateral aspect of the corpus. All simulations were performed using the homogeneous isotropic model, constrained bilaterally at condyles and angles. The models were subjected to a vertical occlusal load of 70 N, applied to the left central incisor. These simulations did not allow for relaxation of constraint in any direction.

Number of constraints	Dentate model			Edentulous model		
	$\varepsilon_1(\mu\varepsilon)$	$\varepsilon_2(\mu\varepsilon)$	$\varepsilon_1/\varepsilon_2$	$\varepsilon_1(\mu\varepsilon)$	$\varepsilon_2(\mu\varepsilon)$	$\varepsilon_1/\varepsilon_2$
25	156	-169	0.92	340	-107	3.17
12	173	-178	0.97	343	-108	3.17
6	193	-211	0.91	377	-127	2.96
3	205	-239	0.85	429	-163	2.63
1	231	-247	0.93	542	-181	2.99

Experimental strain data: $\varepsilon_1 = 755\mu\varepsilon$, $\varepsilon_2 = -221\mu\varepsilon$, $\varepsilon_1/\varepsilon_2 = 3.41$

Table 2-5. Effect of nodal constraint on principal strain values. Principal strains and the principal strain ratios are calculated from the medial aspect of the corpus. All simulations were performed using the homogeneous isotropic model, constrained bilaterally at condyles and angles. The models were subjected to a vertical occlusal load of 70 N, applied to the left central incisor. These simulations did not allow for relaxation of constraint in any direction.

Number of constraints	Dentate model			Edentulous model		
	$\varepsilon_1(\mu\varepsilon)$	$\varepsilon_2(\mu\varepsilon)$	$\varepsilon_1/\varepsilon_2$	$\varepsilon_1(\mu\varepsilon)$	$\varepsilon_2(\mu\varepsilon)$	$\varepsilon_1/\varepsilon_2$
25	95	-36	2.63	74	-42	1.76
12	85	-33	2.57	74	-41	1.80
6	132	-47	2.80	89	-41	2.17
3	172	-58	2.96	139	-59	2.35
1	161	-67	2.40	213	-174	1.22

Experimental strain data: $\varepsilon_1 = 273\mu\varepsilon$, $\varepsilon_2 = -108\mu\varepsilon$, $\varepsilon_1/\varepsilon_2 = 2.52$

Table 2-6. Influence of force orientation on principal strain values. Principal strains and the principal strain ratios are calculated from the lateral aspect of the corpus. Each iteration employs an occlusal load of 70N applied to the left central incisor. These analyses were performed using homogeneous isotropic models, fully constrained bilaterally at condyles and angles. Inclination of the occlusal force vector lies within the frontal plane.

Inclination angle	Dentate model			Edentulous model		
	$\varepsilon_1(\mu\varepsilon)$	$\varepsilon_2(\mu\varepsilon)$	$\varepsilon_1/\varepsilon_2$	$\varepsilon_1(\mu\varepsilon)$	$\varepsilon_2(\mu\varepsilon)$	$\varepsilon_1/\varepsilon_2$
0°	231	-247	0.93	542	-181	2.99
5 °	253	-257	0.98	574	-190	3.02
10°	274	-267	1.02	602	-198	3.04
20°	311	-280	1.11	646	-208	3.10

Experimental strain data: $\varepsilon_1 = 755\mu\varepsilon$, $\varepsilon_2 = -221\mu\varepsilon$, $\varepsilon_1/\varepsilon_2 = 3.41$

Table 2-7. Influence of force orientation on principal strain values. Principal strains and the principal strain ratios are calculated from the medial aspect of the corpus. Each iteration employs an occlusal load of 70N applied to the left central incisor. These analyses were performed using homogeneous isotropic models, fully constrained bilaterally at condyles and angles. Inclination of the occlusal force vector lies within the frontal plane.

Inclination angle	Dentate model			Edentulous model		
	$\varepsilon_1(\mu\varepsilon)$	$\varepsilon_{2(}\mu\varepsilon)$	$\varepsilon_1/\varepsilon_2$	$\varepsilon_1(\mu\varepsilon)$	$\varepsilon_{2(}\mu\varepsilon)$	$\varepsilon_1/\varepsilon_2$
0°	161	-67	2.40	213	-174	1.22
5 °	144	-86	1.67	202	-189	1.06
10°	136	-116	1.17	195	-209	0.93
20°	141	-197	0.71	193	-261	0.73

Experimental strain data: $\varepsilon_1 = 273\mu\varepsilon$, $\varepsilon_2 = -108\mu\varepsilon$, $\varepsilon_1/\varepsilon_2 = 2.52$

Table 2-8. Influence of the degrees of freedom on principal strain values. Principal strains and the principal strain ratios are calculated from the lateral aspect of the corpus. All analyses use homogeneous isotropic models (70 N applied to the left central incisor). Relaxation of the degrees of freedom is restricted to the transverse direction in all cases.

Degree of relaxation	Dentate model			Edentulous model		
	$\varepsilon_1(\mu\varepsilon)$	$\varepsilon_2(\mu\varepsilon)$	$\varepsilon_1/\varepsilon_2$	$\varepsilon_1(\mu\varepsilon)$	$\varepsilon_{2(}\mu\varepsilon)$	$\varepsilon_1/\varepsilon_2$
Fixed	231	-247	0.93	542	-181	2.99
R condyle, R base	439	-243	1.80	769	-241	3.19
R condyle, L condyle	520	-491	1.05	1010	-442	2.28
R condyle, R base, L condyle	648	-421	1.53	1096	-355	3.08

Experimental strain data: $\varepsilon_1 = 755\mu\varepsilon$, $\varepsilon_2 = -221\mu\varepsilon$, $\varepsilon_1/\varepsilon_2 = 3.41$

Table 2-9. Influence of the degrees of freedom on principal strain values. Principal strains and the principal strain ratios are calculated from the medial aspect of the corpus. All analyses use homogeneous isotropic models (70 N applied to the left central incisor). Relaxation of the degrees of freedom is restricted to the transverse direction in all cases.

Degree of relaxation	Dentate model			Edentulous model		
	ε1(με)	ε2(με)	ε1/ε2	ε1(με)	ε2(με)	ε1/ε2
Fixed	161	-67	2.40	213	-174	1.22
R condyle, R base	147	-423	0.34	295	-371	0.79
R condyle, L condyle	426	-385	1.10	557	-474	1.17
R condyle, R base, L condyle	321	-624	0.51	471	-540	0.87

Experimental strain data: $\varepsilon_1 = 273\mu\varepsilon$, $\varepsilon_2 = -108\mu\varepsilon$, $\varepsilon_1/\varepsilon_2 = 2.52$

Table 2-10. Influence of material properties assignment on principal strain values. Principal strains and the principal strain ratios are calculated from the lateral aspect of the corpus. The models were subjected to an occlusal load of 70N, applied to the left central incisor and were fully constrained bilaterally at condyles and angles.

Material	Dentate model			Edentulous model		
	$\varepsilon_1(\mu\varepsilon)$	$\varepsilon_2(\mu\varepsilon)$	$\varepsilon_1/\varepsilon_2$	$\varepsilon_1(\mu\varepsilon)$	$\varepsilon_2(\mu\varepsilon)$	$\varepsilon_1/\varepsilon_2$
Isotropic Homogeneous*	231	-247	0.93	542	-181	2.99
Isotropic Heterogeneous*	193	-223	0.86	569	-180	3.16
Transverse Isotropic Heterogeneous**	136	-169	0.80	565	-197	2.86

Experimental strain data: $\varepsilon1 = 755\mu\varepsilon$, $\varepsilon2 = -221\mu\varepsilon$, $\varepsilon1/\varepsilon2 = 3.41$

*Without directional dependence of material behavior throughout mandible

** With directional dependence of material behavior throughout mandible

Table 2-11. Influence of material properties assignment on principal strain values. Principal strains and the principal strain ratios are calculated from the medial aspect of the corpus. The models were subjected to an occlusal load of 70N, applied to the left central incisor and were fully constrained bilaterally at condyles and angles.

Material	Dentate model			Edentulous model		
	ε1(με)	ε2(με)	ε1/ε2	ε1(με)	ε2(με)	ε1/ε2
Isotropic Homogeneous*	161	-67	2.40	213	-174	1.22
Isotropic Heterogeneous*	187	-78	2.39	179	-78	2.29
Transverse Isotropic Heterogeneous**	181	-65	2.78	167	-74	2.25

Experimental strain data: $\varepsilon_1 = 273\mu\varepsilon$, $\varepsilon_2 = -108\mu\varepsilon$, $\varepsilon_1/\varepsilon_2 = 2.52$

*Without directional dependence of material behavior throughout mandible

** With directional dependence of material behavior throughout mandible

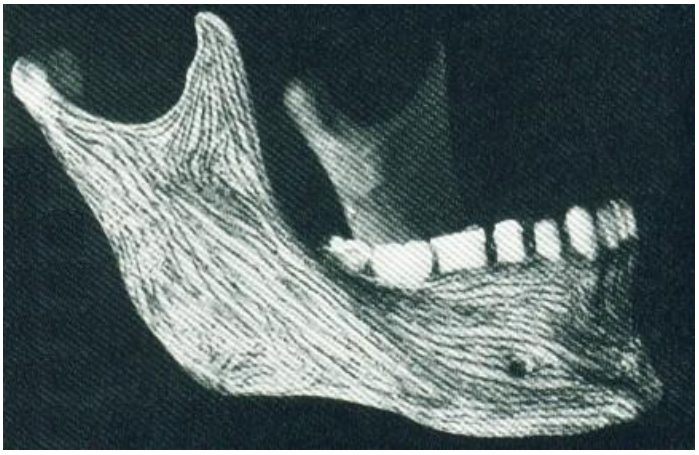

Figure 2-1. Photoelastic method. The coated mandible (Evans 1957).

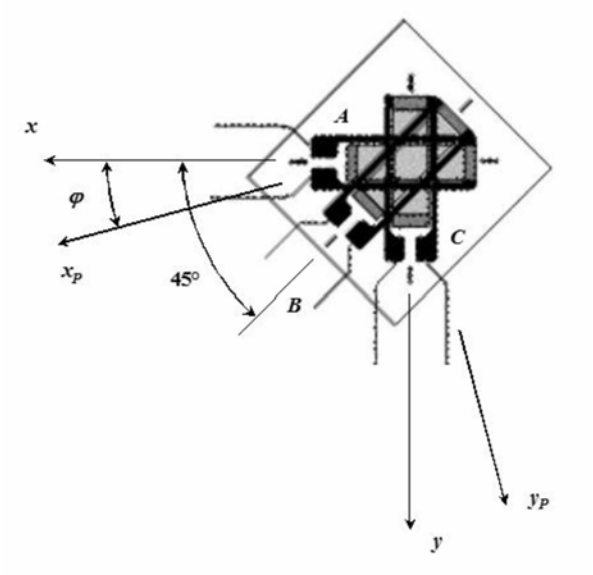

Figure 2-2. Rectangular rosette strain gauge. From the raw strain data from the individual gauge elements, principal strain magnitude and direction were calculated using the formulas presented.

Figure 2-3. *Macaca fascicularis* specimen. The experimental strain analysis was performed on a fresh *Macaca fascicularis* mandible of a six-year old adult female macaque.

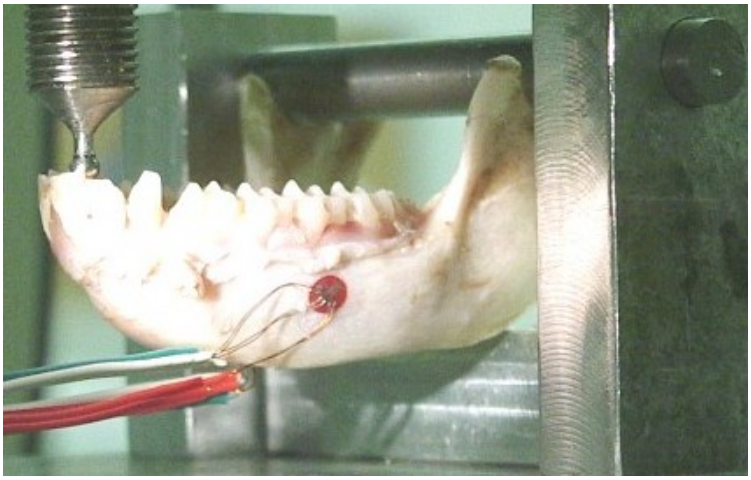

Figure 2-4. Experimental strain analysis—lateral strain gauge. Rectangular rosette strain gauges were bonded to the lateral and the medial aspect of the mandibular corpus, below the left second molar. The metal fixture that restrained the mandible during the procedure was composed from an aluminum base that supported the mandible at each angle and a steel roller which prevented movement at the condyles. The mandible was subjected to a vertical occlusal load applied to the left central incisor.

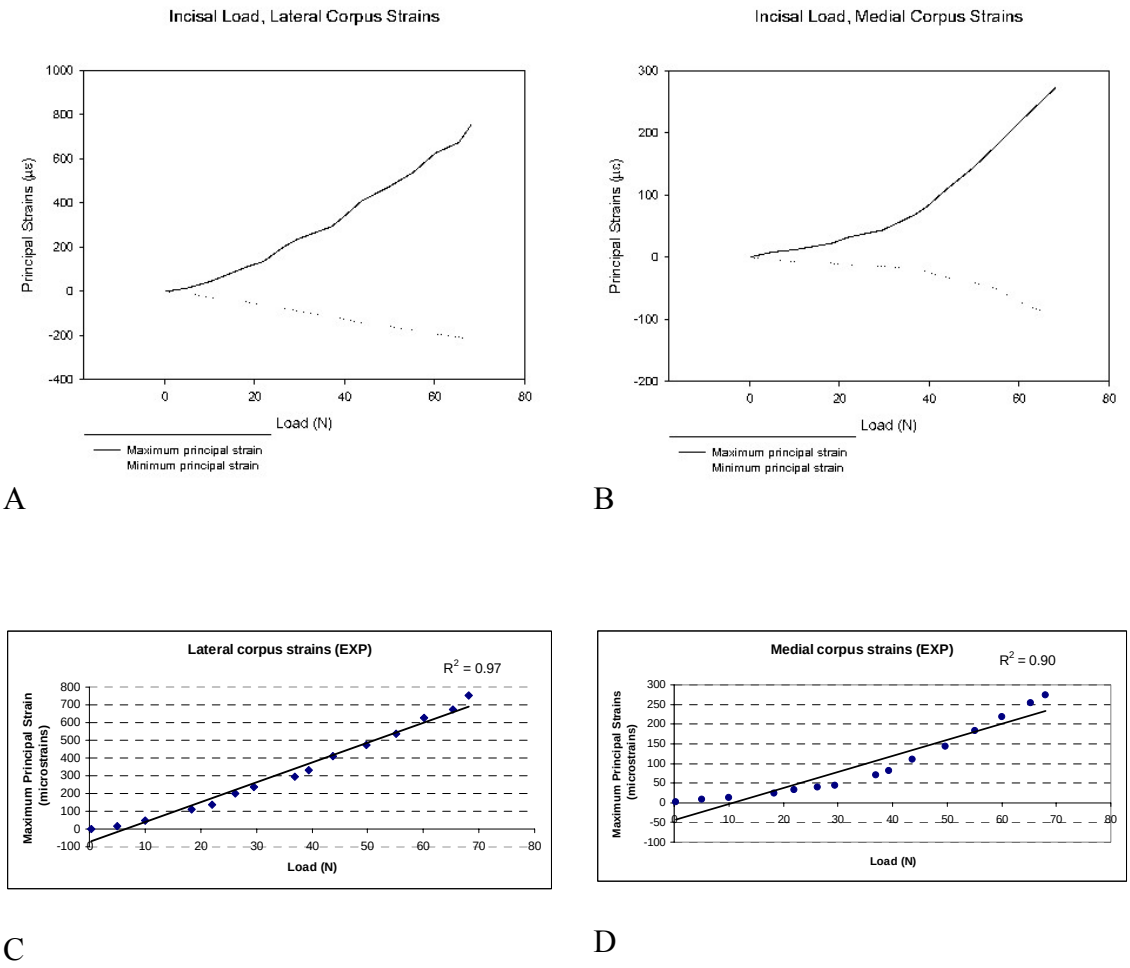

Figure 2-5. Experimental data variation. The variation of the principal strain values versus the applied load for the lateral corpus (A) and medial corpus (B) of the mandible was analyzed. The experimental data variation for the lateral aspect (C) and medial aspect (D) is shown above. The smaller coefficient of determination (R^2) obtained for the medial gage, suggests large variation in the experimental data.

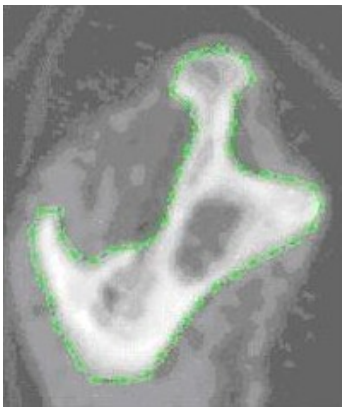

Figure 2-6. Digitized CT cross sections. The geometric model of the mandible was obtained through volumetric reconstruction from CT scans. The current picture represents a cross section through the upper part of the mandibular ramus, coronoid process and condyle.

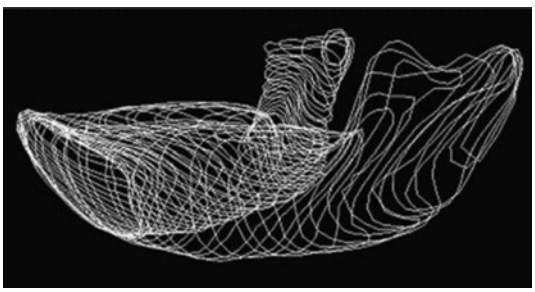
A
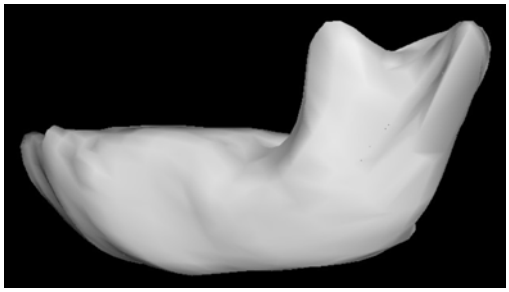
B

Figure 2-7. Geometric mandible model. A) Wireframe representation, without the outer shell. B) Surface representation, with the outer shell. The volume (three-dimensional geometry) of the mandible was reconstructed from a stack of 90 digitized outer contours.

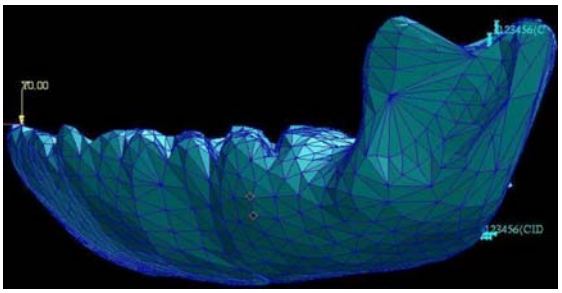
A
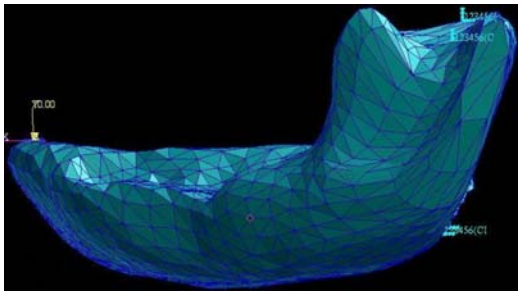
B

Figure 2-8. FE mandible models. A) Dentate FE model. B) Edentulous FE model. Both were reconstructed from the same 90 CT cross sections. The tooth crown and root structures were not digitized for the edentulous model.

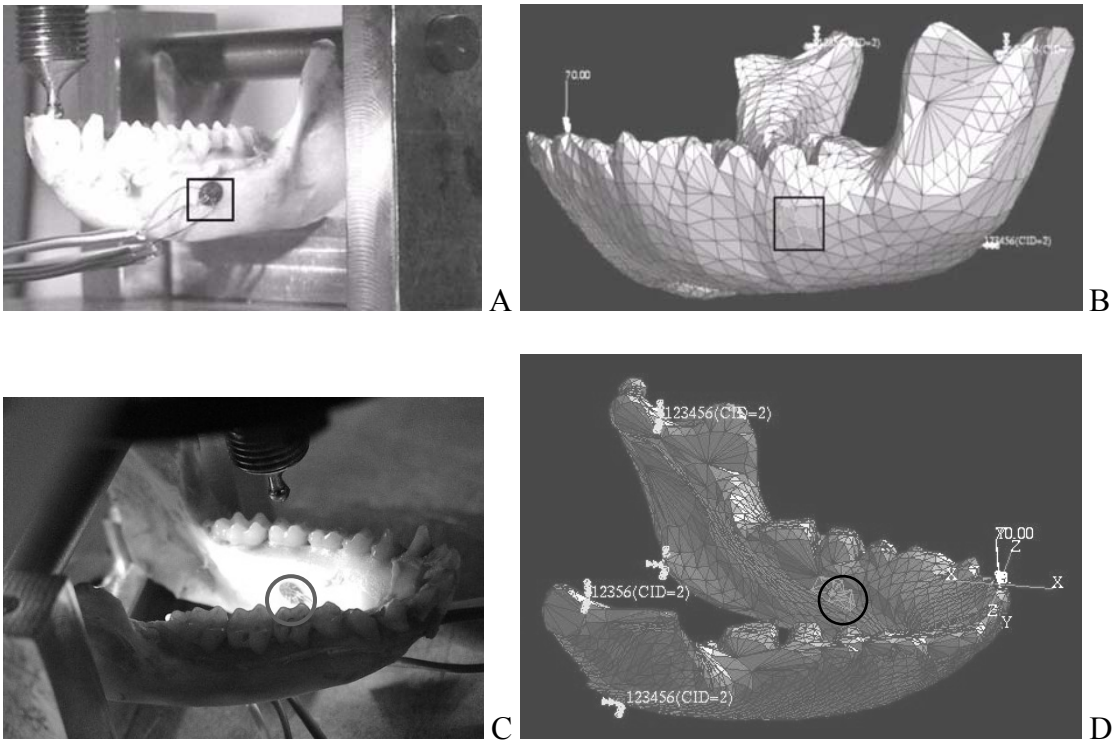

Figure 2-9. Prediction of surface strains from the FE dentate model. A) Experimental analysis—lateral strain gauge. B) FE analysis—lateral strain gauge. C) Experimental analysis—medial strain gauge. D) FE analysis—medial strain gauge. The models were subjected to a vertical occlusal load of 70 N which was applied to the left central incisor and were constrained bilaterally at condyles and angles.

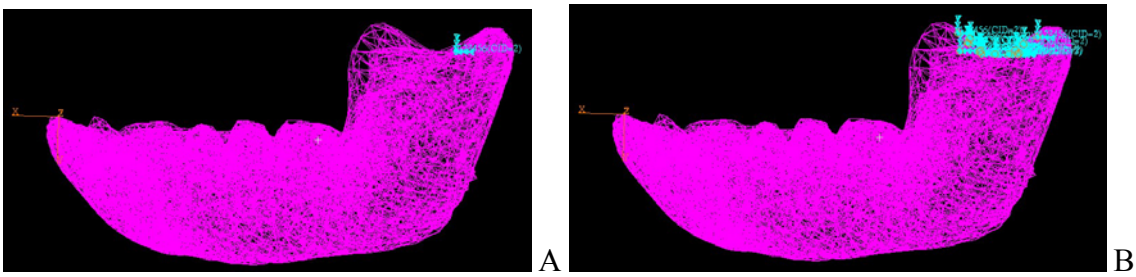

Figure 2-10. Variation in the number of constrained nodes in finite element models. Shown are the two extremes simulated: A) 1 node constrained B) 25 nodes constrained (only condylar constraints shown here). During different FEA iterations, an equal number of nodes were constrained on each side, at condyles and angles. Simulations were performed by reducing the nodal constraints bilaterally below the condyles and at gonion from 25 to 12, 6, 3 and 1 at each location.

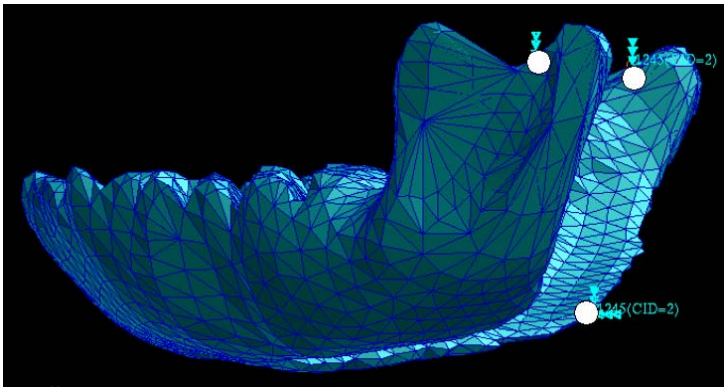

Figure 2-11. Relaxing boundary conditions by reducing the degrees of freedom. To account for the deflection of the specimen during the experiment, simulations were performed by relaxing successively the degrees of freedom at condyles and angles in the transverse direction.

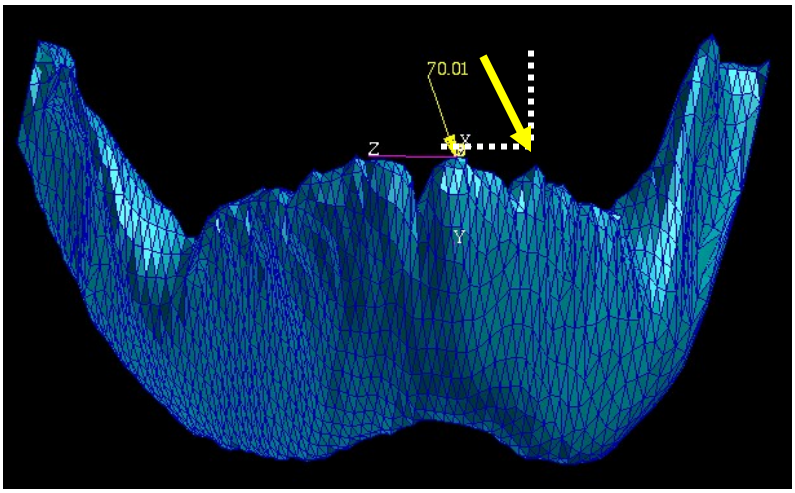

Figure 2-12. Alteration of direction of the applied force. Simulations were performed in which 4 different inclination angle values ($\theta = 0°, 5°, 10°, 20°$) were considered. The force vector was tilted in the frontal plane in an attempt to replicate the conditions of the experiment.

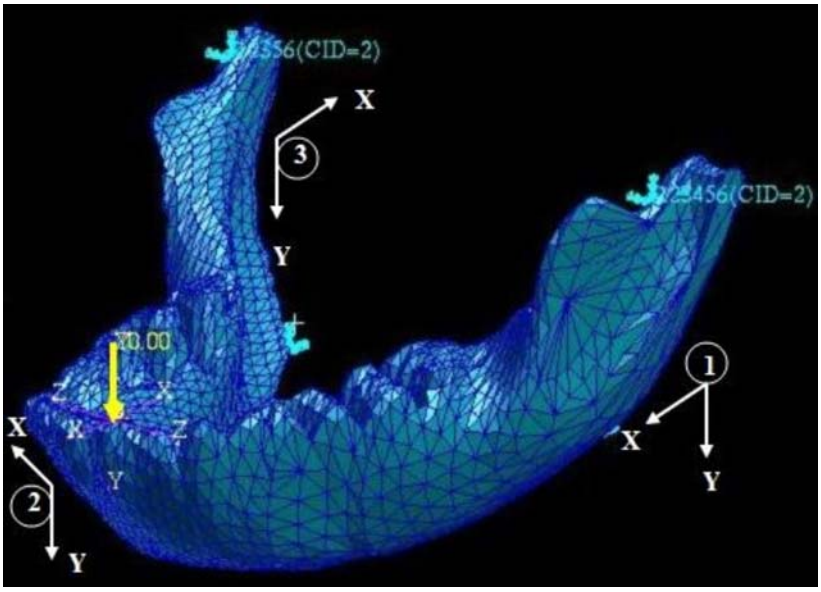

Figure 2-13. Heterogeneous transverse isotropic model showing specification of local material axes for three regions: right region (posterior corpus and ramus), symphyseal region (anterior corpus) and left region (posterior corpus and ramus). One local coordinate system was built for each region, which followed the longitudinal axis from one condyle to the other.

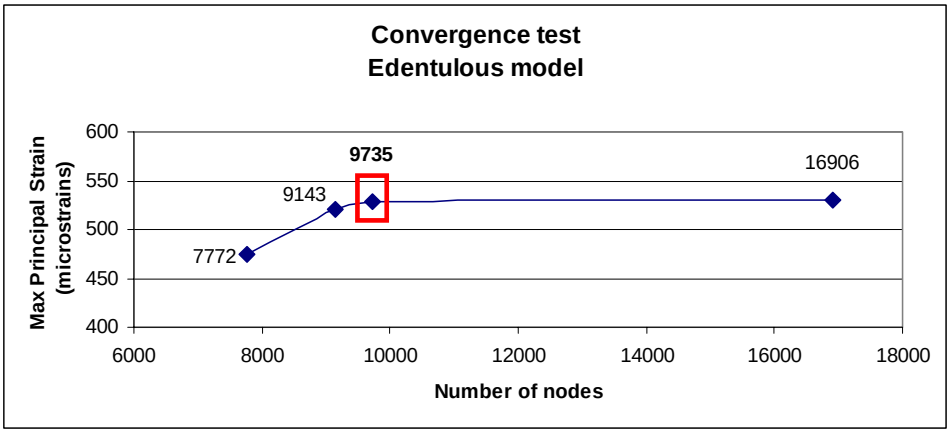

Figure 2-14. Convergence test. A convergence study was performed to determine the accuracy of the numerical models. FE meshes, from coarse to a very refined mesh with increased degrees of freedom, were created by assigning different GEL (global edge length) values. For the edentulous model, the coarsest mesh was created using the global edge length 10 (7,772 elements were created). The most refined mesh was created using the global edge length 0.5 (16,906 elements were created). The model used for simulations was created using a global edge length of 2 (9735 elements were created).

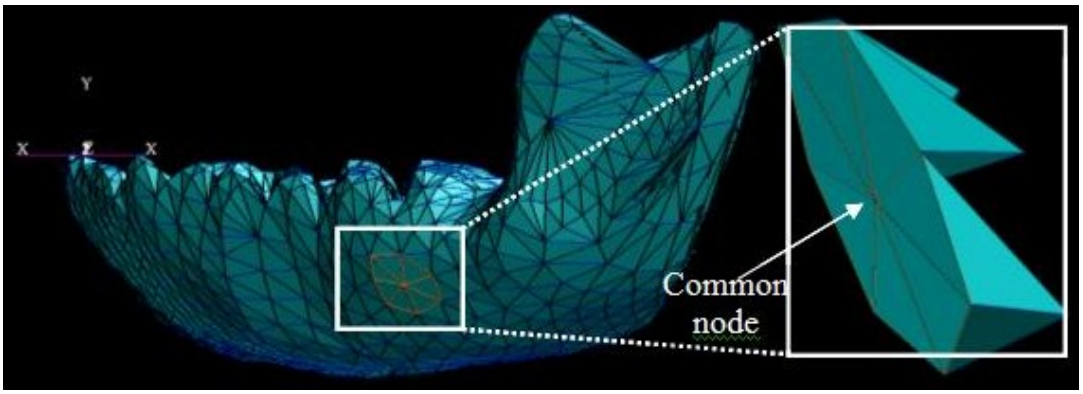

Figure 2-15. Method to record principal strain values based on averaging principal strain values of a node common to neighboring elements.

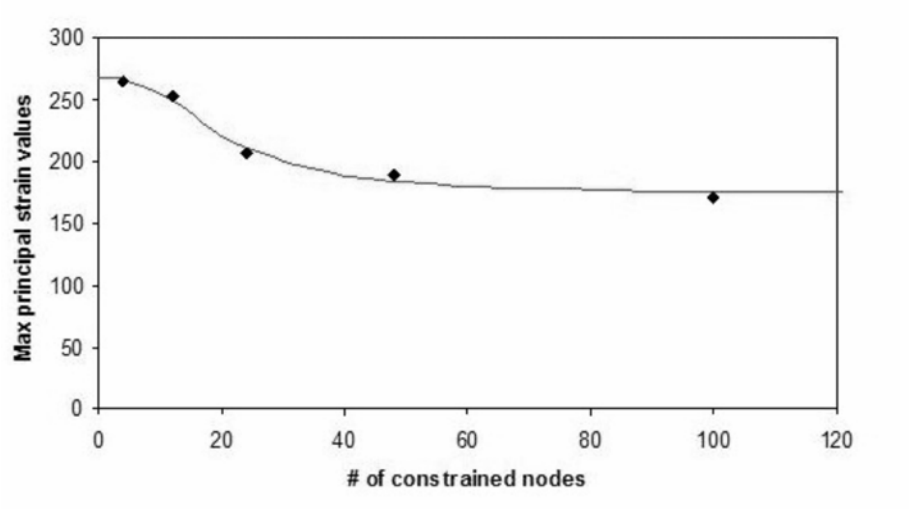

Figure 2-16. Effect of nodal constraint on predicted maximum principal strain values. The absolute number of constrained nodes has the predictable effect of influencing model stiffness. The greater number of nodes constrained results in a stiffer model and consequently produces lower principal strains.

CHAPTER 3
RELATIONSHIP OF STRAIN ENERGY DENSITY TO MORPHOLOGICAL VARIATION IN MACACA MANDIBLE

Introduction

In the last 25 years, extensive research on macaque mastication explored mandibular anatomy, mandibular movements during mastication, investigated biting and reaction forces occurring during mastication, portrayed the stress-strain behavior of the mandibular bone and overall, expanded our understanding of primate masticatory biomechanics. The macaque model is an excellent model for studying mastication, not only because of abundant available data, but also because it is a primate model. Studies on the primate skull are regularly used as reference for studying human masticatory biomechanics.

The mandible is characterized by a very odd and fascinating geometry: the cortical bone is distributed asymmetrically throughout the entire mandible. Despite extensive research on the mastication system, the biomechanical justification for this unique, asymmetrical distribution of cortical bone is still ambiguous. A direct relationship among mandible form, function, and mechanical load history, although crucial from a biomechanical point of view, was often assumed but has never been established. Despite an abundant record of biomechanical studies on mandibular morphology and profiles of strain (Hylander 1979a, Daegling and Grine 1991, Daegling 1993, 2002, 2004, Dechow and Hylander 2000) nothing is known about the relationship among the bone mass variation and Strain Energy Density (SED), one of the most important mechanical stimuli

for bone adaptation. One of the most important applications of FEA in functional morphology is to develop a realistic model of a biological complex structure, such as a mandible, and use it to explore its behavior in response to applied loads. Another significant application of FEA in functional morphology is to investigate complex biological processes, such as the functional adaptation activity in bone. Principles of biomechanics in combination with FEA tool could help unravel the mechanism responsible for the controversial functional morphology of the mandible and generally, enhance our understanding of mechanics and biology of bone. Understanding the functional morphology of the mandible is critical for uncovering the evolutionary transformations in facial bones form and expanding our knowledge of primate origin.

The present study concentrates on the relationship among strain, SED and bone mass variation. An improved mandible model, the mandible with masticatory muscles, is used to simulate the physiologic loading conditions which occur during mastication. Masticatory muscles (left temporalis muscle, left masseter-pterygoid sling, right temporalis muscle and right masseter-pterygoid sling) are simulated as individual vectors. FE analyses are performed in which the mandible is subjected to combined loading: torsion, direct shear and parasagittal bending. The most important biting models are simulated: mastication (open mouth) and clench (closed mouth). Principal strain values and SED data are recorded and used to explore the functional adaptation process in the mandible.

Regional Variation in Cortical Bone

The geometry of the mandibular cross-section is characterized by asymmetry or the absence of symmetry between the lateral and the medial aspect (Figure 3-1). Asymmetry is a characteristic feature of organic things that exist in nature. The shape of the

mandibular cross-section probably reflect, at some degree, the loading environment to which the mandible is subjected.

In the molar region, the lingual aspect of the mandibular corpus is thinner than the lateral aspect. The distribution of cortical bone changes from the molars toward the symphysis, such that under the premolars the thin lingual bone is much less apparent. At the symphysis, the mandibular thickness is greatest along the medial aspect, not on the lateral aspect as in the molar region. The base of the mandibular corpus in the molar region is the thickest part. At midcorpus, the mandibular corpus is thicker on the lateral aspect than on the medial aspect (Daegling 1993). In addition, experimental studies showed that not only the geometrical properties but also the mechanical properties differ significantly throughout the mandible. The mandible is very stiff in the longitudinal direction and usually stiffer on the medial aspect than on the lateral aspect (Dechow and Hylander 2000).

The most used measurable mandibular dimensions are: the arch length (the distance between the second molar and the most anterior incisor), the corpus vertical depth (the minimum distance between the base of the mandible and the alveolar border) and the transverse thickness of the mandibular corpus (usually the maximum thickness, at midcorpus). For this study, six mandibular sections were used: M_3 (third molar), M_2 (second molar), M_1 (first molar), P_4 (fourth premolar), P_3 (third premolar), C/I_2 (canine/incisor) (Daegling 1993).

Both functional and non-functional explanations, as presented in Chapter 1, have been explored by many researchers but currently there is no consensus regarding the unique distribution of bone mass in the mandible. These studies emphasized the

difficulties in studying the mandible due to considerable regional variation in thickness, cortical area, size, shape and mechanical properties throughout the bone. Because of the complexity of the mandible, many challenges are encountered when testing a mandibular specimen experimentally or a mandible model, theoretically.

Loading Patterns, Strain Gradients and Mandible Morphology

Numerous studies explored a functional relationship among the form and the function of the mandible (Hylander 1979a,b, 1984, Demes et al. 1984, Russell 1985, Hylander et al. 1987, 1998, Lahr and Wright 1996, Ross and Hylander 1996). A large body of research explored the relationship among the stress and strain patterns and the mandible morphology (Hylander 1979a, Daegling and Grine 1991, Daegling 1993, 2002, 2004, Dechow and Hylander 2000). Although extensive research exists, a functional correlation between the mandibular morphology and the stress and strain patterns has never been established and it is still one of the most controversial issues in physical anthropology.

Different regions of the mandibular corpus are loaded differently during mastication. In vivo experiments brought evidence that the macaque mandible is subjected to a combination of bending and torsion during mastication (Hylander 1979b, 1984, Hylander and Crompton 1986, Hylander et al. 1987, Hylander and Johnson 1997). Specifically, during the mastication, the mandible is primarily twisted about its long axis (the basal border of the mandible everts while the alveolar process inverts) and sheared perpendicularly to its long axis. In addition, the mandible is subjected to parasagittal and transverse bending (Hylander 1979b). The simultaneous application of twisting, bending and direct shear during mastication is a possible explanation for the unusual asymmetrical distribution of bone in the mandibular corpus (Demes et al. 1984, Daegling 1993).

According to this superposition theory, the shear stresses resulted from torsion and direct shear add up on the lateral aspect and are subtracted on the medial aspect of the mandibular corpus. Four biting styles are usually investigated: unilateral canine, bilateral canine, unilateral molar and bilateral molar (Dumont et al. 2005). Unilateral molar biting is the predominant mastication style for macaques (Hylander 1979b).

There is a considerable difference between how the working side of the mandible behaves when compared with the balancing side during unilateral mastication. The working side is the side of the mandible where the biting force is applied and the balancing side is the side of the mandible without the biting force. It was established that the working side is mostly twisted during unilateral mastication while the balancing site is primarily bent and in addition, twisted. However, given that primates chew on one side, then the other, both sides of the mandible experience twisting and bending regimes.

The loading patterns on the working side of the mandible and the distribution of stresses and strains during mastication were inferred from theoretical and experimental studies (Hylander 1979a,b, 1984, Knoell 1977, Bouvier and Hylander 1996, Daegling and Hylander 1997, 1998, Dechow and Hylander 2000). It is commonly accepted that during mastication, the working side of the mandible is subjected to torsion, direct shear and parasagittal bending or a combination of these.

- Torsion. The mandibular corpus is twisted about its long axis. The basal border of the mandible everts while the alveolar process inverts. Theoretically, to counter torsion, the transverse thickness of the mandibular corpus has to be increased. The maximum stress is at the surface.

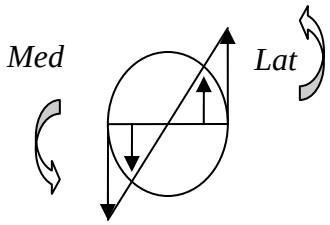

- Parasagittal Bending. The mandibular corpus is slightly bent along the long axis in the sagittal plane. According to Hylander, to counter bending, the mandibular corpus has to be deep. Bending along the long axis will results in compressive stress along the lower border of the mandible and tensile stresses along the alveolar process. Vertical shear stress due to bending varies as a parabola from zero at the bottom to a maximum at the centroid and zero at the top/bottom.

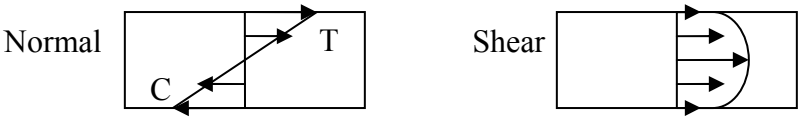

- Direct Shear. The mandibular corpus is subjected to direct shear, perpendicular to the mandible's long axis. To counter direct shear, the cross sectional area of the corpus has to be increased. The stress distribution is uniform.

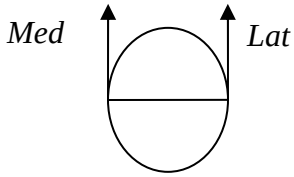

As it can be seen from the next stress distribution diagram, the shear stresses resulted from torsion and direct shear add up on the lateral aspect and are subtracted on the medial aspect of the mandibular corpus.

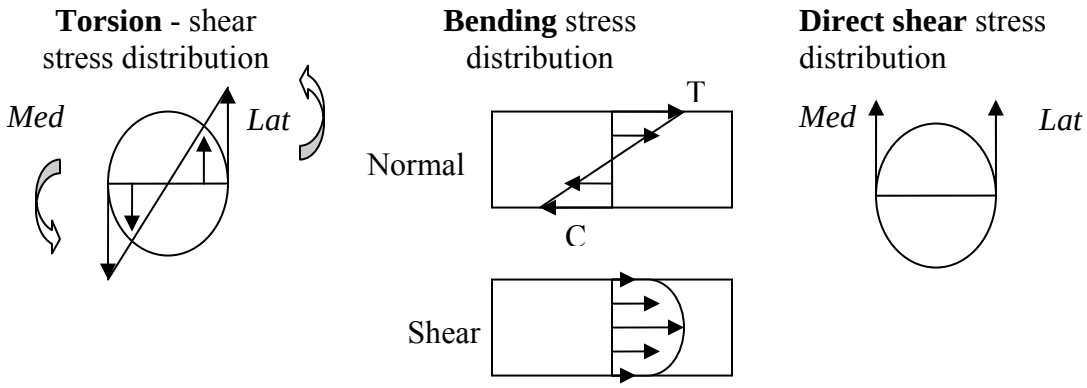

The strain history for the facial bones of *Macaca Fascicularis* is well-documented nowadays. Strain magnitudes are available for various skull regions: mandibular

symphysis (Hylander 1984), zygomatic arch (Bouvier and Hylander 1996, Hylander and Johnson 1997), supraorbital bar (Hylander et al. 1991, Bouvier and Hylander 1996) and mandibular corpus (Hylander 1979a,b, Hylander 1986, Hylander and Crompton 1986, Hylander et al. 1998, Bouvier and Hylander 1996, Dechow and Hylander 2000, Daegling and Hotzman 2003). Usually the strains recorded are in the 250-1000με range which is considered the functional interval (Fritton et al. 2000, Wood and Lieberman 2001, Daegling 2004). In conclusion, non-uniform and steep strain gradients were found for the *Macaca* facial bones: high strain have been found in the anterior zygomatic arch and in the mandibular corpus while low strains have been found in the posterior portion of the zygomatic arch and supraorbital bar. Particularly, in the mandible's case, experiments show that very low strains (below 200με) as well as very high strains (2000με) are present. It seems that for the mandible, the form does not always follow the function, or at least not all parts of the mandible are designed as to maximize strength and minimize bone tissue (Daegling and Hylander 1997, Daegling 1993).

Edentulous vs. Dentate Mandible Models

Two mandible models were obtained initially through 3D reconstruction from 90 CT scans: a dentate and an edentulous model. Both models were imported into a commercial finite element analysis package. As demonstrated in the previous chapter, the edentulous model performed always better than the dentate one in recreating the experimental strains. The dentate model was too stiff and consequently, the strain values obtained from it were extremely low when compared with the experimental strain values.

The finding that an edentulous model is more realistic than a dentate model is extremely significant and has important implications for both comparative studies of the

mandible and other finite element models of the mandible. The implications for comparative research (i.e. studies based on linear measurements of mandibles) are especially significant. Theoretical models used in comparative research are based on circular cross-sectional shape models, solid or hollow ellipse models, asymmetrical ellipse models or closed- or open-section models. To estimate the stresses and strains in the mandibular corpus, various shape indices are calculated. These indices are generally based on measuring the corpus cross sections. Because the appropriate data are generally lacking, the presence of teeth and the surrounding structures and the possible differences between dentate and edentulous models are ignored. For simplicity it is often assumed in comparative studies that "occlusal morphology, enamel thickness and attrition patterns have no necessary impact on stress distributions in the corpus"(Daegling and McGraw 2001). As presented in this dissertation, the FE dentate model is unrealistically stiff. Therefore, the way researchers are currently measuring mandibles is obviously overestimating strength and stiffness, but whether this introduces tolerable errors depends on how tooth roots scale with other mandibular dimensions. The degree of accuracy of these models, which do not account for the presence or absence of teeth within alveoli, in estimating the biomechanical behavior of the mandible or comparing differences between species is thus uncertain.

Various studies explored the influence of teeth, alveoli and periodontal ligaments on the strain history and explained the considerable role they play in the mandible during mastication (Daegling et al. 1992, Chen and Chen 1997, Rees 2001). Theoretically, the teeth and the specialized tissues surrounding the teeth can be simulated in the finite element models. However, due to modeling limitations, difficulties in estimating

boundaries between different tissues or to a lack of material properties data, the teeth and especially the surrounding specialized tissues, such as the periodontal ligament, are modeled as very simple structures or not modeled.

The teeth in a mandible are not inserted into the bone directly, they are isolated from the mandibular bone by the gingival margin and the periodontal ligament. Therefore, teeth do not contribute to the stiffness of the mandible. In this study, because of the limits of spatial resolution in conventional CT, the periodontal ligament was not visualized and consequently impossible to model. As a result, no interface existed between the teeth and alveoli. For the dentate model, the teeth were embedded directly into the mandibular bone and therefore they caused the dentate model to be much stiffer than indicated by experiments on the real mandible. The tooth row in the dentate model acted as a rigid layer on top of the mandible model and impeded the normal behavior of the model. The edentulous model created by "extracting" the teeth yields, as expected, more accurate results and eliminates the challenging task of modeling the periodontal ligament.

Strain Energy Density

The adaptation of bones to the environment is accomplished through many processes, including modeling and remodeling processes. Modeling and remodeling processes are responsible for reshaping and repairing parts of the bone. Modeling involves bone resorption in some place of the bone and formation in others, which result in sculpting the bones. This is usually a process that takes place during childhood. Remodeling affects the internal structure of the bone. Through remodeling, the microscopic damage is repaired and the accumulation of damage is prevented (Martin

2003). Without bone remodeling, the accumulation of fatigue damage could results in frequent bone fractures and our skeleton would collapse.

The most common mechanical stimuli that govern bone adaptation are: strain, stress, strain energy, SED, strain rate, strain frequency and fatigue microdamage. However, despite extensive research over the last 100 years, the mechanical stimuli that govern bone adaptation still remain unknown. Strain parameters or strain perturbations are generally accepted as the most significant mechanical stimuli for bone adaptation (Turner et al. 1997). Research shows that increased physical activity results in increased bone mass and inactivity result in reduced bone mass. Researchers believe that achieving a "favorable strain environment" is more important for bone adaptation than peak strain values (Sommerfeldt and Rubin 2001). Frost in his mechanostat theory described four mechanical usage windows or intervals and strain thresholds (Frost 1994). Furthermore, a static load applied during a long period of time will produce bone loss, therefore not only strain or a strain interval but strain-rate parameter is also important (Roberts and Hart 1997). Other studies indicate that not only the magnitude and the duration of the mechanical loading, but also the frequency of the load application needs to be considered (Forwood and Turner 1995). Rubin and colleagues proposed that bone adaptation is not governed by peak or maximum strains and it is in fact governed by extremely small strains (Rubin et al. 2002, Judex et al. 2006). Thus, extremely low-magnitude, high-frequency mechanical signals rather than low-frequency, high-magnitude stimuli can have a significant influence on bone adaptation and actually trigger bone gain. The bone tissue responds not only to mechanical parameters but to a multitude of biophysical

stimuli. The specific stimuli and the specific mechanical parameters responsible for bone adaptation still remain a source of great controversy.

Strain energy density has been considered by many researchers a critical stimulus for bone adaptation which can successfully predict the bone adaptation activity (Huiskes et al. 1987, Brown et al. 1990, Fyhrie and Carter 1990, Katona et al. 1995, Turner et al. 1997, Barbier et al. 1998, Cowin 2001, Mellal et al. 2004). Strain energy is the energy stored in a material when the material is deformed under an external load. Strain energy is the area under the load deformation curve. The strain energy obtained by applying the load P as the material deforms with a deformation x is:

$$U = \int_0^{x1} P dx$$

Strain energy can be determined from the load-deformation curve. However, it does not give any information about the properties of the material since the results will depend on the dimension of the specimen used. Because of this, the strain energy per unit volume, the strain energy density, is usually considered. SED, when applied to bones, is the rate of variation in bone density (Mellal et al. 2004). Strain energy density is the area under the stress-strain curve.

For a rod, the volume (V) is equal with V=A*L, where A is the cross-sectional area and L the length of the rod.

$$\frac{U}{V} = \int_0^{x1} P dx * \frac{1}{V} \quad ; \quad \frac{U}{V} = \int_0^{x1} \frac{P}{A}\frac{dx}{L} \quad ; \quad \frac{U}{V} = \int_0^{\varepsilon 1} \sigma_x d\varepsilon_x$$

P/A is the normal stress, σx, and x/L is the normal strain, εx. The strain energy density is:

$$u = \int_0^{\varepsilon 1} \sigma_x d\varepsilon_x$$

A strain energy density criterion was further developed in which SED is the main stimulus. The rate of change of apparent density at a particular location in the mandible is described by the following formula:

$$\frac{\partial \rho}{\partial t} = B\left(\frac{u}{\rho} - k\right)$$

where ρ is the apparent density, t is the time, B and k constants that quantify bone gain or loss, and u is the strain energy density. The area in which no net change of bone density occurs, the zone between bone densification and bone resorption, is the lazy zone (bone homeostasis). A lazy zone can be expressed by using the following formulas, where s is expressed in percents and represents the extent of the lazy zone:

$$\frac{\partial \rho}{\partial t} = \begin{cases} B\left(\frac{u}{\rho} - (1+s)k\right) & if \quad \frac{u}{\rho} > (1+s)k \\ 0 & if \quad (1-s)k \le \frac{u}{\rho} \le (1+s)k \\ B\left(\frac{u}{\rho} - (1-s)k\right) & if \quad \frac{u}{\rho} < (1-s)k \end{cases}$$

In 1892, the Wolff's law of bone adaptation was published. This was one of the first studies on bone adaptation. The Wolff's law states that bones react to the loading environment to which they are subjected and adapt accordingly (Martin et al. 1998). However, the mechanisms responsible for bone adaptation were unknown. Wolff suggested that bone is an optimal structure that exhibit maximum efficiency with minimum mass. The implicit assumption underlying Wolff's law is that, if a functional correlation between the morphology and function of the mandible exists and bone is an optimized load bearing structure, there should be near uniform strain levels throughout the bone.

Later, Frost proposed the mechanostat theory according to which bones adapt to mechanical loads in order to sustain those loads without hurting or breaking (Frost 1986, Frost 1998, Schoenau and Frost 2002). The mechanostat is a combination of non-mechanical factors (hormones, calcium, vitamins, etc), mechanical factors (loads, strains, etc), modeling and remodeling mechanisms, thresholds and possibly other mechanisms and propose that the bone adaptation is an error-driven process. Bone will respond and adapt accordingly only when strains are above or below certain thresholds, when the strains are not comprised within the physiologic loading zone. Below a certain strain threshold, called remodeling Minimum Effective Strain (MES), bone loss is predicted. The strains in this window range between 50-200με and below. Between 50-200με and 1500 - 3000με, is the physiologic loading zone, lazy zone, dead zone or equilibrium interval. In this interval bones do not respond to mechanical loads and do not adapt. If the strain levels exceed the 1500 - 3000με threshold, called the modeling Minimum Effective Strain (MES), bone gain is predicted. Above 4000με threshold, called repair Minimum Effective Strain (MES), the pathologic overload zone begins. Frost proposed that the mechanostat model is applicable "in all amphibians, birds, mammals, and reptiles of any size, age and sex" (Frost 1998). However, Frost's theory is a qualitative theory which presumes that local strains regulate bone mass formation or resorption.

The process of functional adaptation is however not fully understood. Mathematical rules or expressions were developed to link mechanical stimuli, which relate to the adaptation process, to stress and strain fields, which relate to a pattern. Strain energy density criterion, based on evaluating a lazy zone interval, was developed to relate the strain energy density stimulus to adaptation and strain gradients.

Theoretical and experimental studies on the mandible offer conflicting conclusions regarding a possible relationship among the strain field and the distribution of bone mass. The principal reasons for this discrepancy arise from the complexity of the mandible. To create a biomechanical model of the mandible is a very challenging task. Theoretical models (solid, hollow, asymmetrical ellipse models) can offer insight into the mandible biomechanics but because they do not account for the intricate materials properties of the mandible, they cannot be used for complex biomechanical analyses. The inconsistency in results might arise also from using different methods to test the mandible. In vivo or in vitro experimental methods are considered limited field methods. The mandible is usually analyzed only in certain regions "of interest." Other limitations contribute to the problem: the load magnitude and the loading environment cannot be controlled in an in vivo experiment. In vitro methods can control the load magnitude but have difficulties is recreating the in vivo environment. The boundary conditions applied in vitro (loading environments, how the mandible was supported, how it was constrained, etc) are not quite similar with the in vivo boundary conditions. The results will be greatly affected by all these changes. Moreover, experimental studies can only estimate from a couple sites "of interests" the strain gradients for the entire mandible.

The best solution to combine many of the advantages of in vivo and in vitro methods is the finite element method. The finite element model of the mandible, even if it is a simplified representation, can be successfully used to estimate the real mandible behavior. The geometry and realistic material properties can be simulated in the model. The load magnitude and the loading environment can be controlled during the analysis. The stress and strain results can be obtained throughout the entire mandible not just in

some regions of interest. Most important, an FEA can predict regions in the model with maximum stress and/or maximum strain values. Strain gradients throughout the model can be easily calculated, plotted and displayed. However, the success of FEA strongly depends on several significant factors: accurate geometry of the FE model, realistic material properties and replicating physiologic boundary conditions (restraints and applied loads).

The current work aims to use FEA to answer questions related to functional morphology that the limited field methods cannot resolve. The objectives of this study are to attempt to explain bone mass variation in the mandible using FEA. The first hypothesis was that the mechanostat theory is applicable to all bones, including the mandible. Therefore, the equilibrium that is supposed to exist under the mechanostat model fit the mandibular strains and SED. The second hypothesis concerns the implicit assumption underlying Wolff's law, that at all locations uniform SED values will be measured. This hypothesis questions whether SED and strains can be related to bone mass variation in a predictable way.

Materials and Methods

Strain Energy Density Criterion

The lazy zone interval was calculated using the parameters available in the literature: k=0.004 J/g, B=1 $(g/cm^3)^2$/MPa time units, s = 10% (Figure 3-2) (Weinans et al. 1992, Turner et al. 1997, Mellal et al. 2004). The lazy zone interval is:

$$0.0036 \leq \frac{u}{\rho} \leq 0.0044 \ \text{MPa}/(\text{gcm}^{-3})$$

The density (ρ) was estimated using the relationship (Carter and Hayes 1977, Huiskes et al. 1987, Weinans et al. 1992):

$E = 3790 \times \rho^3$

The elastic modulus of the model corresponding to cortical bone was chosen as E = 17 GPa therefore the density is ρ=1.65 g/cm^3. The value for the elastic modulus was 17 GPa to correspond with the value assigned to the FE model. Consequently, the calculated lazy zone interval for the strain energy density corresponding to ρ=1.65 g/cm^3 is:

$0.00594 \leq u \leq 0.00726$ (MPa)

Some studies choose a density interval between a minimum density value close to zero (a zero value cannot be use in FEM) and a maximum calculated density value (Weinans et al. 1992, Turner et al. 1997, Mellal et al. 2004):

$\rho_{min} \leq \rho \leq \rho_{max}$; 0.001 g/cm$^3 \leq \rho \leq$ 1.65 g/cm^3

Consequently, the calculated lazy zone interval for the strain energy density corresponding to a density interval of 0.001 g/cm3 $\leq \rho \leq$ 1.65 g/cm3 is:

$0.0000036 \leq u \leq 0.00726$ (MPa)

Finite Element Analysis

The FE analyses were performed using the edentulous mandible model. The most complex case of heterogeneity and directional dependence studied previously was chosen for the analysis. The analyzed model was heterogeneous and transversely isotropic. Material properties were assigned using a local coordinate system: the 3-axis was defined as following the length of the mandible, with the 1-axis mediolaterally oriented and 2-axis superoinferiorly oriented. The sets of material properties were assigned for cortical and trabecular bone. Cortical bone was assigned material properties in the frontal plane and in the longitudinal direction ($E_{1,2cortical}$ = 13 GPa, G_{12} = 5 GPa, $E_{3cortical}$ = 17 GPa, G_{23} = 6.91 GPa, ν_{12} = 0.3 and ν_{23} = 0.229). The trabecular region was modeled as isotropic

($E_{trabecular}$ = 1.5 GPa and $\nu_{trabecular}$ = 0.3). Three regions, right (posterior corpus and ramus), anterior corpus, and left (posterior corpus and ramus) were defined. One local coordinate system was defined for each region. The finite element package was used to assign material properties for cortical and trabecular bone to each region, according to their local coordinate system.

The 3D volumetric reconstruction technique allowed a faithful reproduction of the real mandible specimen. However, as with any model of a biological structure, the model has several limitations. Because the model is developed from a stack of outer contours, a high degree of internal anatomical structures cannot be simulated. The periodontal ligament for example, could not be visualized and simulated. The method of assigning material properties has several disadvantages: limitation in the number of material assigned, averaging data for each voxel, etc. The physiologic loading environment is too complex and mostly unknown and cannot be simulated entirely (assumptions needed for the mastication forces magnitude and orientation). In addition, the mandible model is a linear static model, used in a linear static analysis and, therefore, it cannot inform a dynamic process, such as the bone remodeling process.

A new parameter, masticatory muscles, was introduced in an attempt to improve previous modeling efforts and simulate more realistically the physiologic loading environment (Marinescu et al. 2005). The human masticatory system is well described and analyzed in the literature (Pruim et al. 1978, 1980, Koolstra and van Eijden 1992, 1997a, 1997b, 1999, Koolstra 2002, 2003, Korioth and Hannam 1994a,b, Korioth and Johann 1999). The masticatory system can be modeled as a constrained lever model and it is based on the assumption that the forces in the mandible are related through a triangle

of support (Greaves 2000, Spencer 1998). The unconstrained lever model uses equilibrium equations to determine the relationship among the forces in the mandible (Spencer 1998, 1999). The muscle resultant force (M), the bite force (B) and the joint reaction forces (J_W and J_B) are determined through spatial relationship. The model assumes that the working and the balancing side muscle forces are equal and the muscles resultant force lies in the midline.

The information available about the *Macaca* masticatory system is limited compared with the information available about the human masticatory system. The documentation available concerning *Macaca* masticatory system consists usually of physiologic data or in vivo electromyographic data (EGM). The internal architecture, fiber length and cross sectional area of macaque masseter muscle and pterygoid muscle were described in detail by Anton (Anton 1999, 2000). There are many studies that offer electromyographic data for the *Macaca* masticatory system (Hylander and Johnson 1994, Hylander et al. 2000).

There are multiple problems in simulating the masticatory system. The extremely complex system consists of: the mandible, which is moved in respect with the skull, two intricate temporomandibular joints and masticatory muscles. The mandible has an extremely complicated irregular geometry and it is characterized by a large variation in mechanical properties. The temporomandibular joint is the articulation between the condyle and the temporal bone. The condyle and the temporal bone are separated by a cartilaginous structure called the meniscus. The masticatory system consists of many muscles with different shapes and sizes. It is impossible to determine the contribution of each muscle from in vivo studies. To simulate the masticatory muscles, the muscles

forces or the resultant masticatory force have to be estimated. Both the magnitude and the direction of the force vectors have to be known. Because the masticatory system is such a complex system, the experiments performed are very challenging and the experimental data very difficult to collect and validate. The mastication models are usually based on many assumptions and simplifications (Pruim et al. 1980, Meyer et al. 2000, Erdman et al. 2002, Wagner et al. 2002, Feller et al. 2003). The most used assumptions in simulating the mastication muscles are:

- The forces of the mastication muscles can be simulated as vectors.
- The forces of the masseter and medial pterygoid muscles can be added and simulated through a single vector (the masseter-pterygoid sling).
- The main mastication forces simulated are the forces exerted by the masseter-pterygoid sling and the temporalis muscle.

In the current study, the masseter-pterygoid sling and the temporalis muscles were simulated by applying two loads at condyles and angles, on both sides of the mandible (Figure 3-3). Several researchers attempted to determine the maximum possible mastication force using mathematical models or experimental models, by using electronic strain gauges (Howell and Manly 1948). A few of the magnitudes reported for the maximum possible mastication force are: 250 N (Koolstra and van Eijden 1992) and 300 N (Van Ruijven et al. 2002) for human mandibles and 154-258 N for monkey mandibles (Reitzik et al. 1978). The magnitude of the maximum resultant mastication force was therefore considered equal to 300N. The current model was inspired by the lever model in which the muscle resultant applies a force that is resisted at the biting point. The working and the balancing side muscle forces are considered equal. According to experimental findings, the working to balancing (W/B) strain ratio is usually different than one. Hylander found that the ratio of working-side muscle force to balancing-side

muscle force is approximately 1.5:1 in macaques (Hylander 1979a) and the W/B strain ratio is 1.6 for macaques chewing hard food (Hylander et al. 1998). However, as experimental work showed, for some macaque specimens, the working-side strains are very similar to the balancing-side strains and the W/B strain ratio is very close to one (Hylander et al. 1998, macaque 4, exp.E). Four loads of 75N each were applied to the mandible model to account for the left temporalis muscle, the left masseter-pterygoid sling, the right temporalis muscle and the right masseter-pterygoid sling.

The orientation for the masseter-pterygoid sling was chosen according to the data available for the Macaque masseter muscle. The fibers of the Macaque masseter muscle are oriented between 65° and 85° to the occlusal plane (Anton 1999). The sine of the masseter muscle angle for monkeys is 0.93 which gives a 68° angle from the horizontal, occlusal plane (Dechow and Carlson 1990). Only the angles between the muscles and the occlusal plane were considered in the Dechow and Carlson study. The angle of inclination of the masseter-pterygoid sling in the frontal plane was estimated at 45° (Hylander 1979b). Therefore, in the current study, the masseter-pterygoid sling vector was inclined 45° in the frontal plane and 68° from the occlusal plane. The sine of the temporalis muscle angle for monkeys is 0.87 which gives a 60° angle of inclination from the occlusal plane (Dechow and Carlson 1990). The temporalis was considered to act only in the sagittal plane. The insertions of the masticatory muscles were simulated by points on the mandibular angles and the coronoid process of the mandible, on each side.

The model was constrained at condyles (Hart et al. 1992, Futterling et al. 1998). An equal number of nodes (three) were totally constrained at condyles on each side. Chewing consists of rhythmic open-close jaw movements. Therefore, the two most important

loading cases were simulated: mastication (open mouth) and clench models (closed mouth). Unilateral canine, bilateral canine, unilateral molar and bilateral molar are the most used biting styles (Dumont et al. 2005). Unilateral molar biting case was simulated in the current study because, according to the literature, it is the predominant mastication style for macaques (Hylander 1979b).

The mastication model. The mastication model consists of simultaneous application of bending, torsion and direct shear, a combined loading pattern which is believed to occur most often (Figure 3-4). Torsional loading was accomplished in two ways: by using a tilted occlusal load and by using muscle vectors. The masseter-pterygoid sling vector acts in twisting the mandibular corpus about its long axis in such a way that the basal border of the mandible everts while the alveolar process inverts. This torsional loading was described by Hylander as the primary source of stress (Hylander 1979a,b). The mastication force is tilted by 15° in the frontal plane, toward the right side of the mandible because, previous studies considered more realistic to simulate a tilted bite force. Experimental work showed that a vertical mastication force is highly questionable. It is believed that the lateral component of the bite force contributes to increase twisting of the mandible during mastication (Daegling and Hotzman 2003). Occlusal loading was accomplished by applying a point load (100 N magnitude) to the left second molar. A point load is theoretically applied at one point. However, in order to avoid an infinite stress value (a load applied over a zero area), finite element theory converts the concentrated load into a distributed one over a small area around the point. Therefore, in FE the point load can be considered an uniform distributed loads over a small area of the molar surface.

The clench model. The clench model, described initially by Korioth and colleagues and frequently used in FE, simulates a static molar bite (Korioth et al. 1992). The mandible was restrained at condyles and at the second lower molar. In this model there was no mastication force applied, as in the previous model. The molar was totally constrained in the vertical direction (clench case or close mouth case) and partially constrained in the horizontal plane. The same magnitude and orientation as previously were used for the four muscle vectors.

The masseter muscle of the Macaque is oriented between 65 and 85 degrees to the occlusal plane (Anton 1999). Korioth uses multiple vectors to simulate one masticatory muscle load (Korioth et al. 1992). In the current study, several FE simulations were performed in which the masseter-pterygoid sling vector was replaced by 3 vectors with different orientations: 65°, 75° and 85° from the occlusal plane. The resultant of the three vectors is oriented 75° from the occlusal plane (75N magnitude). Evidently, the FE simulations of the physiological loading environments cannot account for all the factors that influence the masticatory strains measured in vivo, not only because a simplified model is used to approximate the behavior of the real, complex mandible specimen but also because the physiological loading environment is not entirely known.

The experimental data available in the literature for the cortical thickness for *Macaca fascicularis* was used in this study for making the correlation assessment between cortical thickness and SED and strain values (Daegling 1993). Six mandibular sections are used in experimental studies: M_3 (third molar), M_2 (second molar), M_1 (first molar), P_4 (fourth premolar), P_3 (third premolar), C/I_2 (canine/incisor) (Figure 3-5). The variation in transverse cortical thickness in the mandible is presented in Table 3-1. The

same mandibular sections and the same mandibular regions were identified in the FE mandible model. The principal strains and the SED values were automatically calculated for the entire mandible model using the finite element analysis package. The values were manually extracted at each section, for each region.

For each mandibular section, principal strain and SED values were extracted for the lateral, basal and medial region. First, the six sections were identified in the model by using the sections described in the experimental study. Second, for each section, three regions were identified: lateral midcorpus, basal and medial midcorpus. One common node and its neighboring elements were identified for each region. The values for the five or six neighboring elements situated at the each location were found and their values averaged. Consequently one average value was obtained for each region. Eighteen averaged values were obtained in the end: three values (lateral, basal and medial) for each of the six sections.

Results

According to the published experimental data, the cortical thickness varies considerably within each mandibular region and between mandibular sections. In this study, using FEA, SED and principal strain values were obtained at the same locations and plotted against published thickness data. SED and principal strain values were recorded for the mastication model (Table 3-2, Table 3-3, Table 3-4) and clench model (Table 3-5, Table 3-6, Table 3-7). The results were collected from six mandibular sections (third molar, second molar, first molar, fourth premolar, third premolar, canine/incisor) for the lateral midcorpus, base and medial midcorpus.

Strain Energy Density

The SED profiles for the mastication and clench models are very similar. For the lateral midcorpus region, the SED values tend to increase slightly from the anterior corpus toward the molar region (Figure 3-6a). The minimum values are found at the symphysis region and maximum values are found at the molar region. The thickness values increase from the premolar region toward the molar region. If the value for the most anterior section is considered an outlier and is excluded, the correlation between SED and thickness is positive strong. The correlation between SED and thickness for the lateral midcorpus region is 0.673 (p-value $\leq$ 1) for the mastication model and 0.445 (p-value $\leq$ 1) for the clench model.

The SED values recorded for the basal region also tent to increase from the anterior corpus toward the molar region, with small values in the anterior corpus and higher values toward the molar region (Figure 3-6b). In the mandibular base region, the thickness values increase similarly from the premolar region toward the molar region. The overall trend for the medial region is the decrease of the SED values from the anterior corpus toward the molar region (Figure 3-6c). The highest values are encountered in the anterior corpus. The correlation between SED and thickness for the basal region is 0.698 (p-value $\leq$ 1) for the mastication model and 0.795 (p-value $\leq$ 1) for the clench model.

The thickness values on the medial aspect decrease correspondingly, from the anterior corpus toward the molar region. The correlation between SED and thickness for the medial midcorpus region is 0.634 (p-value $\leq$ 1) for the mastication model and 0.504 (p-value $\leq$ 1) for the clench model. An arbitrary path was created along the midcorpus and the overall SED profile was plotted along the path (Figure 3-7). The path was created

in a horizontal plane between the anterior and posterior mandibular sections. The SED values are generally higher on the anterior part of the corpus than on the posterior region of the mandible.

For the mastication model, the SED values found at the lateral or the medial midcorpus are always higher than along the mandibular base (Figure 3-8 a, b). Also, the values found at the lateral midcorpus generally exceed the values found at the medial midcorpus (Figure 3-8c). The only exception is the value for the most anterior mandibular region, the symphysis. Only in this region (C/I_2), the SED value on the medial aspect is higher than the SED value recorded for the lateral aspect. The exact same pattern is encountered for the clench model. The SED values found at the lateral and medial midcorpus are higher than along the mandibular base (Figure 3-9 a, b) and the values found at the lateral midcorpus exceed the values found at the medial midcorpus (Figure 3-9c), with the only exception at the symphysis.

The SED values obtained from all the sections and regions were plotted on the same graph and the lazy zone interval was determined for each model. The SED values obtained in the current study range from $0.00283 \leq U \leq 0.01213$ (MPa). As it can be seen from Figure 3-10a, almost half of the values are within the lazy zone interval for the mastication model. The values situated within the lazy zone interval were collected from the medial midcorpus and basal area. A few of the SED values collected from the lateral midcorpus fall within the lazy zone interval. For the clench model, a few values from the medial midcorpus and basal area are situated within the lazy zone interval (Figure 3-10b). Several SED values are higher than the values comprise in the lazy zone interval, especially for the lateral midcorpus.

Strain

The maximum and minimum principal strain values were recorded for the mastication model (Table 3-2, Table 3-3, Table 3-4) and clench model (Table 3-5, Table 3-6, Table 3-7) for the lateral midcorpus, base and medial midcorpus. The ratio between the maximum and minimum principal strains was obtained and plotted against the mandibular thickness (Figure 3-11). As in the previous case, the strain profiles for the mandibular and clench models are very similar.

For the lateral midcorpus region, the strain values tend to increase from the anterior corpus toward the molar region (Figure 3-11a). The minimum strain values are found at the symphysis and maximum strain values are found in the molar region. The thickness values increase following the same pattern from the premolar region toward the molar region. The correlation between principal strain ratio and thickness for the lateral midcorpus region is 0.990 (p-value $\leq$ 0.001) for the mastication model and 0.966 (p-value $\leq$ 0.007) for the clench model.

For the mandibular base, the strain values increase from the anterior corpus toward the molar region, following very closely the thickness profile (Figure 3-11b). The overall trend for the medial region is the decrease of the strain values from the anterior corpus toward the molar region (Figure 3-11c). High strain values are encountered at the symphysis for both, mastication and clench model. The correlation between principal strain ratio and thickness for the basal region is 0.803 (p-value $\leq$ 1) for the mastication model and 0.761 (p-value $\leq$ 1) for the clench model.

On the medial midcorpus aspect, the thickness values decrease from the anterior corpus toward the molar region. The maximum thickness and strain values are encountered at the symphysis. The correlation between principal strain ratio and

thickness for the medial midcorpus region is 0.638 (p-value ≤ 1) for the mastication model and 0.668 (p-value ≤ 1) for the clench model.

The regional strain values for the mastication and clench models are very comparable. The strain values found at the lateral or the medial midcorpus are generally higher than along the base (Figure 3-12 a, b). The experimental thickness values found at the lateral or the medial midcorpus are lower than along the mandibular base. For the anterior region of the mandible, the strain values found at the medial aspect are higher than the strain values found at the lateral midcorpus for both loading cases. For the posterior region of the mandible, the strain values found at the medial aspect are lower than the strain values found at the lateral midcorpus (Figure 3-12c). Similar strain patterns are encountered for the clench model (Figure 3-13).

Maximum principal strain values obtained from all six sections and three mandibular regions were plotted on the same graph. The maximum principal strain value was encountered at the symphysis, on the medial midcorpus. The minimum principal strain value was found basally, at the anterior part of the mandible. All the maximum principal strain values for mastication and clench models, ranging from 251με to 1421με are within the proposed 50-1500με lazy zone interval (Figure 3-14).

To better understand the strain pattern inside the mandibular bone during mastication, strain profiles were determined within several mandibular cross sections along transverse thickness, from the medial aspect toward the lateral aspect. Strain data was collected and plotted for all the mandibular sections C/I2 (canine/incisor), P3 (third premolar), P4 (fourth premolar), M1 (first molar), M2 (second molar), M3 (third molar), from symphysis, the most anterior cross-section, to the most posterior cross-section, the

molar region. Horizontal paths were created in a horizontal plane between the medial and lateral midcorpus within each cross-section. The maximum principal strain values were plotted along the paths (Figure 3-15). The strain values are higher on the medial aspect than on the lateral aspect for the anterior region of the mandible. On the contrary, the strain values are lower on the medial aspect than on the lateral aspect for the posterior region of the mandible.

To investigate the relation between strain values and the orientation of the muscle vector, several FE simulations were performed in which the orientation of the masseter-pterygoid sling vector from the occlusal plane was altered (Table 3-8, Table 3-9). Initially, the muscle vector is oriented at 68° from the occlusal plane. When the muscle force is simulated by using more vectors, the resultant vector is oriented at 75° from the occlusal plane. The resultant is therefore oriented more vertically than the previous single vector. As results show, using a more vertically oriented muscle vector will result in decreasing the principal strain values.

FE Model Accuracy in Terms of Cortical Asymmetry

In this study, special consideration was given to the degree of FE model accuracy and how the assigned material variation in the model reflects the actual mandibular asymmetry documented for Macaca. There are at least four reasons which explain how the cortical asymmetry was captured in the FE model. These reasons are related to: the geometry of the model, FE mesh generation and element size, method of assigning material properties, and strain results.

Geometry of the model. The chief advantage of this mandible model is that it is developed using volumetric reconstruction from CT scans. This procedure is successfully

used to create specimen-specific FE models characterized by high geometric precision. The geometric model is first reconstructed from CT cross sections. The curves that contour the geometric model were then imported in the finite element analysis package. The model was then populated with tetrahedral elements (Tet10). This model generation method guarantees that the size and shape of the model reflects in great detail the specimen's real biological structure and therefore, reflects the unusual medial versus lateral asymmetry present in the mandible. For example, the medial aspect of the mandibular midcorpus is substantially curved and the overall shape is more complex that the corresponding lateral aspect of the mandibular midcorpus.

FE mesh generation and element size. The model was meshed with a tetrahedral mesh using quadratic tetrahedral elements. A special mesh generation technique, AutoTetMesh, was used in the finite element analysis package to mesh the model. AutoTetMesh is a highly automated technique that allows curvature-based meshing. This technique is especially suitable for complex models because allows the creation of finer mesh in regions of high curvature. Therefore, AutoTetMesh allows mesh refinement based on curvature by distributing larger elements in a less critical region of the model and smaller elements in an area of high curvature and therefore, higher stress. This automated meshing technique offers the significant advantage of refining the mesh locally, as needed. Mesh refinement improve the solution, maximize the accuracy of the model and minimize the computational expense.

The cross-sections through the FE mandibular corpus show that smaller elements are encountered on the medial aspect of the mandibular corpus and larger element are encountered on the lateral aspect. This distribution coincides exactly with the cortical

bone distribution in the mandible. At midcorpus, the mandibular corpus is thinner on the medial aspect than on the lateral aspect. This asymmetrical distribution in the FE model is due to the difference in geometry between the two regions. The medial aspect is highly curved at midcorpus. Thus, this region is considered a "critical" region, prone to higher stress, and it was meshed with smaller elements. The geometry of the lateral aspect is simpler, not curved, therefore this region is considered a regular region and it was meshed with larger elements.

To estimate the medial and lateral "cortical thickness" in the FE model, the element sizes were measured in the following way. Starting from the node previously chosen at midcorpus on the medial or the lateral side for each of the six cross-sections, the distance between two neighboring nodes was measured. Because the size of the elements varies, the measurement was repeated three times, in three different directions, and the three values averaged. Therefore, in the end, one value was obtained and used to represent the element size or the "cortical thickness" in the lateral or medial region. To allow the comparison between the cross-sections, the results are presented in percentage of the total distance (or the transversal thickness of the corpus) between the medial and lateral nodes within a cross section.

To obtain an estimate of the medial and lateral cortical thickness of the mandible specimen used in this study, images representing P3, P4, M1, M2, and M3 cross sections were analyzed using ImageJ, an image processing program (ImageJ, National Institute of Health, NIH Version v1.37s). The program can be used to measure lengths using real world measurement units, such as mm. The thickness at the symphysis could not be determined from the available images. The lateral thickness, medial thickness and total

transverse thickness along midcorpus were measured using ImageJ for each cross section. The results are presented in percentage of the total transverse thickness between the medial and lateral aspects of the midcorpus.

Method of assigning material properties. Material properties were assigned to the model using Bonemat program (Laboratorio di Technologia Medica, Bologna, Italy, Zannoni et al. 1998 and Taddei et al. 2004). The program assigns material properties based on CT numbers as described in Chapter 2. Bonemat program reads the CT dataset containing the CT numbers and the FEA mesh generated from it containing the information about all the elements of the mesh. The materials properties are automatically calculated using a linear relationship among CT numbers (expressed in HU—Hounsfild Units) and apparent bone density, and a power relationship among apparent density and Young's modulus. Therefore, each element is selected and placed in a group of elements based on the original CT numbers, as stored in the CT scan data. The significant advantage of this method of assigning material properties is that, theoretically, every element could have its own material properties based on CT numbers and its location in the mandible model. However, this approach would be too time-consuming. In the end, the model had 3 groups of elements: E_A = 15.4 GPa, E_B = 9.08 GPa, E_C = 3.7 GPa, and $\nu_A = \nu_B = \nu_C = 0.3$. For the dentate model, there were 12,353 elements in the Group A (90.72%), 65 elements in the Group B (0.48%) and 1,198 elements in Group C (8.80%). For the edentulous model, there were 8,428 elements in the Group A (86.57%), 62 elements in the Group B (0.64) and 1,245 elements in Group C (12.79%). As expected, the number of elements in Group A, with higher elastic modulus, is reduced for the edentulous model.

Strain profiles. To evaluate the strain pattern inside the mandibular bone and to asses the model accuracy, strain profiles were determined within several mandibular cross sections. Principal strain data was plotted for all the mandibular sections C/I2 (canine/incisor), P3 (third premolar), P4 (fourth premolar), M1 (first molar), M2 (second molar), M3 (third molar), from symphysis to the molar region. The strain data along the transverse thickness shows that, as expected, the values rise toward the lateral or medial surface where the cortical bone exists and fall down toward the middle of the path, between the lateral and medial aspects of the corpus, where the trabecular bone is usually found. Strain gradients were reported for 6 cross sections and for two different loading environments.

Discussion

The mandible is subjected to a multitude of loads during mastication and obviously, the FE simulation of the physiological loading environment cannot account for all the factors that influence the in vivo masticatory strains. The physiological loading environment is not entirely known but it is established that it consists of a combination of torsion, shear and bending. Hylander reported high strain values of up to 2000με from in vivo strain gauge experiments performed during mastication (Hylander 1986). Later, Dechow and Hylander obtained lower values (388με) from the macaque in vivo strain gauge experiments (Dechow and Hylander 2000). In the current study, principal strain results obtained on the lateral aspect, below the left second molar during mastication, were very similar with the published experimental strain results: maximum principal strain +1178με, minimum principal strain -1114με. The experimental strains recorded on

the mandible's lateral aspect, below the left second molar are in the functional interval of 200-2000με (Hylander 1979b, Dechow and Hylander 2000, Daegling 2004).

The mandibular thickness varies significantly throughout the mandible. At the symphysis, the mandibular thickness is greatest lingually, along the medial aspect. However, in the molar region, the medial aspect of the corpus is thinner than the lateral aspect. Especially at midcorpus, the mandibular corpus is thicker on the lateral aspect than on the medial aspect (Daegling 1993). The thickness varies slightly on the lateral midcorpus, increasing from the anterior corpus toward the molar region.

The FE model captures in great detail the asymmetrical distribution of the cortical bone in the real mandible. The accuracy of the model in terms of cortical asymmetry was established using the specimen-specific geometry of the model, FE automatic mesh generation and mesh refinement, method of assigning material properties based on CT numbers and strain results. As it can be seen from Figure 3-16, Table 3-10, Table 3-11, the elements (representing the FE cortical thickness) on the medial aspect of the mandibular corpus are always smaller than the elements for the lateral aspect in all cases considered. This is also true for the data recorded from the *Macaca* specimen used in this study. The cortical thickness data for *Macaca* available on the literature show that the lateral aspect of the mandible is thicker than the medial aspect in the posterior region of the mandible. In the anterior region, the lateral aspect of the mandible is thinner than the medial aspect. As expected, the thickness profile obtained for the FE model is more similar with the thickness profile of the *Macaca* specimen than with the thickness profile obtained from the thickness data available on the literature. Moreover, the percent values representing the relationship among the lateral or medial thickness to the total transverse

thickness for the FE cortical thickness and specimen cortical thickness are very similar. Even if just best estimates for the element size and specimen thickness are used for comparison, this finding adds confidence in the accuracy of the model in terms of cortical asymmetry previously established.

The FE strain curves obtained from mandibular cross sections offer a unique opportunity to discover and visualize the strain field inside the mandibular bone. Finite element method has this distinctive advantage over the conventional experimental limited filed methods of visualizing inside a model. The strain values are higher on the medial aspect than on the lateral aspect for the anterior region of the mandible. On the contrary, the strain values are lower on the medial aspect than on the lateral aspect for the posterior region of the mandible. The strain curve inside the bone is always concave upward, as expected. The strain values rise toward the lateral or medial surface where the hard cortical bone exists and fall down toward the middle of the path, between the lateral and medial aspects of the corpus, where the trabecular bone is usually found. The same concave upward strain profile is recorded for both mastication and clench loading types. The FE strain curves obtained from mandibular cross sections offer valuable information not only about the strain field inside the mandibular bone, impossible to determine experimentally, but also about the accuracy of the model. The curves are always concave upward, as it was expected from a model with cortical bone outside and trabecular bone inside. Furthermore, the FE strain curves are very similar for two different loading environments.

On the lateral midcorpus, the SED and principal strain values generally increase from the anterior corpus toward the molar region. The maximum SED and strain values

are found in the molar region. The base of the mandibular corpus is very thick with the thickest part in the molar area. The SED and the principal strain values recorded for the basal region tent to increase from the anterior corpus toward the molar region. The higher values, calculated for the base of the mandibular corpus, are found also in the molar region. On the medial aspect, the cortical thickness decreases from the anterior section toward the molar section, having the largest value at the anterior corpus. The overall trend for the medial region is the decrease of the SED and principal strain values from the anterior corpus toward the molar region. The highest SED and principal strain values are encountered at the anterior corpus.

SED and strain values found at midcorpus always exceed the values found at the mandibular base for both mastication and clench models. The findings are in agreement with the results published by other researchers (Daegling and Hylander 1998, 2000). Experiments show that under a torsional loading regime, the strains at midcorpus will exceed the values found at the mandibular base. Therefore, in this study, the high principal strains at midcorpus are due to shear strains arising under torsional loading regime. This result also agrees with the experimental observation according to which the values at midcorpus are usually significantly different than the values obtained at the basal corpus (Daegling and Hylander 1998). Moreover, during mastication, vertical shear stress due to parasagittal bending will vary as a parabola from zero at the bottom to a maximum at the centroid (midcorpus) and zero at the top and bottom. Therefore, using stress distribution diagram, higher values were theoretically expected at midcorpus than at the base.

Under the molars, the bone is thicker on the lateral aspect than along the medial aspect. Generally, the SED values found at the lateral midcorpus are higher than the SED values for the medial midcorpus for both mastication and clench models. For the posterior region of the mandible, the strain values found at the lateral midcorpus are higher than the strain values for the medial midcorpus. However, for the anterior region of the mandible, the strain values found at the medial aspect are higher than the strain values found at the lateral midcorpus. The lateral versus medial strain difference is supported by experimental findings. In vivo bone strain data published by Dechow and Hylander show a consistent strain difference between the lateral versus medial aspects of the mandibular corpus (Dechow and Hylander 2000). The lateral strain values were greater than the lingual strain values. The lateral versus medial strain difference was present in the in vitro bone strain results published by Daegling and Hylander (Daegling and Hylander 1998). The lateral strain values were lower than the lingual strain values.

At the symphysis, the cortical bone is distributed exactly the opposite, being thicker lingually than along the lateral aspect. This exact variation is observed from the SED and strain values calculated for the most anterior section (C/I_2). Only for this section, the SED value for the medial aspect exceeded the value for the lateral midcorpus. The mandible model was subjected to a combined loading: superposition of bending, torsion and direct shear. The shear stresses resulted from torsion and direct shear theoretically will add up on the lateral aspect and subtract on the medial aspect of the mandibular corpus (Hylander 1984). According to this theory, high stress, strain and consequently SED values are expected on the lateral aspect of the mandibular corpus and lower stress, strain and SED values are expected on the medial aspect.

The strain energy density values calculated by FEA are in the same range with SED values obtained in similar studies (Mellal et al. 2004). The calculated lazy zone interval for the strain energy density corresponding to a density interval of 0.001 g/cm3 $\leq \rho \leq$ 1.65 g/cm3 is $0.0000036 \leq u \leq 0.00726$ (MPa). The SED values obtained in the current study range from $0.00283 \leq U \leq 0.01213$ (MPa). More than 50% of the calculated SED values are within the lazy zone interval. The values within the lazy zone interval were collected from the medial midcorpus and especially basal area. Several SED values are higher than the values comprises in the lazy zone interval, especially for the lateral midcorpus. All the SED values collected from the base are within the lazy zone interval. Therefore, the current model reject a null hypothesis of uniform SEDs everywhere, which is the implicit assumption underlying Wolff's Law.

According to strain energy density criterion, certain regions of the mandibular bone are not in an equilibrium state or in bone homeostasis. The SED values were not uniform throughout the bone and only 50% of the values were within the lazy zone interval. However, non-uniform SED values may not be an indication of a high bone turnover; it could also signify that the strain energy density criterion is not a suitable bone adaptation predictor.

If form follows function, the SED values are expected to be nearly uniform throughout the bone, and similar values to be collected from thick and thin mandibular sections. The results show that, for example, SED values found at the lateral midcorpus, a thick mandibular section, generally exceed the values found at the medial midcorpus, a thinner mandibular section. A correlation between thickness and strains based on risk of fracture is encountered in engineering structures. Structurally, bone design is a tradeoff

between bone mass and risk of fracture. The trade-off is less acute for light bones than for heavy bones. Therefore, rather than expect an uniform SED throughout the entire bone, it is more reasonable to expect a slight rise in SED values as the thickness increases.

The maximum principal strain values obtained in the current study range from $251\mu\varepsilon \leq \varepsilon_1 \leq 1421\mu\varepsilon$. Below $50\mu\varepsilon$, bone loss is predicted. If the strain levels exceed $1500\mu\varepsilon$, bone gain is predicted. Between $50 \div 1500\mu\varepsilon$, the adapted window or lazy zone interval, bone homeostasis is predicted. According to the strain criterion, all the strain values obtained in this study are situated in the adapted window range or in the lazy zone interval and therefore, no bone adaptation is predicted. The equilibrium that ought to exist under the mechanostat theory seems to fit the mandibular strains. According to Frost and other researchers, the goal of the bone is to main strain values within the equilibrium or physiologic strain range. In this range, the bone turnover is regulated by non-mechanical stimuli. The results presented in this dissertation agree with these theoretical assumptions.

Bone strain gradients in the FE mandible model are influenced by local geometry, material properties and loading. Bone strain gradients in the real mandibular bone are influenced by a constellation of factors, including geometry, material properties and mechanical loading. Modeling and remodeling processes, that developmentally and evolutionary determine bone strain patterns, are responsible for morphological variation in the mandibular bone. Modeling and remodeling processes are responsible for shaping and repairing parts of the bone. Modeling affects the external structure of the bone and involves changes in bone mass, which result in sculpting the bones. Remodeling affects the internal structure of the bone. Through remodeling, the microscopic damage is

repaired and the accumulation of damage is prevented (Martin 2003). Without bone remodeling, the accumulation of fatigue damage could results in frequent bone fractures and our skeleton would collapse.

Developmental adaptation or functional adaptation is the process which helps a living system to adjust to its environment. Particularly, the functional adaptation of bone is the ability to sense, respond and adapt to mechanical loading environment. It was shown through numerous studies that usually bone adapts itself to exercise, disuse, diet and disease. Evolutionary adaptation or historical adaptation is the process which helps a living system to cope with a changing environment over time, by changing a characteristic trait, based on natural selection. In this study, FEM is more relevant to understanding evolutionary adaptation of the mandibular bone rather than developmental adaptation. The mandible model is a linear static model, used in a linear static analysis and, therefore, it cannot inform a dynamic process, such as bone remodeling process. In this study the FE model was used to explore the asymmetrical distribution of bone mass (transverse cortical thickness) in the mandible. Thus, the mandible model can better inform the modeling concept, which involves changes in bone mass specifically.

Strain energy density criterion predicts that only the mandibular base is in homeostasis. Strain criterion predicts bone homeostasis everywhere in the mandible. Bouvier and Hylander investigated the remodeling activity in high- and low-strain regions of the macaque face (Bouvier and Hylander 1996). A very low rate of remodeling was found in the adult Macaca face. Therefore, based on the experimental results, the assumption for an adult mandible is that the mandibular bone is in homeostasis.

The inconsistency in the results obtained from the two criteria is caused mainly by the dissimilarity in the criteria used. Strain energy density criterion is purely theoretical and hypothetical, based on mathematical theories for bone adaptation. Strain criterion is based on experimentally measured bone strain. One common problem when using strain energy density criterion is that the calculated SED lazy zone interval is too narrow (Mellal et al. 2004). A factor that might contribute to the discrepancy in the results is that, in the present study, the SED lazy zone interval is calculated based on parameters proposed in the literature by other authors, parameters that are not specific for the present case. The lazy zone interval is calculated by using a formula for strain energy density, density and several constants. The constants were used initially in the literature for calculating long bone adaptation (femur). For example, parameter B represents bone gain or bone loss in long bones. B is usually assumed equal to unity. Parameter k represents the threshold for bone adaptation in long bones and its value is usually set to 0.004. Parameter s represents the extent of the lazy zone interval and is usually set to 10%. These parameters are not available for mandibular bone. The input parameters, parameters taken from publications on long bone adaptation, are not bone-specific and are used to represent bone adaptation in general (Weinans et al. 1992, Turner et al. 1997, Mellal et al. 2004). The lazy zone interval can be altered greatly by varying one of all the input parameters. For example, the interval can be increased by increasing the extent of the lazy zone interval to 20%, by increasing the threshold for bone adaptation to 1 or by using a larger value for the bone gain or bone loss parameter.

The calculated lazy zone interval depends strongly not only on the parameters chosen, but also on the relationship among parameters, for example the relationship

among elastic modulus and the apparent density. In this study the elastic modulus was set to 17GPa. The relationship between elastic modulus and density was estimated using a cubic relationship (Carter and Hayes 1977, Huiskes et al. 1987, Weinans et al. 1992). If the value for the elastic modulus is increased (other studies assign a larger value for the elastic modulus of cortical bone), the density will increase and consequently the values defining the lazy zone interval will increase. Similarly, a lower elastic modulus value will produce lower values for the lazy zone interval. Furthermore, the extent of the lazy zone interval varies according to the density interval used. If a large density interval is used, a wider lazy zone interval is obtained. Unfortunately, the predictions for the strain energy criterion are usually made in relation to the calculated SED lazy zone interval available in the literature, for long bone adaptation.

The strain versus SED results are, however, in concordance with the results obtained by other researchers. In a study concerning dental implants which compared strain energy density stimulus and strain stimulus, all calculated strain values were situated within the lazy zone interval, whereas, SED values indicate bone adaptation (Mellal et al. 2004). The discrepancy in the results was linked to a lazy zone that is too narrow. In another study, a proximal femur model was developed to explore trabecular bone adaptation using both, the strain and the SED criteria (Turner et al. 1997). The strain criterion was successfully used to predicted realistic density distribution. The SED criterion did not produce a convergent solution. The different results obtained by using SED criterion are probably due in part to the increased complexity of the algorithm and in the same time, oversimplification, the inability to simulate a complex biological structure such as bone tissue. In conclusion, strain criterion based on measured strain

remains a more reliable tool for estimating the lazy zone interval and the adaptation activity in bone.

In conclusion, according to the mechanostat model, the goal of bone is to maintain strain within a physiologic strain range or equilibrium interval. The first hypothesis was that the mechanostat theory is applicable to all bones, including the mandible, in other words, the mandibular bone in equilibrium. The "equilibrium" proposed by the mechanostat model seems to fit the mandibular strains. However, only 50% of the SED values are within the equilibrium interval. The other hypothesis was that at all locations uniform SED values will be measured, the implicit assumption underlying Wolff's Law. If a functional correlation between the morphology and function of the mandible exists and bone is an optimized load bearing structure, there should be near uniform SED levels throughout the bone. The results show that SED and strain values do not consistently correlate with bone mass variation. The null hypothesis of uniform SED everywhere was rejected.

Experimental work on facial bones provides no support for those hypotheses that assume a functional correlation between morphology and stress and/or strain. The study performed by Hylander et al. (1991) on well-developed browridges of primates clearly shows that, contrary to our expectations, bone strains recorded from the robust supraorbital region are extremely small. Therefore, in this case, a predictable relationship among bone-strain magnitudes and morphological variation does not exist. Perhaps a functional relationship in the skull does exist but it is context-specific or region-specific, i.e. it is applicable in some regions of the skull but not in others (Daegling 2004).

Another very important conclusion concerning functional adaptation and regulation of bone mass can be inferred from the results. The results obtained question whether peak functional strains can be related to bone mass variation in a predictable way. The mandibular bone is responding to a mechanical stimulus from the environment, but it seems it is not what physical anthropologists usually are concerned with. Studies performed by Rubin and colleagues suggested that bone adaptation is not governed by peak or maximum strains and it is in fact governed by extremely small strains (Rubin et al. 2002, Judex et al. 2006). Thus, extremely low-magnitude, high-frequency mechanical stimuli can have a considerable impact on bone adaptation.

When the masseter-pterygoid sling force is simulated by using a more vertically oriented vector, the maximum principal strain values are reduced as expected. The direction of maximum principal strain is usually given relative to the long axis of the mandible (the X axis). The strain gage was placed on the mandibular corpus with gage elements A and C aligned with the longitudinal (the X axis) and respectively vertical (Y axis) axes. According to the experimental results performed on the specimen, the maximum principal strain direction is oriented nearly longitudinally with respect to the mandibular corpus (the X axis).

The current research project explored using finite element methods a very important and controversial topic: the unique morphology of the mandible. The study advanced knowledge on the exploration of whether form follows function but more research is needed in this field. Further work on functional adaptation could offer an explanation of how current morphological shape of the mandibular bone was established. Moreover, the relationship could be used to predict how current morphology would

change in the future. The current project aimed to investigate the unusual morphology of the mandible and to extend our knowledge in mandible biomechanics.

Table 3-1. Regional cortical thickness for macaque jaws*. Units in mm.

Section	Lateral region	Basal region	Medial region
C/I2	1.1	1.3	1.1
P3	0.8	1.2	1.0
P4	0.8	1.5	0.9
M1	0.9	1.9	0.8
M2	1.0	1.9	0.7
M3	1.0	1.5	0.6

*Daegling 1993

Table 3-2. Mastication model. SED, maximum and minimum principal strain and cortical thickness data for lateral midcorpus region.

Sections	SED (MPa)	Max strain (με)	Min strain (με)	Thickness (mm)
C/I2	0.005113	386	-987	1.1
P3	0.008551	611	-1315	0.8
P4	0.010723	681	-1388	0.8
M1	0.010938	877	-1118	0.9
M2	0.010622	1179	-1115	1
M3	0.012132	1093	-1126	1

Table 3-3. Mastication model. SED, maximum and minimum principal strain and cortical thickness data for basal region.

Sections	SED (MPa)	Max strain (με)	Min strain (με)	Thickness (mm)
C/I2	0.002833	367	-647	1.3
P3	0.004023	448	-811	1.2
P4	0.005435	700	-796	1.5
M1	0.006737	995	-737	1.9
M2	0.004763	822	-551	1.9
M3	0.005307	903	-587	1.5

Table 3-4. Mastication model. SED, maximum and minimum principal strain and cortical thickness data for medial midcorpus.

Sections	SED (MPa)	Max strain (με)	Min strain (με)	Thickness (mm)
C/I2	0.010616	1421	-468	1.1
P3	0.007596	1008	-669	1
P4	0.007142	1127	-709	0.9
M1	0.010275	1116	-788	0.8
M2	0.005517	1141	-531	0.7
M3	0.006251	889	-942	0.6

Table 3-5. Clench model. SED, maximum and minimum principal strain and cortical thickness data for lateral midcorpus region.

Sections	SED (MPa)	Max strain (με)	Min strain (με)	Thickness (mm)
C/I_2	0.004052	325	-881	1.1
P_3	0.008382	551	-1288	0.8
P_4	0.012636	579	-1514	0.8
M_1	0.012042	578	-1107	0.9
M_2	0.011143	1046	-1204	1
M_3	0.013272	936	-1221	1

Table 3-6. Clench model. SED, maximum and minimum principal strain and cortical thickness data for basal region.

Sections	SED (MPa)	Max strain (με)	Min strain (με)	Thickness (mm)
C/I_2	0.001529	251	-459	1.3
P_3	0.002917	343	-663	1.2
P_4	0.004298	550	-671	1.5
M_1	0.005817	873	-641	1.9
M_2	0.005154	844	-490	1.9
M_3	0.005427	937	-539	1.5

Table 3-7. Clench model. SED, maximum and minimum principal strain and cortical thickness data for medial midcorpus region.

Sections	SED (MPa)	Max strain (με)	Min strain (με)	Thickness (mm)
C/I_2	0.007987	1332	-394	1.1
P_3	0.007692	1062	-567	1
P_4	0.007704	1222	-600	0.9
M_1	0.010798	1226	-664	0.8
M_2	0.005476	1111	-442	0.7
M_3	0.004589	783	-673	0.6

Table 3-8. SED and principal strain values for mastication and clench models when one or more vectors are used to simulate the masseter-pterygoid sling load. The values are reported for the lateral midcorpus, below second molar.

Model	One muscle vector (68°)			Multiple vectors (Resultant=75°)		
	SED (MPa)	Strain (με)		SED (MPa)	Strain (με)	
		ε1	ε2		ε1	ε2
Mastication	0.010622	1179	-1115	0.010757	1164	-1141
Clench	0.011143	1046	-1204	0.010766	1017	-1187

Table 3-9. SED and principal strain values for mastication and clench models when one or more vectors are used to simulate the masseter-pterygoid sling load. The values are reported for the medial midcorpus, below second molar.

Model	One muscle vector (68°)			Multiple vectors (Resultant=75°)		
	SED (MPa)	Strain(με)		SED (MPa)	Strain(με)	
		ε1	ε2		ε1	ε2
Mastication	0.005517	1114	-531	0.005407	1131	-510
Clench	0.005476	1111	-442	0.005439	1105	-443

Table 3-10. Cortical thickness comparison for the lateral midcorpus region. The size of the FE elements representing "FE cortical thickness" versus specimen cortical thickness and cortical thickness published in the literature.

Sections	FE cortical thickness (%)	Specimen (%)	Published data (mm)*
C/I2	35.50	-	1.1
P3	40.66	25.10	0.8
P4	40.03	30.23	0.8
M1	37.85	35.71	0.9
M2	35.09	36.36	1
M3	30.38	27.91	1

*Daegling 1993

Table 3-11. Cortical thickness comparison for the medial midcorpus region. The size of the FE elements representing "FE cortical thickness" versus specimen cortical thickness and cortical thickness published in the literature.

Sections	FE cortical thickness (%)	Specimen (%)	Published data (mm)*
C/I2	21.43	-	1.1
P3	27.96	22.73	1
P4	30.65	23.26	0.9
M1	33.15	28.63	0.8
M2	28.50	29.90	0.7
M3	27.93	23.26	0.6

*Daegling 1993

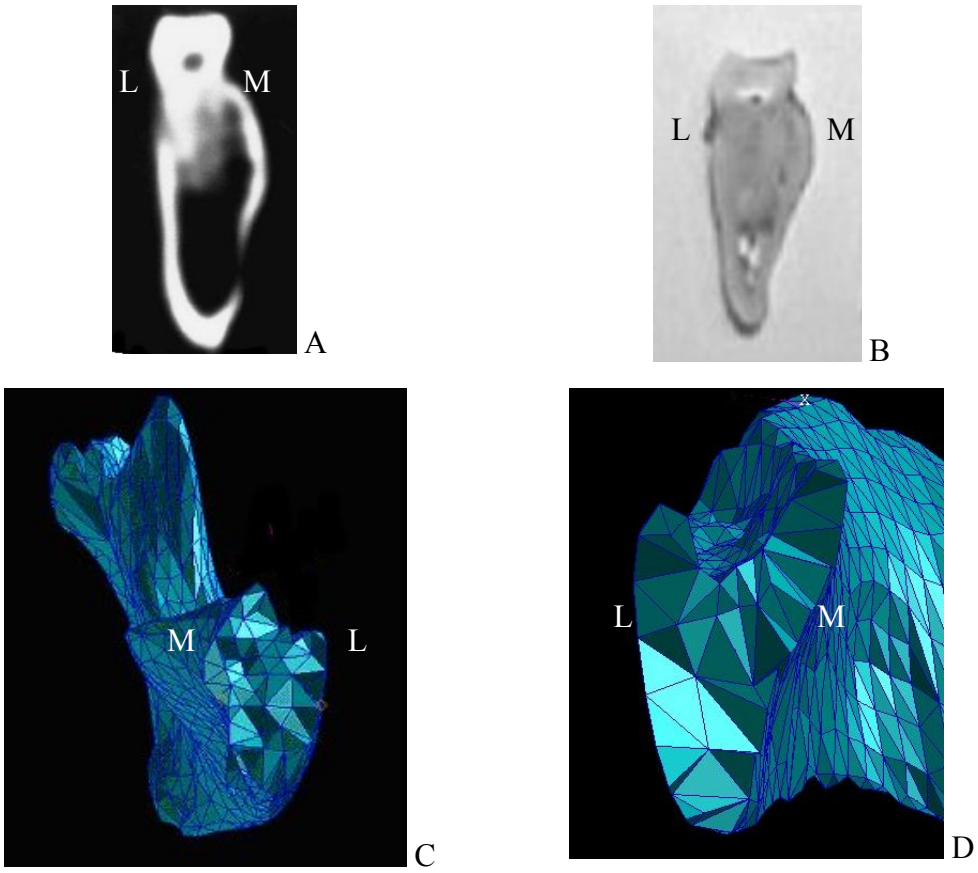

Figure 3-1. Mandibular cross-sections: A) CT scan, B) mandibular cross-section, C) FE cross-section, anterior view, D) FE cross-section, posterior view. The mandibular cross-section is asymmetrical, and presents considerable geometric dissimilarity between the medial (M) and lateral (L) aspects of the corpus.

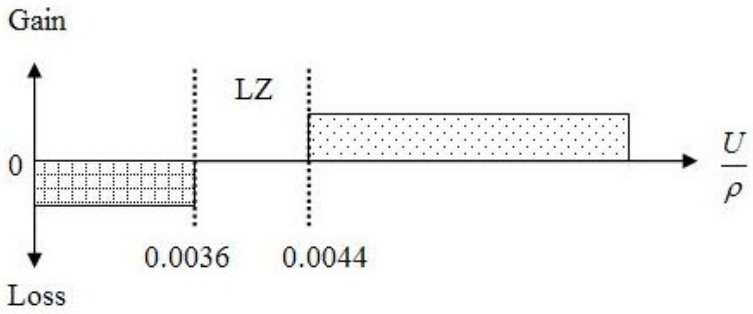

Figure 3-2. Calculated lazy zone interval. The lazy zone is the functional strain or strain energy density interval for which bone homeostasis is predicted. Homeostasis means that bone resorption and bone formation are in equilibrium. Values higher than the values within the lazy zone predict bone gain and values lower than the values within the interval predict bone loss.

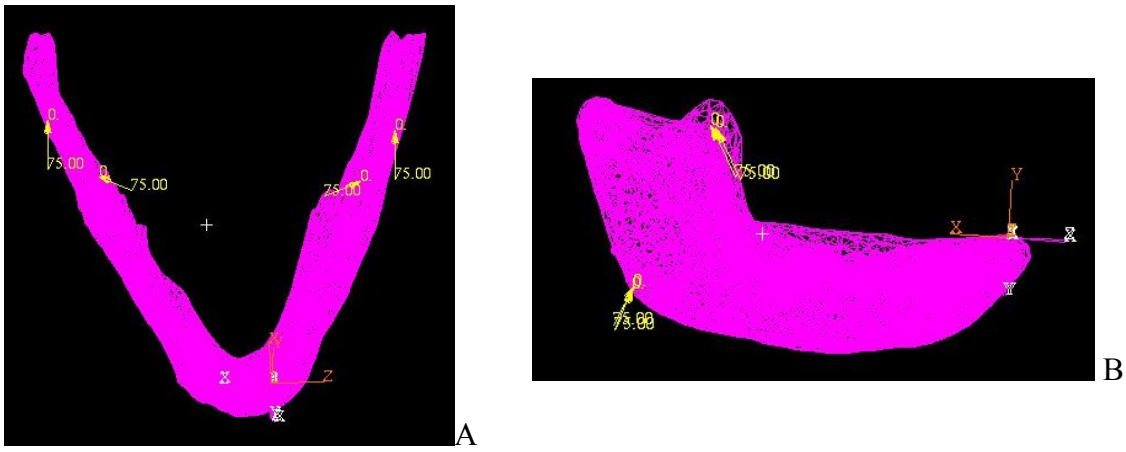

A B

Figure 3-3. The masseter-pterygoid sling and the temporalis muscles simulation. A) Top and B) lateral view of the FE mandible. The insertions of the masticatory muscles were simulated by points on the mandibular angles and the coronoid process of the mandible, on each side. Four loads of 75N each were applied to the mandible model to account for the left temporalis muscle, the left masseter-pterygoid sling, the right temporalis muscle and the right masseter-pterygoid sling.

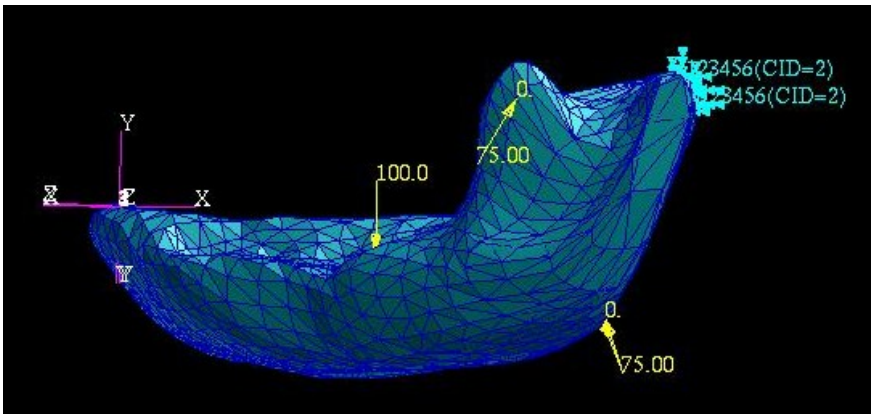

Figure 3-4. Mandible model subjected to combined loading. The model was constrained at condyles. An equal number of nodes (three nodes) were totally constrained at condyles on each side. The mastication force is tilted by 15° in the frontal plane, toward the right side of the mandible. The model was subjected to combined loading: simultaneous application of bending, torsion and direct shear.

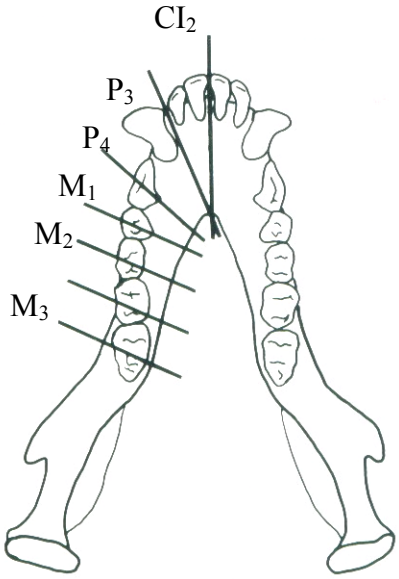

Figure 3-5. Mandibular sections: M_3 (third molar), M_2 (second molar), M_1 (first molar), P_4 (fourth premolar), P_3 (third premolar), C/I_2 (canine/incisor) (from Daegling DJ 1993. The relationship of in vivo bone strain to mandibular corpus morphology in Macaca fascicularis. J Hum Evol 25: 247–269).

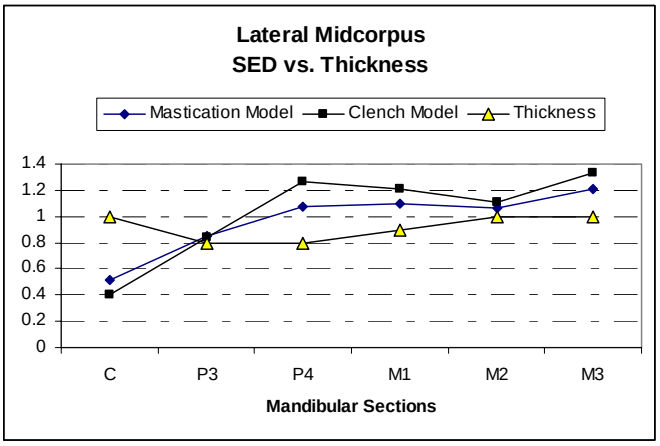

A)

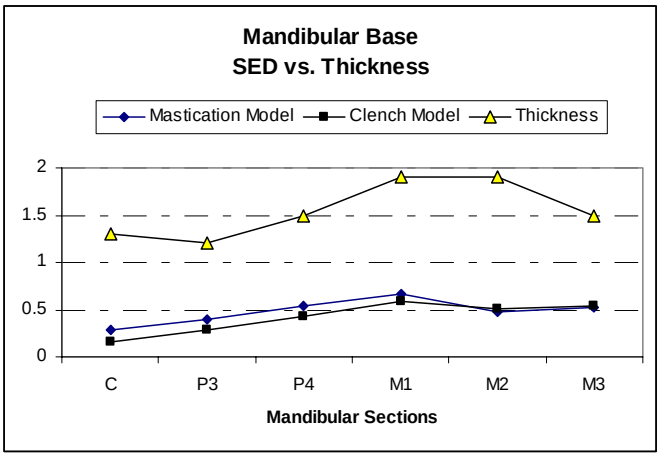

B)

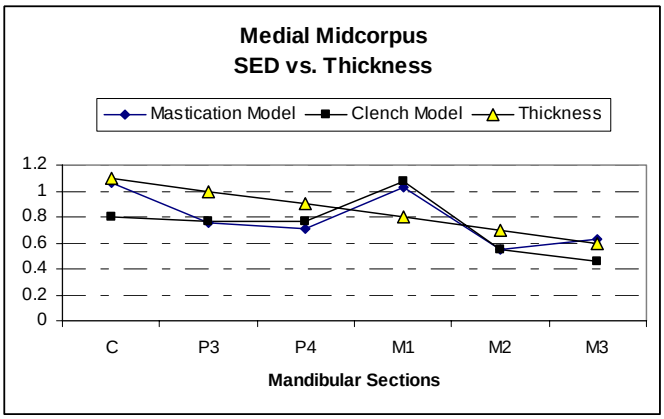

C)

Figure 3-6. SED and thickness data for various mandibular regions: A) lateral midcorpus region. For the lateral region, the SED values tend to increase slightly from the anterior corpus toward the molar region; B) basal region. The SED values recorded for the basal region also tent to increase slightly from the anterior corpus toward the molar region, with small values in the anterior corpus and higher values toward the molar region; C) medial midcorpus region. The overall trend for the medial region is the decrease of the SED values from the anterior corpus toward the molar region.

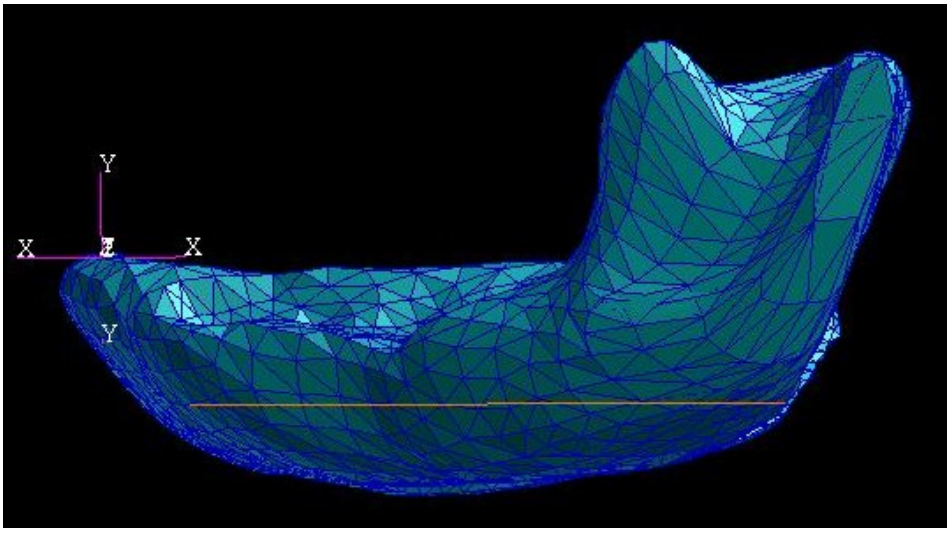

A)

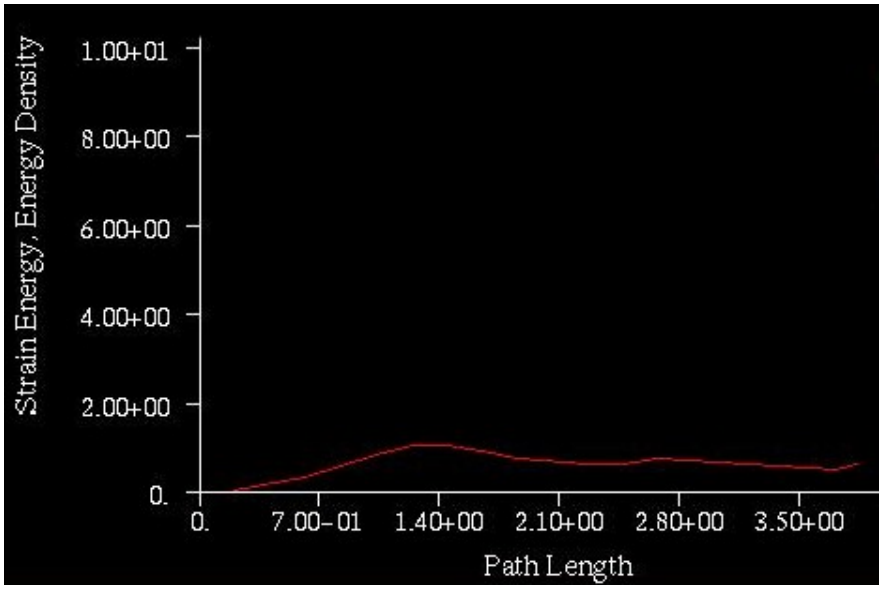

B)

Figure 3-7. SED profile along midcorpus. An arbitrary path was created along the midcorpus and the overall SED profile was plotted along the path. A) Mandible model and an arbitrary path. B) SED values were plotted along an arbitrary path created on the mandibular corpus.

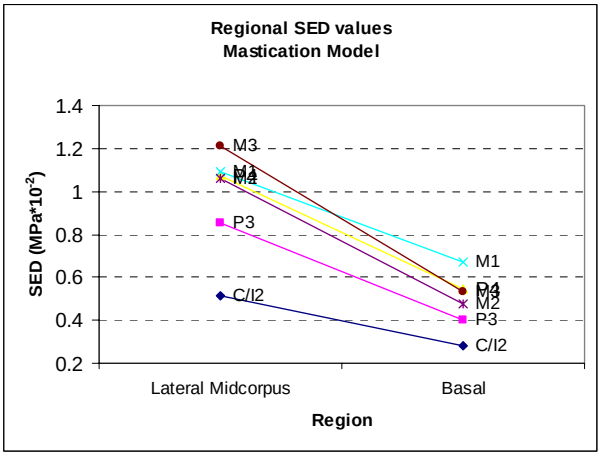

A)

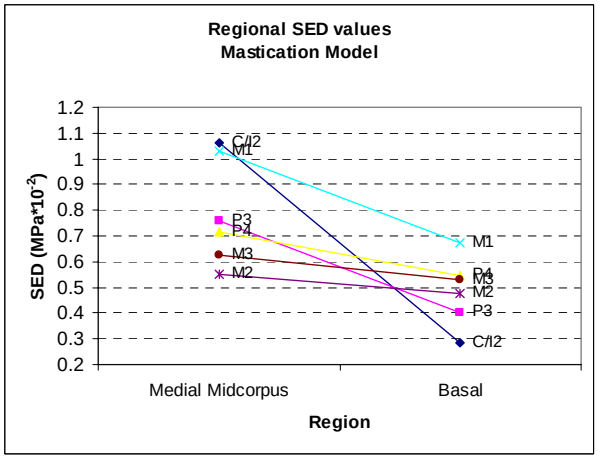

B)

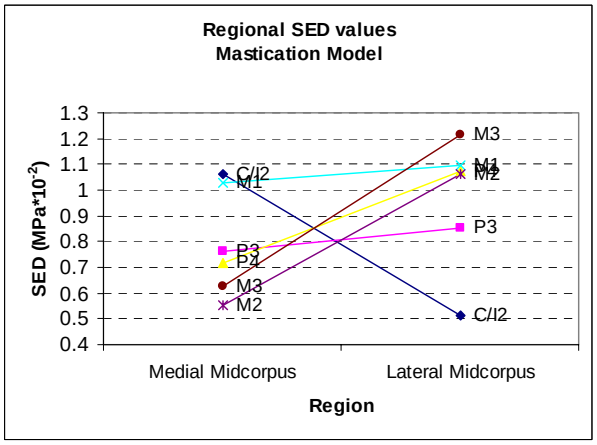

C)

Figure 3-8. Regional SED values for the mastication model: SED values are consistently higher: A) at the lateral midcorpus than basally; B) at the medial midcorpus than basally; C) the lateral midcorpus than at the medial midcorpus. The only exception is at symphysis (C/I2) where the medial SED values are higher than the lateral SED values. The same variation is observed in cortical bone distribution. Mandibular sections: M3 (third molar), M_2 (second molar), M_1 (first molar), P_4 (fourth premolar), P_3 (third premolar), C/I_2 (canine/incisor).

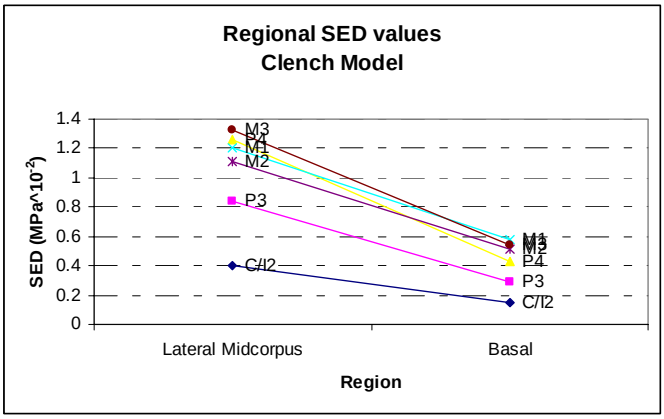

A)

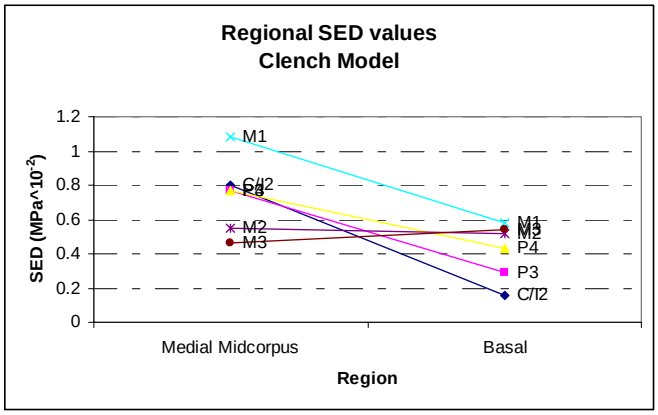

B)

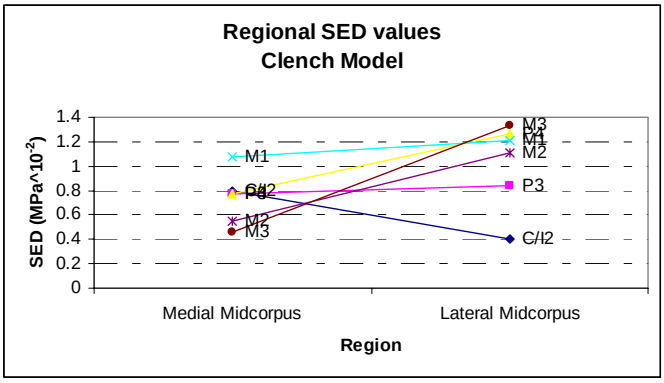

C)

Figure 3-9. Regional SED values for the clench model: SED values are consistently higher: A) at the lateral midcorpus than basally; B) at the medial midcorpus than basally; C) the lateral midcorpus than at the medial midcorpus. The only exception is at symphysis (C/I2) where the medial SED values are higher than the lateral SED values. The same variation is observed in cortical bone distribution. Mandibular sections: M3 (third molar), M_2 (second molar), M_1 (first molar), P_4 (fourth premolar), P_3 (third premolar), C/I_2 (canine/incisor).

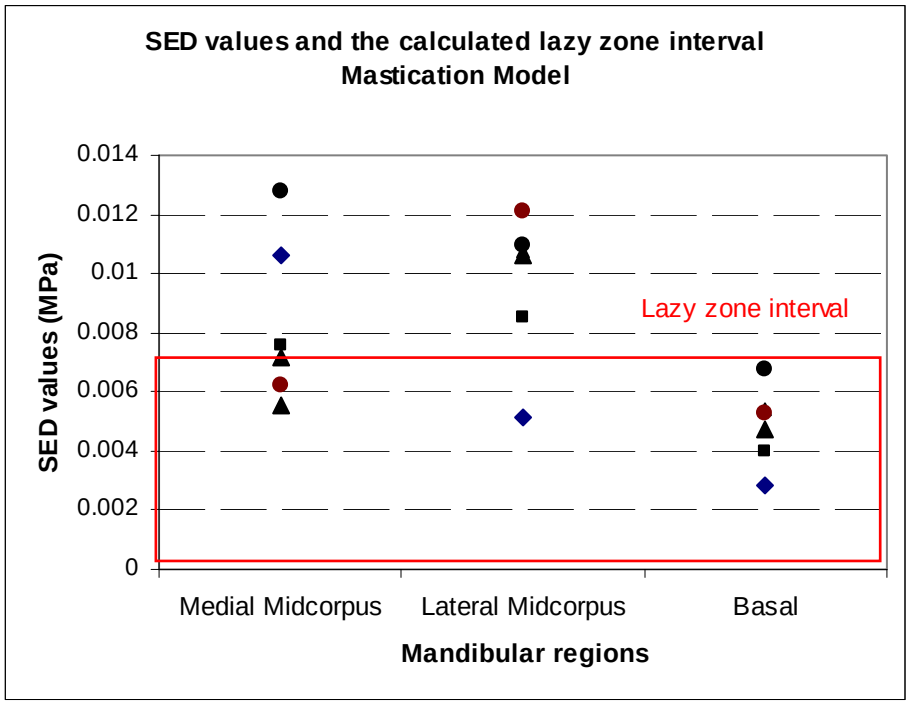

A)

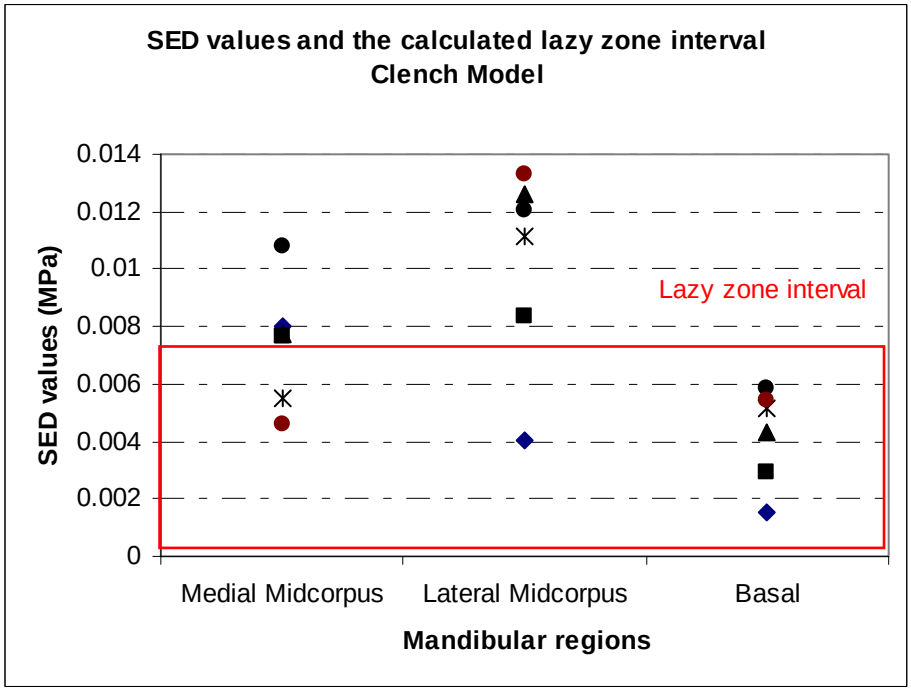

B)

Figure 3-10. Regional SED values and the calculated lazy zone interval. A) For the mastication model, numerous calculated SED values are within the lazy zone interval. B) For the clench model, many SED values collected from the medial midcorpus and basal area are within the lazy zone interval.

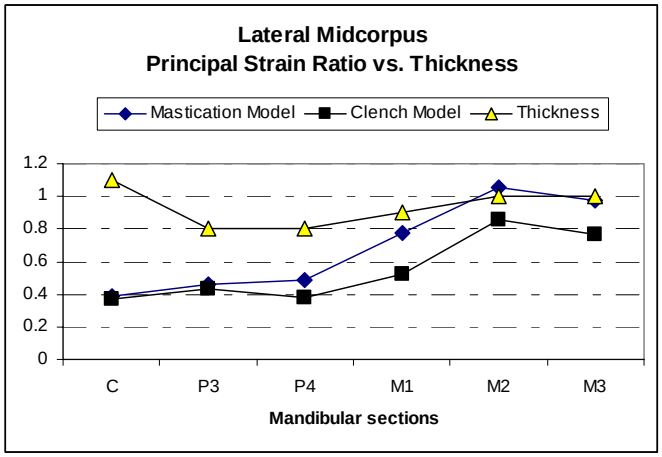

A)

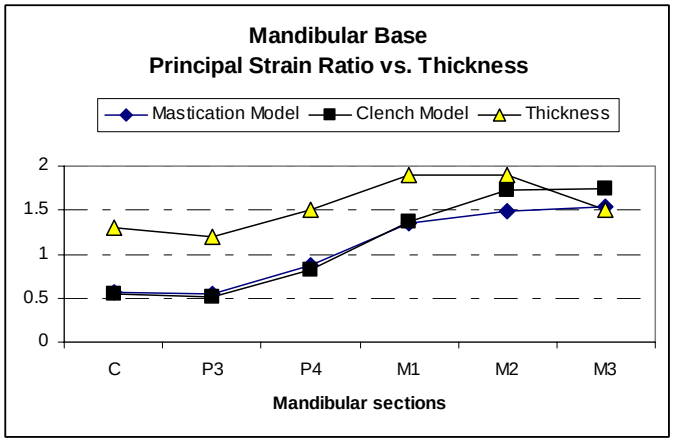

B)

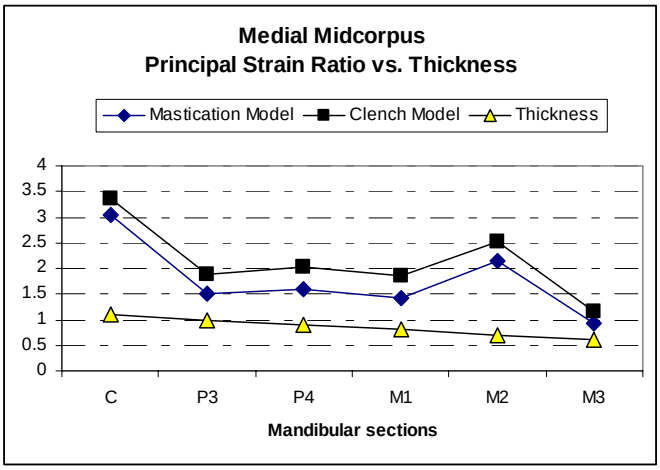

C)

Figure 3-11. Principal strain ratio and thickness data for various mandibular regions: A) lateral midcorpus region. For the lateral region, strain values tend to increase from the anterior corpus toward the molar region. B) basal region. The strain values recorded for the basal region also tent to increase slightly from the anterior corpus toward the molar region. C) medial midcorpus region. The overall trend is the decrease of the SED values from the anterior corpus toward the molar region.

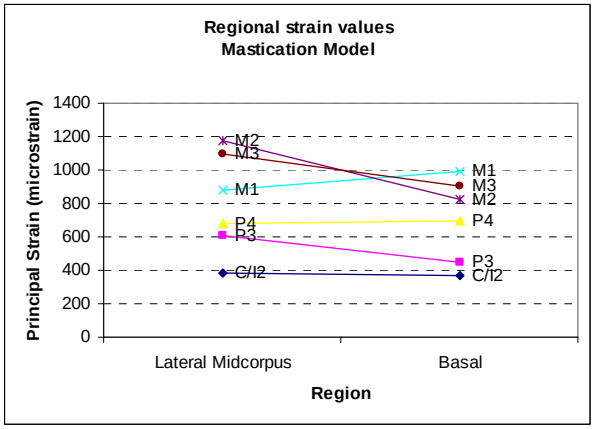

A)

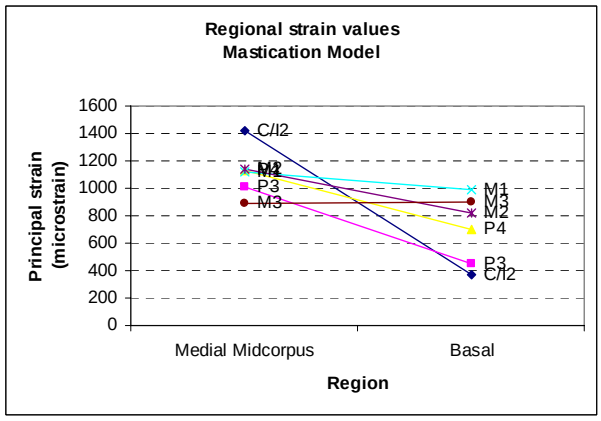

B)

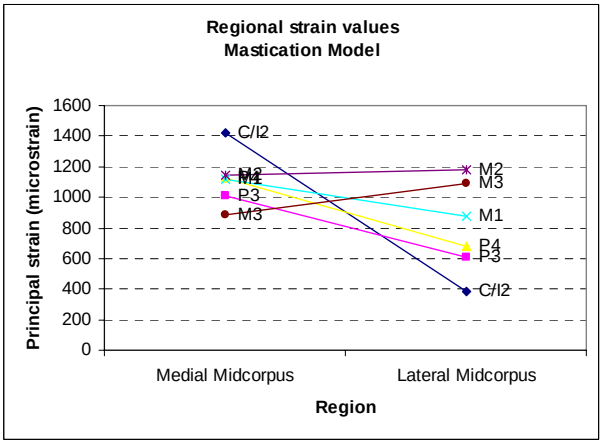

C)

Figure 3-12. Regional principal strain values for the mastication model: strain values are consistently higher A) at the lateral midcorpus than basally; B) at the medial midcorpus than basally; C) at the medial midcorpus than at the lateral midcorpus. At symphysis (C/I2) the medial values are much higher than the lateral values. The same variation is observed in bone distribution: at the symphysis and at the anterior corpus, the cortical bone is thicker on the medial aspect than along the lateral aspect. Mandibular sections: M_3 (third molar), M_2 (second molar), M_1 (first molar), P_4 (fourth premolar), P_3 (third premolar), C/I_2 (canine/incisor).

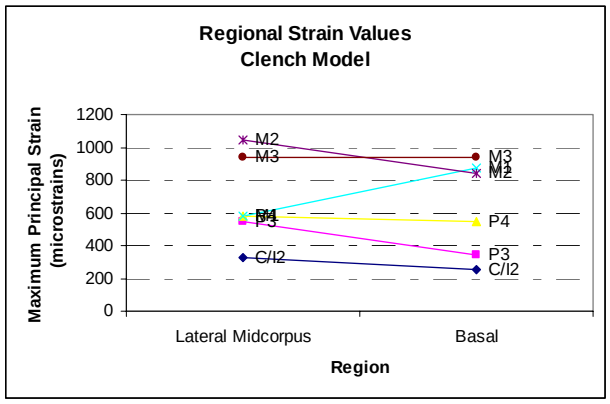

A)

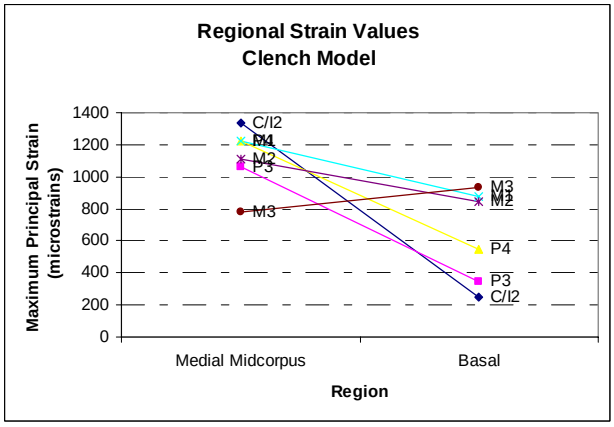

B)

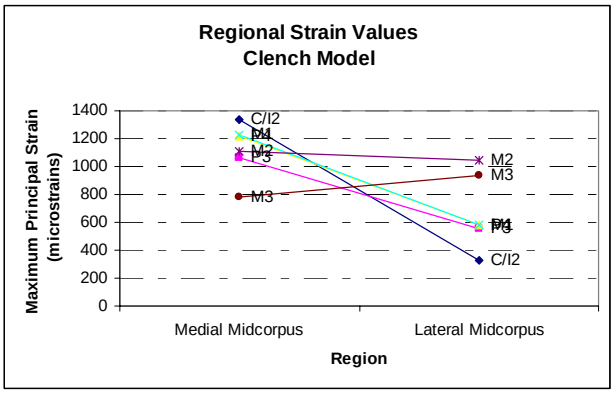

C)

Figure 3-13. Regional strain values for the clench model: principal strain values are generally higher: A) at the lateral midcorpus than basally; B) at the medial midcorpus than basally; C) at the medial midcorpus than at the lateral midcorpus. Mandibular sections: M3 (third molar), M2 (second molar), M1 (first molar), P4 (fourth premolar), P3 (third premolar), C/I2 (canine/incisor).

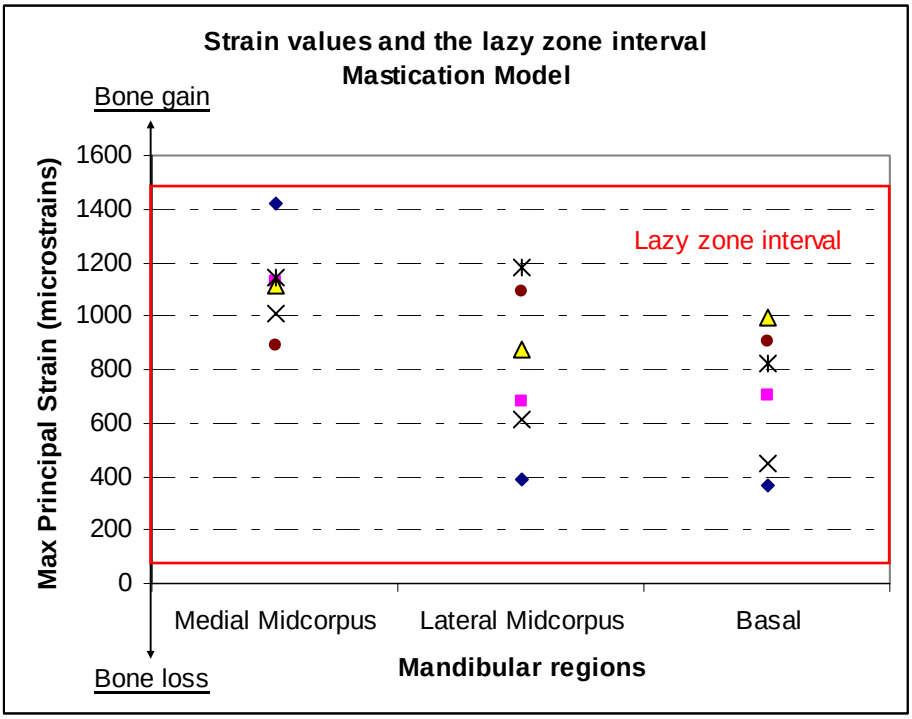

A)

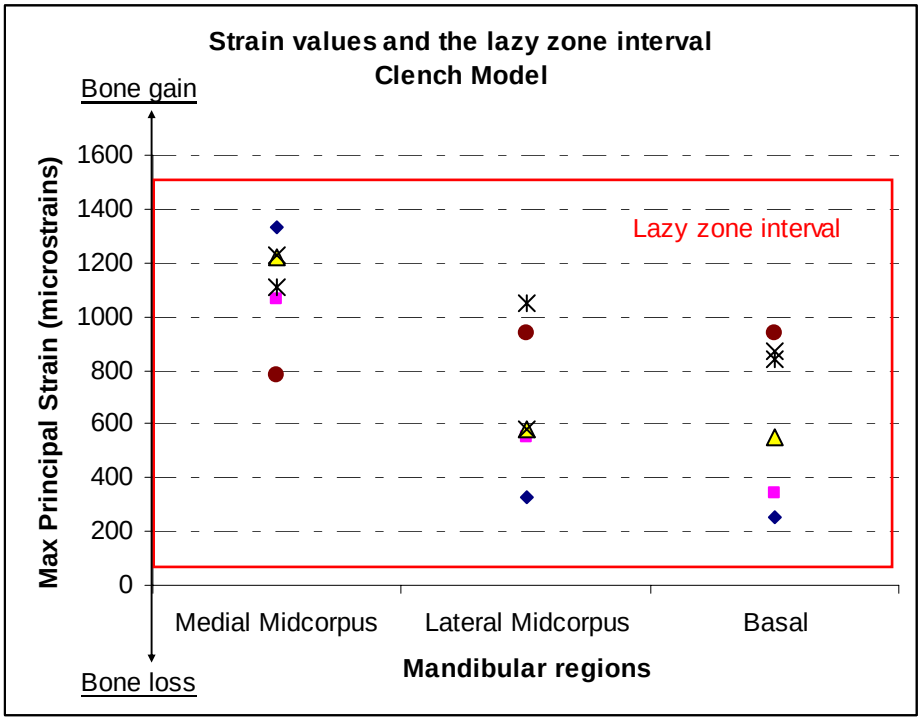

B)

Figure 3-14. Regional strain values and the lazy zone interval. For both biting models, A) the mastication model and B) the clench model, all the calculated strain values are within the lazy zone interval (50-1500με).

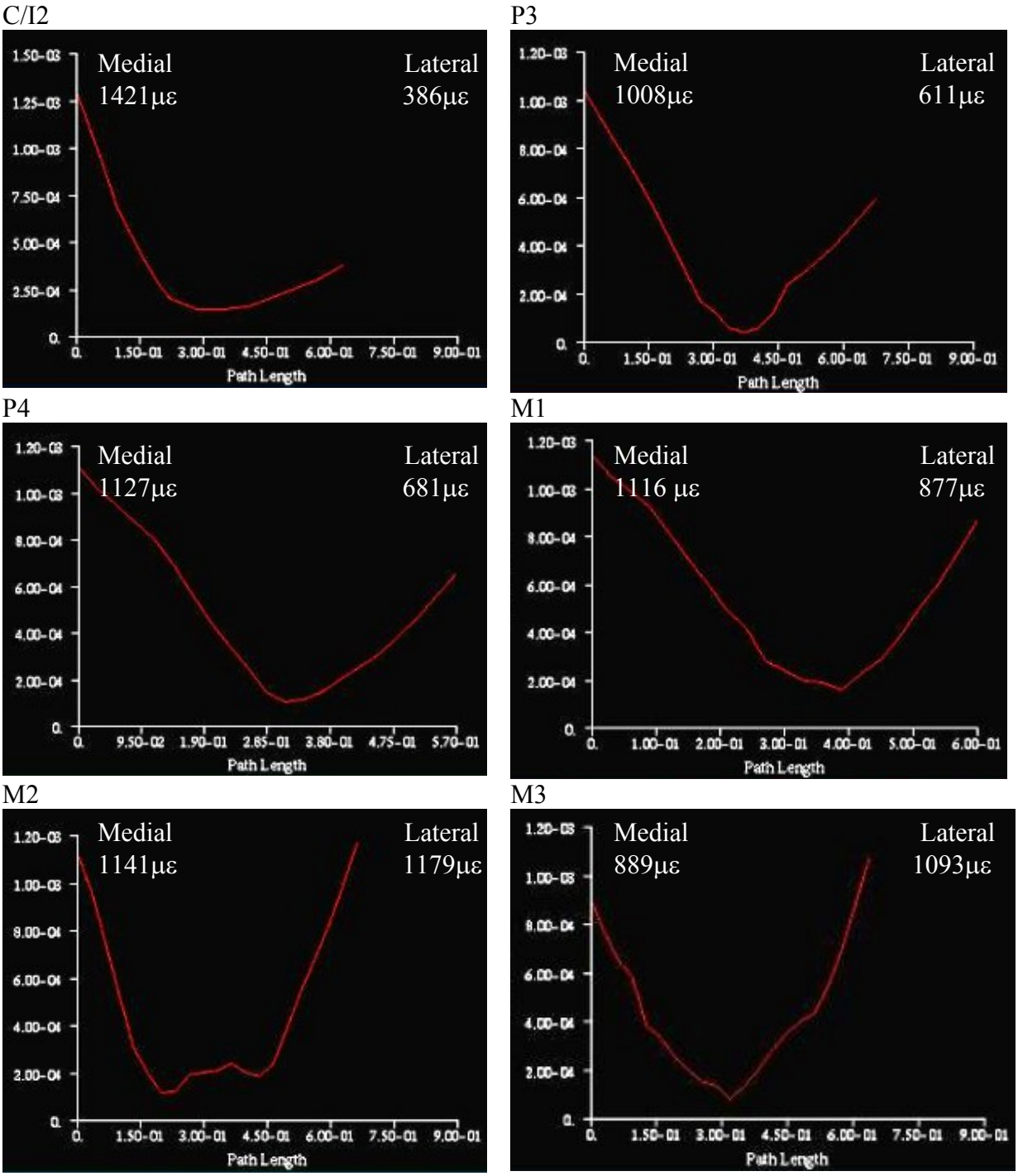

Figure 3-15. Principal strain profiles in mandibular cross-sections, from symphysis, the most anterior cross-section, to the most posterior cross-section, the molar region during mastication. Mandibular sections: M3 (third molar), M2 (second molar), M1 (first molar), P4 (fourth premolar), P3 (third premolar), C/I2 (canine/incisor).

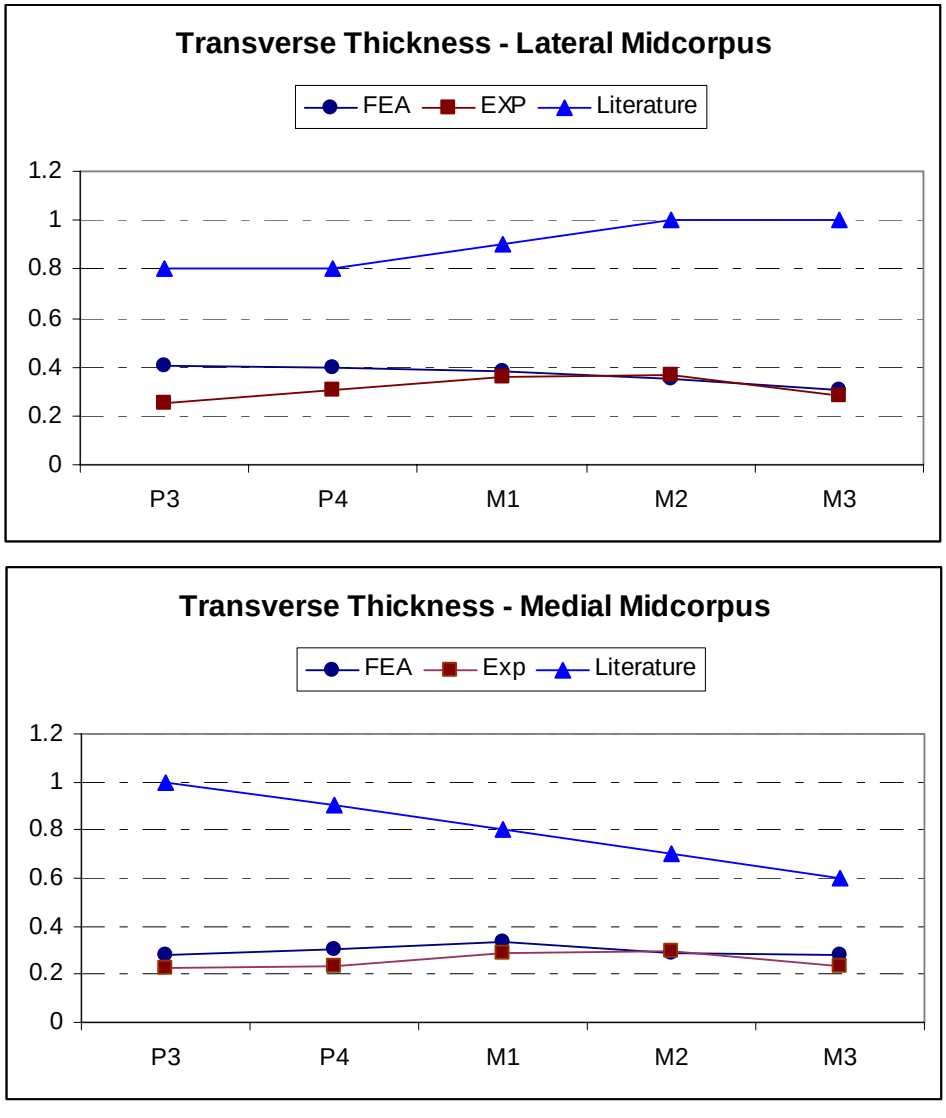

Figure 3-16. Cortical thickness comparison. Comparison between transverse cortical thickness data for the FEA model (element size), EXP model (*Macaca* specimen), and data available in the literature (Daegling 1993): A) lateral midcorpus; B) medial midcorpus. Mandibular sections: M3 (third molar), M2 (second molar), M1 (first molar), P4 (fourth premolar), P3 (third premolar).

CHAPTER 4
CONCLUSIONS AND PERSPECTIVES

The main goals of the current study were to design a realistic mandible model, to validate the model and then analyze it using finite element methods. Another goal of the current study was to use the validated model to explore the correlation between mandibular morphology with patterns of strain and strain energy density. It is well known that usually bones respond to mechanical loads imposed on them. However, in the mandible's case, the functional relationship is still ambiguous and controversial.

An in vitro strain gauge experiment was conducted on a fresh adult mandible of *Macaca fascicularis*. Rectangular strain gauges were bonded to the lateral and medial aspects of the mandibular corpus, below the left second molar. The mandible was constrained bilaterally, at condyles and angles, using a metal fixture. The fixture was composed from a base that supported the mandible at each angle and a roller which prevented movement at the condyles. An occlusal load (70N) was applied to the left central incisor. Surface bone strain data were obtained from mechanical testing of the mandible. The maximum and minimum principal strains and their ratio were calculated.

The mandible was then scanned in a series of parasagittal planes. Each scan was segmented to obtain digitized contours. The mandible model was obtained through volumetric reconstruction from 90 CT scans. Two models were developed: a dentate and an edentulous model. The edentulous model was reconstructed from the same cross sections used for reconstructing the dentate model, without digitizing the teeth. The models were imported in into a finite element analysis package.

Under various conditions of material and structural complexity, two finite element models were constructed: a dentate and an edentulous model. The two geometric models were transformed into solids and then meshed with a tetrahedral mesh using quadratic elements. The FE dentate model had 13,616 quadratic tetrahedral elements. The FE edentulous model had 9,735 quadratic tetrahedral elements. The models include data on spatial variation (heterogeneity) and directional dependence (anisotropy) of elastic properties obtained from micromechanical tests on the specimen. Three models were developed: an isotropic homogeneous model, an isotropic heterogeneous model and a transversely isotropic heterogeneous model.

Validation of the FE model is accomplished using surface bone strain data obtained from the in vitro strain gauge experiment and convergence studies. The FE models were subjected to a vertical occlusal load (70N) which was applied to the left central incisor. The models were constrained bilaterally, at condyles and angles. Several analyses were performed to explore the effects of changing boundary conditions (altering the degrees of freedom, changing the number of nodes constrained and changing the force orientation) and material properties on strain values predicted at the gauge location.

The first part of the study presents the creation and the validation of the mandible model and the challenges encountered when attempting to produce a realistic model and to validate a complex FEM. The strain results show that the dentate model is too stiff and consequently, the strain values obtained from it are extremely low when compared with the experimental strain values. The strain results obtained from analyzing the edentulous model are more congruent with the experimental strain data. Determination of appropriate boundary conditions and material properties are as critical as recreation of

precise geometry for finite element model validation. The specimen deflected during the experiment because of the mandible asymmetrical geometry; movement occurred in the transverse direction at the constraint locations. Congruent finite element results were obtained by relaxing the degrees of freedom in the transverse direction (1.85% error between experimental and FE strain data for the lateral gauge and 8.05% error for the medial gauge). The overall percent error is below 10% which is the accepted error in the FE studies. A convergence test was performed to determine the accuracy of the numerical model. The error between the mesh used in the simulations and the most refined mesh in the current study is very small (0.37%). The results obtained from the convergence study add additional confidence in the FE results.

There are many studies which explored in the last decades the mandibular anatomy, mandibular movements during mastication, investigated biting and reaction forces occurring during mastication and portrayed the stress-strain behavior of the mandibular bone. However, the relationship between the loading environment, stress-strain patterns and morphology is still unknown. Some studies suggested that the mastication forces are not functionally linked to the mandible's morphology and in fact, the mandibular structure could be the result of genetic determinants or numerous non-mechanical factors that occurred during evolution. Perhaps the mandibular corpus is deep and thick to accommodate large teeth, more specifically their long roots. Hylander and colleagues explored the functional significance of well-developed brow-ridges in of *Macaca fascicularis* using strain gauges (Hylander et al, 1991). The strains recorded were, unexpectedly, very low. Many other studies showed that bone strain values collected for various "robust" facial bones during mastication, including the mandible, were very low.

The results suggested that facial bones in *Macaca fascicularis* could actually be "overdesigned". The asymmetrical distribution of cortical bone in the mandible is unique and fascinating. The biomechanical justification for this asymmetrical distribution of cortical bone is ambiguous. The mandible is laterally thick and lingually thin. At midcorpus, the cortical bone on the lateral aspect is thicker than on the lingual aspect. It was proposed that simultaneous application of twisting, bending and direct shear might explain why the cortical bone is distributed the way it is in the mandibular corpus. Thus, one of the most essential questions concerning mandible's morphology still remains unanswered. The main objective of the present study was to use FEA to explore the cortical asymmetry concept.

The last part of the current study aims to investigate the relationship of strain and strain energy density to bone mass variation in the macaque mandible. The previous modeling efforts are improved by simulating the masticatory muscles. The muscles - left temporalis muscle, left masseter-pterygoid sling, right temporalis muscle and right masseter-pterygoid sling - are simulated as individual vectors. Strain interval and strain energy density criterion are used to explore variations in the mandibular bone mass when the mandible is subjected to combined loading (torsion, direct shear and parasagittal bending).

Six mandibular sections - M_3 (third molar), M_2 (second molar), M_1 (first molar), P_4 (fourth premolar), P_3 (third premolar), C/I_2 (canine/incisor) - and three mandibular regions - lateral midcorpus, basal and medial midcorpus - were identified in the FE mandible model. The sections, the regions and the cortical thickness values for Macaca fascicularis were available in the literature (Daegling 1993).

SED and the maximum and minimum principal strain values were recorded for the mastication model and clench model for the lateral midcorpus, base and medial midcorpus. The ratio between the maximum and minimum principal strains was obtained and plotted against the mandibular thickness. The variables, the thickness and the SED and the thickness and the strain, vary in a similar manner within the mandibular sections. The patterns are consistent across various mandibular sections. However, the values found at the lateral or the medial midcorpus are always higher than along the mandibular base. The values for the lateral midcorpus are higher than the values for the medial midcorpus. The values obtained from all the sections and regions were plotted on the same graph and the lazy zone interval was determined. More than 50% of the SED values are within the lazy zone interval. Non-uniform SED values were obtained. According with the strain criterion, all the strain values obtained in this study are situated in the adapted window range or in the lazy zone interval (50÷1500με). The slight discrepancy in the results is explained in this study and in other similar studies by the narrow normal interval or lazy zone interval obtained when using SED criterion.

In conclusion, according with the mechanostat model, the goal of bone is to maintain strain within a physiologic strain range or equilibrium interval. The first hypothesis was that the mechanostat theory is applicable to all bones, including the mandible, in other words, the mandibular bone in equilibrium. The "equilibrium" proposed by the mechanostat model seems to fit the mandibular strains. However, only 50% of the SED values are within the equilibrium interval. The other hypothesis was that at all locations uniform SED values will be measured, the implicit assumption underlying Wolff's Law. If a functional correlation between the morphology and function of the

mandible exists and bone is an optimized load bearing structure, there should be near uniform SED levels throughout the bone. The null hypothesis of uniform SED everywhere was rejected.

Improved depiction of periodontal structures will lead to improved model and an ideal congruence between the experimental data and the finite element recreation of that data. Modeling physiological loads and constraints is likely to be the greatest future challenge in physical anthropology for successful application of finite element methods for modeling in vivo mechanical behavior. Understanding the functional morphology of the mandible is critical for uncovering the evolutionary transformations in facial bones form and discovering new knowledge of primate origin.

LIST OF REFERENCES

Akay, M., Aslan, N. (1996) Numerical and experimental stress analysis of a polymeric composite hip joint prosthesis. *J Biomed Mater Res*. **31**(2):167-82.

Anton, S.C. (1999) Macaque masseter muscle: internal architecture, fiber length, and cross-sectional area. *Int J Primatol*. **20**: 441–462.

Anton, S.C. (2000) Macaque pterygoid muscles: internal architecture, fiber length, and cross-sectional area. *Int J Primatol*. **21**: 131–156.

Ashman, R.B., Van Buskirk, W.C. (1987) The elastic properties of a human mandible. *Adv Dent Res*. **1**(1): 64-7.

Ashman, R.B., Rosinia, G., Cowin, S.C., Fontenot, M.G., Rice, J.C. (1985) The bone tissue of the canine mandible is elastically isotropic. *J Biomech*. **18**(9): 717-21.

Barbier, L., Vander Sloten, J., Krzesinski, G., Schepers, E., Van der Perre, G. (1998) Finite element analysis of non-axial versus axial loading of oral implants in the mandible of the dog. *J Oral Rehabil*. **25**(11): 847-58.

Barker, D.S., Netherway, D.J., Krishnan, J., Hearn, T.C. (2005) Validation of a finite element model of the human metacarpal. *Med Eng Phys*. **27**: 103-113.

Berkovitz, B.K.B., Moxham, B.K., Brown, M.W. (1988) *A Textbook of Head and Neck Anatomy*. London, England: Wolfe Medical Publications.

Blazevich, A.J., Gill, N.D., Bronks, R., Newton, R.U. (2003) Training-specific muscle architecture adaptation after 5-wk training in athletes. *Med Sci Sports Exerc*. **35**(12): 2013-22.

Brown, T.D., Pedersen, D.R., Gray, M.L., Brand, R.A., Rubin, C.T. (1990) Toward an identification of mechanical parameters initiating periosteal remodeling: a combined experimental and analytic approach. *J Biomech*. **23**(9): 893-905.

Bonfield, W., Datta, P.K.(1974) Young's modulus of compact bone. *J Biomech*. **7**(2): 147-9.

Bouvier, M., Hylander, W.L. (1981) Effect of bone strain on cortical bone structure in macaques (Macaca mulatta). *J Morphol*. **167**(1): 1-12.

Bouvier, M., Hylander, W.L. (1996) The mechanical or metabolic function of secondary osteonal bone in the monkey Macaca fascicularis. *Arch Oral Biol*. **41**(10): 941-50.

Carter, D.R. (1987) Mechanical loading history and skeletal biology. *J Biomech*. **20**: 1095-1109.

Carter, D.R., Hayes, W.C. (1977) The compressive behavior of bone as a two-phase porous structure. *J Bone Joint Surg Am*. **59**(7): 954-62.

Carter, D.R., Spengler, D.M. (1978) Mechanical properties and composition of cortical bone. *Clin Orthop*. **135**: 192-217.

Carter, D.R., Harris, W.H., Vasu, R., Caler, W.E. (1981) The mechanical and biological response of cortical bone to in vivo strain histories. In: *Mechanical Properties of Bone.* New York, NJ: American Society of Mechanical Engineers.

Carter, D.R., Beaupré, G.S., Giori, N.J., Helms, J.A. (1998) Mechanobiology of skeletal regeneration. *Clin Orthop*. **355**(Suppl): S41-55.

Chen, X., Chen, H. (1998) The influence of alveolar structures on the torsional strain field in a gorilla corporeal cross-section. *J Hum Evol*. **35**(6):611-33.

Ciarelli, M.J., Goldstein, S.A., Kuhn, J.L., Cody, D.D., Brown, M.B. (1991) Evaluation of orthogonal mechanical properties and density of human trabecular bone from the major metaphyseal regions with materials testing and computed tomography. *J Orthop Res*. **9**(5): 674-82.

Coleman, J.C., Hart, R.T., Owan, I., Tankano, Y., Burr, D.B. (2002) Characterization of dynamic three-dimensional strain fields in the canine radius. *J Biomech*. **35**(12):1677-83. Erratum in: *J Biomech* 2003 Jun;**36**(6): 895.

Cowin, S.C. (2001) *Bone Mechanics Handbook*. Boca Raton, FL: CRC Press.

Currey, J.D. (2002) *Bones: Structure and Mechanics*. Princeton, NJ: Princeton University Press.

Daegling, D.J. (1993) The relationship of in vivo bone strain to mandibular corpus morphology in Macaca fascicularis. *J Hum Evol*. **25**: 247–269.

Daegling, D.J. (2002) Bone geometry in cercopithecoid mandibles. *Arch Oral Biol*. **47**(4): 315-25.

Daegling, D.J. (2004) Relationship of strain magnitude to morphological variation in the primate skull. *Am J Phys Anthropol*. **124**(4): 346-52.

Daegling, D.J., Grine, F.E. (1991) Compact bone distribution and biomechanics of early hominid mandibles. *Am J Phys Anthropol*. **86**: 321-339.

Daegling, D.J., Ravosa, M.J., Johnson, K.R., Hylander, W.L. (1992) Influence of teeth, alveoli, and periodontal ligaments on torsional rigidity in human mandibles. *Am J Phys Anthropol*. **89**(1):59-72.

Daegling, D.J., Hylander, W.L. (1994a) Strain distribution in the human mandible. *Am J Phys Anthropol*. Suppl **18**:75.

Daegling, D.J., Hylander, W.L. (1994b) Profiles of strain in the human mandible. *J Dent Res.* **73**(Special Issue:IADR Abstracts):195.

Daegling, D.J., Hylander, W.L. (1997) Occlusal forces and mandibular bone strain: is the primate jaw "overdesigned"?. *J Hum Evol*. **33**(6): 705-17.

Daegling, D.J., Hylander, W.L. (1998) Biomechanics of torsion in the human mandible. *Am J Phys Anthropol*. **105**:73-87.

Daegling, D.J., Hylander, W.L. (2000) Experimental observation, theoretical models, and biomechanical inference in the study of mandibular form. *Am J Phys Anthropol*. **112**(4): 541-51.

Daegling, D.J., McGraw, W.S. (2001) Feeding, diet and jaw form in West African *Colobus* and *Procolobus*. *Int. J. Primatol*. **22**:1033-1055.

Daegling, D.J., Hotzman, J.L. (2003) Functional significance of cortical bone distribution in anthropoid mandibles: an in vitro assessment of bone strain under combined loads. *Am J Phys Anthropol*. **122**(1): 38-50.

Daegling, D.J., Marinescu, R., Venkataraman, S., Rapoff, A.J. (2003) Effects of structural heterogeneity and anisotropy on finite element model predictions for a mandible of a *Macaca fascicularis*. *Am J Phys Anthropol*. Suppl 36:83.

Dally, J.W., Riley, W.F. (1991) *Experimental Stress Analysis*. New York, NY: McGraw-Hill Co.

Dalstra, M., Huiskes, R., van Erning, L. (1995) Development and validation of a three-dimensional finite element model of the pelvic bone. *J Biomech Eng*. **117**(3): 272-278.

Dechow, P.C., Carlson, D.S. (1990) Occlusal force and craniofacial biomechanics during growth in rhesus monkeys. *Am J Phys Anthropol*. **83**(2): 219-37.

Dechow, P.C., Schwartz-Dabney, C.L., Ashman, R.B. (1992) Elastic Properties of the Human Mandibular Corpus. In: *Bone Biodynamics in Orthodontic and Orthopedic Treatment*. Ann Arbor, MI: University of Michigan Press.

Dechow, P.C., Hylander, W.L. (2000) Elastic properties and masticatory bone stress in the macaque mandible. *Am J Phys Anthropol*. **112**(4):553-74.

Demes, B., Preuschoft, H., Wolff, J.E.A. (1984) Stress-strength relationships in the mandibles of hominoids. In: *Food Acquisition and Processing in Primates*. New York, NY: Plenum Press.

Driessen, N.J., Wilson, W., Bouten, C.V., Baaijens, F.P. (2004) A computational model for collagen fibre remodelling in the arterial wall. *J Theor Biol*. **226**(1): 53-64.

Dumont, E.R., Piccirillo, J., Grosse, I.R. (2005) Finite-element analysis of biting behavior and bone stress in the facial skeletons of bats. *Anat Rec A Discov Mol Cell Evol Biol*. **283**(2): 319-30.

Emory University, Atlanta SEER Cancer Registry, October 9, 2006 http://training.seer.cancer.gov/module_anatomy/unit3_2_bone_tissue.html

Erdmann, B., Kober, C., Lang, J., Deuflhard, P., Zeilhofer, H.F., Sader, R. (2002) Efficient and reliable finite element methods for simulation of the human mandible. Proceedings of 9th Workshop on The Finite Element Method in Biomedical Engineering, Biomechanics and Related Fields, Ulm, Germany.

Evans, F.G. (1957) *Stress and Strain in Bones, Their Relation to Fractures and Osteogenesis*. Springfield, IL: Charles C. Thomas Publisher, Bannerstone House.

Evans, F.G. (1973) *Mechanical Properties of Bone*. Springfield, IL: Charles C. Thomas Publisher, Bannerstone House.

Fajardo, R.J., Muller, R. (2001) Three-dimensional analysis of nonhuman primate trabecular architecture using micro-computed tomography. *Am J Phys Anthropol*. **115**(4): 327-36.

Feller, K.U., Schneider, M., Hlawitschka. M., Pfeifer, G., Lauer, G., Eckelt, U. (2003) Analysis of complications in fractures of the mandibular angle-a study with finite element computation and evaluation of data of 277 patients. *J Craniomaxillofac Surg*. **31**(5): 290-5.

Fyhrie, D.P., Carter, D.R. (1990) Femoral head apparent density distribution predicted from bone stresses. *J Biomech*. **23**(1): 1-10.

Forwood, M.R., Turner, C.H. (1995) Skeletal adaptations to mechanical usage: results from tibial loading studies in rats. *Bone*. **17**(4 Suppl): 197S-205S.

Fritton, S.P., McLeod, K.J., Rubin, C.T. (2000) Quantifying the strain history of bone: spatial uniformity and self-similarity of low-magnitude strains. *J Biomech*. **33**(3): 317-25.

Frost, H.M. (1964) *The Laws of Bone Structure*. Springfield, IL: Charles C. Thomas Publisher.

Frost, H.M. (1986) *Intermediary Organization of the Skeleton*. Boca Raton, FL: CRC Press.

Frost, H.M. (1990a) Skeletal structural adaptations to mechanical usage (SATMU): 1. Redefining Wolff's law: the bone modeling problem. *Anat Rec*. **226**(4): 403-413.

Frost, H.M. (1990b) Skeletal structural adaptations to mechanical usage (SATMU): 2. Redefining Wolff's law: the remodeling problem. *Anat Rec*. **226**(4): 414-22.

Frost, H.M. (1994) Wolff's Law and bone's structural adaptations to mechanical usage: an overview for clinicians. *Angle Orthod*. **64**(3): 175-88.

Frost, H.M. (1998) Changing concepts in skeletal physiology: Wolff's law, the mechanostat, and the "Utah Paradigm". *Am J Hum Biol*. **10**: 599-605.

Futterling, S., Klein, R., Straßer, W., and Weber, H. (1998) Automated Finite Element Modeling of a Human Mandible With Dental Implants, Proceedings of the Sixth International Conference in Central Europe on Computer Graphics and Visualization '98, Vol. 1, part 1, 103–110.

Giesen, E.B., Ding, M., Dalstra, M., van Eijden, T.M. (2003) Reduced mechanical load decreases the density, stiffness, and strength of cancellous bone of the mandibular condyle. *Clin Biomech.* **18**(4): 358-63.

Gray, H. (2000) *Anatomy of the Human Body.* Philadelphia, PA: Lea & Febiger.

Greaves, W.S. (2000) Location of the vector of jaw muscle force in mammals. *J Morphol*. **243**(3): 293-9.

Gross, T.S., Edwards, J.L., McLeod, K.J., Rubin, C.T. (1997) Strain gradients correlate with sites of periosteal bone formation. *J Bone Miner Res*. **12**(6):982-8.

Gross, T.S., Srinivasan, S., Liu, C.C., Clemens, T.L., Bain, S.D. (2002) Noninvasive loading of the murine tibia: an in vivo model for the study of mechanotransduction. *J Bone Miner Res*. **17**(3):493-501.

Guo, X.E., Eichler, M.J., Takai, E., Kim, C.H. (2002) Quantification of a rat tail vertebra model for trabecular bone adaptation studies. *J Biomech*. **35**(3): 363-8.

Gupta, K.K., Knoell, A.C., Grenoble, D.E. (1973) Mathematical modeling and structural analysis of the mandible. *Biomater Med Devices Artif Organs*. **1**(3): 469-79.

Gupta, S., van der Helm, F.C., Sterk, J.C., van Keulen, F., Kaptein, B.L. (2004) Development and experimental validation of a three-dimensional finite element model of the human scapula. *Proc Inst Mech Eng*. **218**(2):127-42.

Hart, R.T., Thongpreda, N. (1988) A finite element based study of the biomechanics of the mandible. *Eng Medicine Biology Soc.* IEEE, 1986-1987.

Hart, R.T., Hennebel, V.V., Thongpreda, N., Van Buskirk, W.C., Anderson, R.C. (1992) Modeling the biomechanics of the mandible: a three-dimensional finite element study. *J Biomech*. **25**(3): 261-286.

Hayes, W.C., Bouxsein, M.L. (1997) Biomechanics of cortical and trabecular bone: Implications for assessment of fracture risk. In: *Basic Orthopaedic Biomechanics*. Philadelphia, PA: Lippincott-Raven Publishers.

Hengsberger, S., Enstroem, J., Peyrin, F., Zysset, P. (2003) How is the indentation modulus of bone tissue related to its macroscopic elastic response? A validation study. *J Biomech*. **36**(10): 1503-9.

Hollister, S.J., Brennan, J.M., Kikuchi, N. (1994) A homogenization sampling procedure for calculating trabecular bone effective stiffness and tissue level stress. *J Biomech*. **27**(4): 433-44.

Hvid, I., Bentzen, S.M., Linde, F., Mosekilde, L., Pongsoipetch, B. (1989) X-ray quantitative computed tomography: the relations to physical properties of proximal tibial trabecular bone specimens. *J Biomech*. **22**(8-9): 837-44.

Hylander, W.L. (1979a) The functional significance of primate mandibular form. *J Morphol*. **160**(2): 223-40.

Hylander, W.L. (1979b) Mandibular function in *Galago crassicaudatus* and *Macaca fascicularis*: an in vivo approach to stress analysis of the mandible. *J Morphol*. **159**: 253–296.

Hylander, W.L. (1984) Stress and strain in the mandibular symphysis of primates: a test of competing hypotheses. *Am J Phys Anthropol*. **64**(1): 1-46.

Hylander, W.L. (1986) In-vivo bone strain as an indicator of masticatory bite force in *Macaca fascicularis*. *Arch Oral Biol*. **31**(3): 149-57.

Hylander, W.L. (1988) Implications of *in vivo* experiments for interpreting the functional significance of "robust" australopithecine jaws. In: *Evolutionary History of the Robust Australopithecines*. New York, NY: Aldine de Gruyter.

Hylander, W.L., Crompton, A.W. (1986) Jaw movements and patterns of mandibular bone strain during mastication in the monkey Macaca fascicularis. *Arch Oral Biol*. **31**(12): 841-8.

Hylander, W.L., Johnson, K.R., Crompton, A.W. (1987) Loading patterns and jaw movements during mastication in Macaca fascicularis: a bone-strain, electromyographic, and cineradiographic analysis. *Am J Phys Anthropol*. **72**(3): 287-314.

Hylander, W.L., Picq, P.G., Johnson, K.R. (1991) Masticatory-stress hypotheses and the supraorbital region of primates. *Am J Phys Anthropol*. **86**(1): 1-36.

Hylander, W.L., Johnson, K.R. (1994) Jaw muscle function and wishboning of the mandible during mastication in macaques and baboons. *Am J Phys Anthropol*. **94**(4): 523-47.

Hylander, W.L., Johnson, K.R. (1997) In vivo bone strain patterns in the zygomatic arch of macaques and the significance of these patterns for functional interpretations of craniofacial form. *Am J Phys Anthropol*. **102**(2): 203-32.

Hylander, W.L., Ravosa, M.J., Ross, C.F., Johnson, K.R. (1998) Mandibular corpus strain in primates: further evidence for a functional link between symphyseal fusion and jaw-adductor muscle force. *Am J Phys Anthropol*. **107**(3): 257-71.

Hylander, W.L., Ravosa, M.J., Ross, C.F., Wall, C.E., Johnson, K.R. (2000) Symphyseal fusion and jaw-adductor muscle force: an EMG study. *Am J Phys Anthropol*. **112**: 469–492.

Huiskes, R., Weinans, H., Grootenboer, H.J., Dalstra, M., Fudala, B., Slooff, T.J. (1987) Adaptive bone-remodeling theory applied to prosthetic-design analysis. *J Biomech*. **20**(11-12): 1135-50.

Huiskes, R., Hollister, S.J. (1993) From structure to process, from organ to cell: recent developments of FE-analysis in orthopaedic biomechanics. *J Biomech Eng*. **115**(4B):520-7.

Johnston, I.A. (2003) Muscle metabolism and growth in Antarctic fishes (suborder Notothenioidei): evolution in a cold environment. *Comp Biochem Physiol B Biochem Mol Biol*. **136**(4): 701-13.

Judex, S., Lei, X., Han, D., Rubin, C. (2006) Low-magnitude mechanical signals that stimulate bone formation in the ovariectomized rat are dependent on the applied frequency but not on the strain magnitude. *J Biomech*. 2006 Jun 29; [Epub ahead of print]

Katona, T.R., Paydar, N.H., Akay, H.U., Roberts, W.E. (1995) Stress analysis of bone modeling response to rat molar orthodontics. *J Biomech*. **28**(1): 27-38.

Keyak, J.H., Meagher, J.M., Skinner, H.B., Mote, C.D. Jr. (1990) Automated three-dimensional finite element modelling of bone: a new method. *J Biomed Eng*. **12**(5): 389-97.

Keyak, J.H., Fourkas, M.G., Meagher, J.M., Skinner, H.B. (1993) Validation of an automated method of three-dimensional finite element modelling of bone. *J Biomech Eng*. **15**: 505-509.

Kiliaridis, S., Bresin, A., Holm, J., Strid, K.G. (1996) Effects of masticatory muscle function on bone mass in the mandible of the growing rat. *Acta Anat (Basel)*. **155**(3):200-5.

Knoell, A.C. (1977) A Mathematical Model of an In Vitro Human Mandible. *J Biomech*. **10**: 159-166.

Koolstra, J.H. (2002) Dynamics of the human masticatory system. *Crit Rev Oral Biol Med*. **13**(4): 366-76.

Koolstra, J.H. (2003) Number crunching with the human masticatory system. *Adv Dent Res*. **82**(9):672-6.

Koolstra, J.H., van Eijden, T.M. (1992) Application and validation of a three-dimensional mathematical model of the human masticatory system in vivo. *J Biomech*. **25**(2): 175-87.

Koolstra, J.H., van Eijden, T.M. (1997a) Dynamics of the human masticatory muscles during a jaw open-close movement. *J Biomech*. **30**(9): 883-9.

Koolstra, J.H., van Eijden, T.M. (1997b) The jaw open-close movements predicted by biomechanical modeling. *J Biomech*. **30**(9): 943-50.

Koolstra, J.H., van Eijden, T.M. (1999) Three-dimensional dynamical capabilities of the human masticatory muscles. *J Biomech*. **32**(2): 145-52.

Korioth, T.W., Romilly, D.P., Hannam, A.G. (1992) Three-dimensional finite element stress analysis of the dentate human mandible. *Am J Phys Anthropol*. **88**(1): 69-96.

Korioth, T.W., Hannam, A.G. (1994a) Deformation of the human mandible during simulated tooth clenching. *Adv Dent Res*. **73**(1): 56-66.

Korioth, T.W., Hannam, A.G. (1994b) Mandibular forces during simulated tooth clenching. *J Orofac Pain*. **8**(2): 178-89.

Korioth, T.W., Johann, A.R. (1999) Influence of mandibular superstructure shape on implant stresses during simulated posterior biting. *J Prosthet Dent*. **82**(1): 67-72.

Kotha, S.P., Guzelsu, N. (2003) Tensile damage and its effects on cortical bone. *J Biomech*. **36**(11): 1683-9.

Lahr, M.M., Wright, H.V.S. (1996) The question of robusticity and the relationship between cranial size and shape in Homo sapiens. *J Hum Evol*. **31**(2): 157–191.

Lanyon, L.E., Goodship, A.E., Pye, C.J., MacFie, J.H. (1982) Mechanically adaptive bone remodeling. *J Biomech*. **15**(3): 141-54.

Lee, K.C., Maxwell, A., Lanyon, L.E. (2002) Validation of a technique for studying functional adaptation of the mouse ulna in response to mechanical loading. *Bone*. **31**(3): 407-12.

Lengsfeld, M., Schmitt, J., Alter, P., Kaminsky, J., Leppek, R. (1998) Comparison of geometry-based and CT voxel-based finite element modelling and experimental validation. *Med Eng Phys*. **20**(7): 515-22.

Lettry, S., Seedhom, B.B., Berry, E., Cuppone, M. (2003) Quality assessment of the cortical bone of the human mandible. *Bone*. **32**(1): 35-44.

Liebschner, M.A., Kopperdahl, D.L., Rosenberg, W.S., Keaveny, T.M. (2003) Finite element modeling of the human thoracolumbar spine. *Spine*. **28**: 559-565.

Liebschner, M.A. (2004) Biomechanical considerations of animal models used in tissue engineering of bone. *Biomaterials*. **25**(9): 1697-714.

Marinescu, R., Daegling, D.J., Rapoff, A.J. (2005) Finite-element modeling of the anthropoid mandible: the effects of altered boundary conditions. *Anat Rec A Discov Mol Cell Evol Biol*. **283**(2): 300-9.

Martin, R.B., Burr, D.B., Sharkey, N.A. (1998) *Skeletal Tissue Mechanics*. New York, NY: Springer-Verlag New York, Inc.

Martin, R.B. (2003) Fatigue microdamage as an essential element of bone mechanics and biology. *Calcif Tissue Int*. **73**(2):101-7.

McNamara, B.P., Cristofolini, L., Toni, A., Taylor, D. (1997) Relationship between bone-prosthesis bonding and load transfer in total hip reconstruction. *J Biomech*. **30**(6):621-30.

Mellal, A., Wiskott, H.W., Botsis, J., Scherrer, S.S., Belser, U.C. (2004) Stimulating effect of implant loading on surrounding bone. Comparison of three numerical models and validation by in vivo data. *Clin Oral Implants Res*. **15**(2): 239-48.

Meijer, H.J., Starmans, F.J., Steen, W.H., Bosman, F. (1993) A three-dimensional, finite-element analysis of bone around dental implants in an edentulous human mandible. *Arch Oral Biol*. **38**(6): 491-6.

Metzger, K.A., Daniel, W.J., Ross, C.F. (2005) Comparison of beam theory and finite-element analysis with in vivo bone strain data from the alligator cranium. *Anat Rec A Discov Mol Cell Evol Biol*. **283**(2):331-48.

Meyer, C., Kahn, J.L., Lambert, A., Boutemy, P., Wilk, A. (2000) Development of a static simulator of the mandible. *J Craniomaxillofac Surg*. **28**(5): 278-86.

Nail, G.A., Dechow, P.C., Ashman, R.B. (1989) Elastic properties of mandibular bone in rhesus monkeys (abstract). *J Dent Res.* **68**(Spec Iss):294

Oreskes, N., Shrader-Frechette, K., Belitz, K. (1994) Certification, validation, and confirmation of numerical models in the earth sciences. *Science*. **263**: 641-646.

Pauwels, F. (1980) *Biomechanics of the Locomotor Apparatus*. New York, NY: Springer-Verlag Berlin.

Pettersson, U., Nordstrom, P., Lorentzon, R. (1999) A comparison of bone mineral density and muscle strength in young male adults with different exercise level. *Calcif Tissue Int*. **64**(6):490-8.

Pruim, G.J., Tenbosch, J.J., Dejongh, H.J. (1978) Jaw muscle EMG-activity and static loading of mandible. *J Biomech*. **11**: 389–395.

Pruim, G.J., Dejongh, H.J., Tenbosch, J.J. (1980) Forces acting on the mandible during bilateral static bite at different bite force levels. J Biomech. 13: 755–763.

Rees, J.S. (2001) An investigation into the importance of the periodontal ligament and alveolar bone as supporting structures in finite element studies. *J Oral Rehabil*. **28**(5):425-32.

Reilly, D.T., Burstein, A.H., Frankel, V.H. (1974) The elastic modulus for bone. *J Biomech*. **7**(3): 271-5.

Reitzik, M., Lownie, J.F., Cleaton-jones, P., Austin, J. (1978) Experimental fractures of monkey mandibles. *Int J Oral Surg*. **7**(2): 100-3.

Remmler, D., Olson, L., Ekstrom, R., Duke, D., Matamoros, A., Matthews, D., Ullrich, C.G. (1998) Pre-surgical CT/FEA for craniofacial distraction: I. Methodology, development, and validation of the cranial finite element model. *Med Eng Phys*. **20**(8): 607-19.

Rho, J.Y., Hobatho, M.C., Ashman, R.B. (1995) Relations of mechanical properties to density and CT numbers in human bone. *Med Eng Phys*. **17**(5): 347-55.

Rho, J.Y., Tsui, T.Y., Pharr, G.M. (1997) Elastic properties of human cortical and trabecular lamellar bone measured by nanoindentation. *Biomaterials*. **18**: 1325–1330

Rho, J.Y., Kuhn-Spearing, L., Zioupos, P. (1998) Mechanical properties and the hierarchical structure of bone. *Med Eng Phys*. **20**(2): 92-102.

Rho, J.Y., Zioupos, P., Currey, J.D., Pharr, G.M. (1999) Variations in the individual thick lamellar properties within osteons by nanoindentation. *Bone*. **25**(3): 295-300.

Roberts, M.D., Hart, R.T. (1997) A frequency dependent bone remodeling algorithm applied to a surface remodeling cantilever beam system. Proc. Sixteenth Southern Biomedical Engineering Conference, Biloxi, MS, 394-397.

Ross, C.F., Hylander, W.L. (1996) In vivo and in vitro bone strain in the owl monkey circumorbital region and the function of the postorbital septum. *Am J Phys Anthropol*. **101**(2): 183-215.

Rubin, C.T. (1984) Skeletal strain and the functional significance of bone architecture. *Calcif Tissue Int*. **36** Suppl 1:S11-8.

Rubin, C.T., Lanyon, L.E. (1982) Limb mechanics as a function of speed and gait: a study of functional strains in the radius and tibia of horse and dog. *J Exp Biol*. **101**:187-211.

Rubin, C.T., Lanyon, L.E. (1985) Regulation of bone mass by mechanical strain magnitude. *Calcif Tissue Int*. **37**(4):411-7.

Rubin, C.T., Gross, T.S., Donahue, H., Guilak, F., McLeod, K. (1994) Physical and environmental influences on bone formation. In: *Bone Formation and Repair.* Rosemont, Ill: American Academy of Orthopaedic Surgeons, pp 61–78.

Rubin, C., Turner, A.S., Mallinckrodt, C., Jerome, C., McLeod, K., Bain, S. (2002) Mechanical strain, induced noninvasively in the high-frequency domain, is anabolic to cancellous bone, but not cortical bone. *Bone*. **30**(3):445-52.

Russell, M.D. (1985) The Supraorbital Torus: "A Most Remarkable Peculiarity". *Current Anthropology*. **26**(3): 337-360.

Schoenau, E., Frost, H.M. (2002) The "muscle-bone unit" in children and adolescents. *Calcif Tissue Int*. **20**: 405–407.

Schwartz-Dabney, C.L., Dechow, P.C. (2003) Variations in cortical material properties throughout the human dentate mandible. *Am J Phys Anthropol*. **120**(3):252-77.

SciSoft, October 9, 2006 www.zib.de

Snyder, S.M., Schneider, E. (1991) Estimation of mechanical properties of cortical bone by computed tomography. *J Orthop Res*. **9**(3): 422-31.

Sommerfeldt, D.W., Rubin, C.T. (2001) Biology of bone and how it orchestrates the form and function of the skeleton. *Eur Spine J*. **10** Suppl 2: S86-95.

Spencer, M.A. (1998) Force production in the primate masticatory system: electromyographic tests of biomechanical hypotheses. *J Hum Evol*. **34**(1): 25-54.

Spencer, M.A. (1999) Constraints on masticatory system evolution in anthropoid primates. *Am J Phys Anthropol*. **108**(4): 483-506.

Strait, D.S., Dechow, P.C., Richmond, B.G., Ross, C.F., Spencer, M.A. (2003) Finite element analysis applied to masticatory biomechanics. *Am J Phys Anthropol*. Suppl 36:202.

Taddei, F., Pancanti, A., Viceconti, M. (2004) An improved method for the automatic mapping of computed tomography numbers onto finite-element models. *Med Eng Phys.* **26**: 61-69.

Taylor, D., O'Reilly, P., Vallet, L., Lee, T.C. (2003) The fatigue strength of compact bone in torsion. *J Biomech*. **36**(8): 1103-9.

Turner, C.H., Anne, V., Pidaparti, R.M. (1997) A uniform strain criterion for trabecular bone adaptation: do continuum-level strain gradients drive adaptation? *J Biomech*. **30**(6): 555-63.

Ueki, K., Nakagawa, K., Marukawa, K., Takatsuka, S., Yamamoto, E. (2005) The relationship between temporomandibular joint disc morphology and stress angulation in skeletal Class III patients. *Eur J Orthod*. **27**(5):501-6.

Van Buskirk, W.C., Ashman, R.B. (1981) The elastic moduli of bone, in *Mechanical Properties of Bone.* Joint ASME-ASCE Applied Mechanics, Fluids Engineering and Bioengineering Conference, Boulder, CO.

Van Rietbergen, B., Weinans, H., Huiskes, R., Odgaard, A. (1995) A new method to determine trabecular bone elastic properties and loading using micromechanical finite element models. *J Biomech*. **28**(1): 69-81.

Van Ruijven, L.J., Giesen, E.B., van Eijden T.M. (2002) Mechanical significance of the trabecular microstructure of the human mandibular condyle. *J Dent Res*. **81**: 706-10.

Van Ruijven, L.J., Giesen, E.B., Farella, M., van Eijden, T.M. (2003) Prediction of mechanical properties of the cancellous bone of the mandibular condyle. *J Dent Res*. **82**(10): 819-23.

Viceconti, M., Olsen, S., Nolte, L.P., Burton, K. (2005) Extracting clinically relevant data from finite element simulations. *Clin Biomech* (Bristol, Avon). **20**(5):451-4. Erratum in: *Clin Biomech* (Bristol, Avon). **20**(9):1010.

Vico, L., Lafage-Proust, M.H., Alexandre, C. (1998) Effects of gravitational changes on the bone system in vitro and in vivo. *Bone*. **22**(5 Suppl):95S-100S.

Vollmer, D., Meyer, U., Joos, U., Vega, A., Piffko, J. (2000) Experimental and finite element study of a human mandible. *J Craniomaxillofac Surg*. **28**(2): 91-6.

Zannoni, C., Mantovani, R., Viceconti, M. (1998) Material properties assignment to finite element models of bone structures: a new method. *Medical Engineering and Physics*. 20(10):735-40.

Yamada, H., Evans, G. (1970) *Strength of Biological Materials*. Baltimore, MD: Williams and Wilkins Company.

Yang, Y.J., Damron, T. Histology of Bone, November 20, 2006 http://www.emedicine.com/orthoped/topic403.htm

Wagner, A., Krach, W., Schicho, K., Undt, G., Ploder, O., Ewers, R. (2002) A 3-dimensional finite-element analysis investigating the biomechanical behavior of the mandible and plate osteosynthesis in cases of fractures of the condylar process. *Oral Surg Oral Med Oral Pathol Oral Radiol Endod*. **94**(6): 678-86.

Ward, S.C. (1991) Taxonomy, paleobiology and adaptations of the "robust" australopithecines. *J Hum Evol*. **21**: 469-483.

Weinans, H., Huiskes. R., Grootenboer, H.J. (1992) The behavior of adaptive bone-remodeling simulation models. *J Biomech*. **25**(12): 1425-41.

Wilson, C.M., Bakewell, S.E., Miller, M.R., Hart, N.D., McMorrow, R.C., Barry, P.W., Collier, D.J., Watt, S.J., Pollard, A.J. (2002) Increased resting bronchial tone in normal subjects acclimatised to altitude. *Thorax*. **57**(5): 400-4.

Wiskott, H.W., Belser, U.C. (1999) Lack of integration of smooth titanium surfaces: a working hypothesis based on strains generated in the surrounding bone. *Clin Oral Implants Res*. **10**(6): 429-44.

Wood, B.A., Lieberman, D.E. (2001) Craniodental variation in Paranthropus boisei: A developmental and functional perspective. *Am J Phys Anthropol*. **116**: 13-25.

BIOGRAPHICAL SKETCH

Ruxandra Cristiana Marinescu Tanasoca graduated in 1998 with a Bachelor of Science in materials science and engineering from Polytechnic University of Bucharest, Romania. In 2001 she received her Master of Science in mechanical engineering from Ohio University, Athens, OH. Deciding to pursue a PhD in biomedical engineering, she joined the Department of Biomedical Engineering at the University of Florida, Gainesville, FL, in June 2002.